OBSERVING SHORT-TERM GEOMORPHIC CHANGE IN A HUMAN-MODIFIED RIVER USING TERRESTRIAL REPEAT PHOTOGRAPHS AND TRADITIONAL SURVEYS: UNCOMPAHGRE RIVER, COLORADO, USA

A Thesis

by

TYLER J. DEPKE

Submitted to the Office of Graduate Studies of
Texas A&M University
in partial fulfillment of the requirements for the degree of

MASTER OF SCIENCE

May 2012

Major Subject: Geology

Observing Short-Term Geomorphic Change in a Human-Modified River Using Terrestrial Repeat Photographs and Traditional Surveys: Uncompahgre River, Colorado, USA

OBSERVING SHORT-TERM GEOMORPHIC CHANGE IN A HUMAN-MODIFIED RIVER USING TERRESTRIAL REPEAT PHOTOGRAPHS AND TRADITIONAL SURVEYS: UNCOMPAHGRE RIVER, COLORADO, USA

A Thesis

by

TYLER J. DEPKE

Submitted to the Office of Graduate Studies of
Texas A&M University
in partial fulfillment of the requirements for the degree of

MASTER OF SCIENCE

Approved by:

Chair of Committee,	John R. Giardino
Committee Members,	John D. Vitek
	Chris Houser
Head of Department,	John R. Giardino

May 2012

Major Subject: Geology

ABSTRACT

Observing Short-Term Geomorphic Change in a Human-Modified River Using Terrestrial Repeat Photographs and Traditional Surveys: Uncompahgre River, Colorado, USA. (May 2012)

Tyler J. Depke, B.S., Hope College

Chair of Advisory Committee: Dr. John R. Giardino

The Uncompahgre River in Ouray, CO, was modified in 1996 from a braided river system to a meandering river channel. Large boulders of riprap were placed along designed meanders to prevent erosion and enable the development of permanent human structures on the flood plain. Deposition of gravel bars in the modified channel occurs annually during the summer. This gravel is "mined" by the City of Ouray; however, the effects of this excavation and the original modification were never assessed.

This study provides an assessment by quantifying cross-sectional area change, cumulative grain-size distributions, shear stresses, slopes, and sinuosities using traditional survey methods. In addition, volume change of a gravel bar inside the modified channel was estimated using extreme oblique photographs (>45º from nadir) that were obtained from nearby cliffs. Close-range photogrammetry was used in the natural channel downstream to evaluate photogrammetric methods using different lenses, image sensors, and camera geometries.

Both traditional and photogrammetric methods clearly indicated significant deposition in the modified channel, whereas erosion occurred directly downstream from the modified channel, but did not occur at a reach 1.5 km downstream. In the natural channel, no cross-sectional area change occurred, grains were poorly sorted, and the longitudinal slope was ~four times steeper than the modified channel. Shear stress ratios were used as an erosion threshold, which did not correlate with actual cross-sectional area change, but a decrease in shear stress ratios from May 2011 to September 2011 were associated with erosion. Average RMSE values for DEMs created from extreme-oblique photographs of a gravel bar in May 2011 and September 2011 were 0.140 m and 0.324 m, respectively. Using a DEM of difference with a t-statistic filter revealed that $115 m^3$ of gravel was deposited.

The Uncompahgre River showed similar geomorphic characteristics to other rivers in southwest Colorado, however, the slope of the natural and modified channels were much steeper than other rivers. Extreme-oblique photography and unconventional sensors both yielded reliable results, showing that these atypical techniques can be used in terrestrial photogrammetric applications such as, post-restoration assessments, as long as proper base-to-height ratios are achieved.

DEDICATION

This paper is dedicated to my friend and colleague Carolyn Sexton. Throughout my entire experience at Texas A&M, the good, the bad, the mediocre, the awkward, the funny, or the sad, she helped me along the journey and challenged me to become a better person. Whether it was the ridiculously long drives through west Texas, fearlessly obtaining cross-section data, or my outrageous underestimations of how long it would take to finish a task in the field, her freak out sessions kept me safe and made me realize that I might be just a little crazy. Carolyn, if you had a tree core for every awesome total station shot you did, Rick's lab would look like a lumberyard and you would never be able to finish your thesis!

ACKNOWLEDGEMENTS

I would like to thank God first and foremost for putting me in the situation to spend 2 wonderful years at Texas A&M and giving me the ability to learn what I needed to learn while at graduate school. I hope that everything that I did in writing this thesis, collecting data, performing analysis, and planning the research will be seen as a reflection of the character of your Son Jesus. Let this manuscript be a small glimpse into the intricacies of the amazing world You created so that people can appreciate Your creation and see your handiwork in the details, even in the field of geology.

> "The heavens declare the glory of God;
> the skies proclaim the work of his hands.
> Day after day they pour forth speech;
> night after night they reveal knowledge.
> They have no speech, they use no words;
> no sound is heard from them."
>
> -Psalm 19:1-3

> "Only a rookie who knows nothing about science would say science takes away from faith. If you really study science, it will bring you closer to God."
>
> -Dr. James Tour

I would like to thank Dr. Rick Giardino for his overwhelming dedication to his students every step along the way. Whether it's accepting you as his student when you had no one else to go to, sawing plywood at 11PM during the week, or editing countless drafts of proposals, abstracts, and theses, it has been a blessing to have Rick as an advisor and mentor. I arrived at Texas A&M with little exposure to graduate studies

confused at what I wanted to do. A high school teacher once told me, “Don’t take classes that interest you. Take classes from the professors that interest you.” Thanks again Rick.

I would also like to thank the members of my committee, Dr. Jack Vitek and Dr. Chris Houser for their guidance, advice, and support throughout the entirety of this research. I would like to give a special thanks to Dr. Andrew Klein for providing insight regarding remote sensing concepts and helping focus my research interests.

I would especially like to thank Dr. Giardino, Dr. Houser, Dr. Chris Matthewson, and Dr. Nasir Gharaibeh for letting me use their equipment in the field. This research could not have been completed otherwise. Thank you Sanjay Tewari for teaching me the total station interface and helping me get that bad boy running.

To the absolutely amazing field assistants that put up with me bossing you around, I would like to show you my appreciation by offering you a juice box. Helen, Marge, Carolyn, Bree, and Jonathan, I love you guys.

I would like to thank Patrick Rondinelli and Dan Fossey from the City of Ouray for helping me become acquainted with the Uncompahgre River Restoration project and providing background information. To Daniel Dgenhardt, thank you for your participation and helping me collect data. Thank you Pam and Bob Larson for helping me locate local benchmarks and providing the necessary information about them.

I can honestly say that I have never experienced the kindness and generosity shown to Carolyn and myself as that given by Eric and Phylius Fagrelius during fieldwork excursions. We unfortunately live in a world where letting random strangers into your home has become taboo, shunned upon, and even dangerous. However, your

willingness to let two random people reside in your house on multiple occasions is an act of compassion that I cannot compare to others. In addition, your homemade cooking, interesting conversations, and general character are absolutely outstanding. No trip to Colorado, nor to any mountainous region of the world will ever be complete without the absolutely amazing hospitality and love of Eric and Phylius Fagrelius. Next time I go to Colorado, I will make sure to stop by Ouray to see what is cooking on the stove and if Eric has acquired any more garden trellises.

To Dr. Jim Chandler, thank you for all of your help trying to get the first steps of analysis finished from the other side of the globe. On some days, your help and encouragement was all I had. Thank you Neffra Mathews from the BLM in Colorado for your help looking for software programs during the first steps of this research project.

I would especially like to thank all the students in HAARP who provided feedback and insight for drafts of proposals, help with analysis, etc. I would especially like to thank Adam Lee for his GIS expertise and the late nights filled with deep analysis that would have taken me forever combined with occasional theological conversations. Thank you Sally Scott for collaborating and helping with a few very useful GIS procedures.

Thank you Dr. Charles Eppes and Dr. Larry Fleinhardt for providing a reasonable amount of creative distraction while performing analysis and writing. A summary of the methods of analysis and writing are summed up in your philosophy of when work is best done.

"Less distracting at night, deeper thinking."

-Dr. Larry Fleinhardt

Finally, I would like to thank my mother and father for their encouragement to "Go Big or Go Home" when applying for graduate schools. If it were not for their advice, I would not have even looked at Texas A&M, let alone spent 2 years of my life in College Station earning a graduate degree there. Thank you for the encouragement throughout the entirety of my graduate school career and thanks for reading my papers that I'm sure were just as exciting as your ordinary reading. Thank you for sharing the horror stories of physically cutting a pasting a thesis by hand with scissors and glue. I am thankful for the technology that has allowed me to avoid that, but I will make sure that my grandkids know that "things aren't how they used to be" when they are using computers that won't even require them to type. Thanks again, I love y'all!

NOMENCLATURE

AOI	Area of Interest
CRP	Close-Range Photogrammetry
cfs	Cubic Feet per Second
CMOS	Complementary Metal-Oxide-Semiconductor
cms	Cubic Meters per Second
DEM	Digital Elevation Model
DIY	Do-It-Yourself
DTM	Digital Terrain Model
DSLR	Digital Single-Lens Reflex
EM1	East Mountain Site #1
EO	Exterior Orientation
EXIF	Exchangeable Image File Format
GCP	Ground Control Point
GPS	Global Positioning System
GSD	Ground Sample Distance
IO	Interior Orientation
MP	Megapixels
NOAA	National Oceanic and Atmospheric Association
PLOTS	Public Laboratory for Open Technology and Science
R1-R5	River Site #1-#5

R2XS3	River Site #2, Cross-Section #3
RMSE	Root Mean Square Error
SPS	Sensor Pixel Size
UAV	Unmanned Aerial Vehicle
WM1	West Mountain Site #1

TABLE OF CONTENTS

Page

ABSTRACT iii

DEDICATION v

ACKNOWLEDGEMENTS vi

NOMENCLATURE x

TABLE OF CONTENTS xii

LIST OF FIGURES xiv

LIST OF TABLES xix

CHAPTER

I INTRODUCTION 1

- Problem Statement 1
- Hypotheses and Objectives 2
- Research Importance 3

II GEOMORPHIC CHANGES OF RIVER RESTORATION ON THE UNCOMPAHGRE RIVER IN OURAY, COLORADO, USA 5

- Introduction 5
- Background for River Restoration 7
- Study Area 18
- Methods of Study 30
- Results 39
- Discussion 56
- Conclusions 58

III TERRESTRIAL PHOTOGRAMMETRY USING CONSUMER-GRADE CAMERAS TO STUDY SHORT-TERM TEMPORAL CHANGE: UNCOMPAHGRE RIVER, COLORADO, USA 61

CHAPTER Page

Introduction 61
Background on Photogrammetry 63
Study Area 80
Methodology 86
Data and Results 94
Discussion 117
Conclusions 121

IV DISCUSSION 124

Broader Impacts 124
Limitations 125
Future Recommendations 126

V CONCLUSIONS 130

Summary 130

REFERENCES 134

APPENDIX 140

VITA 159

LIST OF FIGURES

FIGURE		Page
1	The potential of entrainment of sediment in the Uncompahgre River at Ridgeway for calculated 2-year, 5-year, and 10-year floods	12
2	Map showing the location of the Uncompahgre River in Colorado	19
3	Map of all five USGS gauging stations located on the Uncompahgre River	20
4	Mean daily discharge values for all available data for the Uncompahgre River near Ouray, CO	22
5	Discharge values collected at 15-minute intervals for June 11- 26, 2011.	23
6	A hypothetical example illustrating how the timing of freeze-thaw and peak streamflow can influence the timing and magnitude of erosion	25
7	Repeat photographs looking south from the northern terminus of the modification project	26
8	Looking northwest onto the Uncompahgre River on the southern side of Ouray, CO	27
9	Repeat photographs located at about the midway point of the channel modification	28
10	Mid-channel bars have developed inside the modified “meandering” channel	30
11	Map of the Uncompahgre River Valley on the north side of Ouray, CO .	31
12	Error determination of cross-sectional area via two consecutive surveys of the same cross-section	33
13	Map of cross-sections at R1	34
14	Map of cross-sections at R2 and R3	35
15	Map of cross-sections at R4	36

FIGURE Page

16 The net area change of each cross-section measured from May 2011 to Sept 2011 39

17 Shear Stress Ratios of each Cross-Section for May and September 2011 41

18 Cross-section of R2XS4 43

19 Cross-section of R2XS5 44

20 Pebble counts from R1, R2, and R5 taken in early May 2011 shown as curves of cumulative size distributions 45

21 Pebble counts from R1- R5 taken in mid September 2011 shown as curves of cumulative size distributions 46

22 Pebble counts at R1 taken in early May and mid September of 2011 shown as curves of cumulative size distributions compared against the natural channel 47

23 Pebble counts at R2 taken in early May and mid September of 2011 shown as curves of cumulative size distributions compared against the natural channel 48

24 Pebble counts at R5 taken in early May and mid September of 2011 shown as curves of cumulative size distributions 49

25 Sinuosity and slope measurements for the modified portion of the Uncompahgre River made in Google Earth® 50

26 Sinuosity and slope measurements made in Google Earth® for the natural portion of the Uncompahgre River directly downstream from the modified portion 51

27 Slope and sinuosity relationships based on experimental flume studies at constant discharge (Schumm and Khan, 1972) 52

28 Theoretical threshold between meandering and braided channels plotted using channel slope and estimated 2-year flood 54

29 Slope % values by site for May and September of 2011 54

FIGURE Page

30 Longitudinal profiles of the Uncompahgre River acquired from total station surveys of the water surface from May 2011 55

31 Longitudinal profiles of the Uncompahgre River acquired from total station surveys of the water surface from September 2011 55

32 Optimal camera station setup for terrestrial photogrammetry of a vertical planar object. Modified from (Matthews, 2008) 73

33 Acceptable oblique camera position in relation to land surface..... 74

34 R2 during late September 2010 82

35 Oblique close-up of the gravel bar at R2..... 83

36 Looking west at R3 in September 2011 84

37 Looking west at R4 in September 2011 85

38 Looking west at R5 in September 2011 86

39 Oblique aerial image of R2 captured in September 2010 just before artificial bar was removed by the City of Ouray 87

40 DTM of R4 in May 2011..... 89

41 DTM of R4 in September 2011 89

42 The relationship between the base-to-height ratio and DEM accuracy for different terrain classified by local slopes 90

43 Proper predicted radial distortion for 70mm lens from images rotated approximately 180º images from one vertical side to another vertical side 95

44 Improper predicted of radial distortion for 70mm lens from images that were only taken in a horizontal position 95

45 Proper predicted tangential distortion for 70mm lens from images rotated approximately 180º images from one vertical side to another vertical side. 96

FIGURE Page

46 Improper predicted of tangential distortion for 70mm lens from images that were only taken in a horizontal position 96

47 Screen shot of image used in DTM processing with an image mask only covering the gravel bar 97

48 Repeat cross-sectional data for R2XS2 from May 2011 and September 2011 acquired from total station surveys and DEMs produced using photogrammetric analysis 98

49 Repeat cross-sectional data for R2XS3 from May 2011 and September 2011 acquired from total station surveys and DEMs produced using photogrammetric analysis 99

50 Repeat cross-sectional data for R2XS4 from May 2011 and September 2011 acquired from total station surveys and DEMs produced using photogrammetric analysis 100

51 Repeat cross-sectional data for R2XS5 from May 2011 and September 2011 acquired from total station surveys and DEMs produced using photogrammetric analysis 101

52 Histogram of the 200 checkpoints used to determine elevation errors produced on DEMs 104

53 Photogrammetric scene of R5 showing the river bank and camera positions taken with a Reconyx time-lapse capsule. 105

54 Photogrammetric scene of R5 showing the riverbank and camera positions taken with a 50mm lens 106

55 Raw DEM of difference from May 2011 to Sept 2011 110

56 Classifications of the t-statistic filter created from equation 20 111

57 DEM of difference from May 2011 to Sept 2011 after applying the t-statistic filter in Fig. 56 112

58 Histogram of DEM of change at R2 showing the distribution a pixel values in terms of frequency and elevation 113

FIGURE Page

59 DEM of difference of R4 obtained using a fixed 50mm and a 70mm lens in May 2011 (Top) and Sept 2011 (Bottom) 115

60 Histograms of DEM of Difference from R4 showing that models created in May 2011 contain much less error than DEMs created in September 2011 116

61 18MP Sensor from Canon Rebel T2i (Left) vs 3.1MP Sensor in Reconyx time-lapse capsules (Right) 119

LIST OF TABLES

TABLE		Page
1	Details for each USGS gauging stations on the Uncompahgre River	21
2	Annual maximums of mean daily discharges for all gauge data in Ouray, CO	23
3	Sinuosity and slope values for the modified portion of the Uncompahgre River	50
4	Sinuosity and slope measurements values for the natural portion of the Uncompahgre River directly downstream from the modified portion	51
5	Oblique photograph camera positions from cliffs	87
6	RMSE values for DTMs of R2	102
7	Summary of DEM error from total station checkpoints	104
8	RMSE values for both the DEM created from the Recoynx time-lapse capsule and the point cloud data generated from the 50mm lens at R5	107

CHAPTER I

INTRODUCTION

Problem Statement

A section of the Uncompahgre River in Ouray, CO, has been modified from a braided river system to a meandering river system through anthropogenic channel alteration. Riprap was installed to stabilize banks, prevent erosion, and maintain fixed meanders to increase usable land on the floodplain for building homes, hotels, and a riverwalk recreation area. In the modified section of the river, sediment is annually dredged from newly created point bars, crushed, and sold as aggregate gravel to be used for construction. In 2010, the City of Ouray paid $15,000 to repair the channel from the erosion that had occurred from the spring runoff. Unfortunately, knowledge of the rates of change and volume of material removed are unknown.

This study will estimate the quantity of material deposited/eroded at specific sites within the modified channel and downstream in an unmodified portion of the channel using a series of digital photographs and traditional cross-section surveys. The digital images were processed using photogrammetric techniques to create digital elevation models (DEMs) to determine temporal and spatial patterns of geomorphic changes. Time-lapse photography, or short-temporal photography has the potential to capture

---

This thesis follows the style of *Geomorphology*.

geomorphic changes at a seasonal time scale and even for individual flows. Time-lapse capsules were setup in the natural portion of the stream channel to capture small, high-frequency geomorphic changes. Traditional cross-sectional surveys were used to validate DEMs created from oblique and close-range photographs and to provide an independent data set for analysis.

River restoration has been performed at a number of different locations in southwest Colorado (Elliott and Capesius, 2009; Wohl, 2006); however, the outcomes of restoration projects are often not assessed. This study provides a post analysis of restoration, which is significant because it adds to the limited database of knowledge for the region concerning the character of rivers after restoration has been completed. Although river restoration, or river modification has become a very popular method of creating more buildable land on flood plains and aesthetically pleasing recreational areas, assessing the outcomes of engineering projects is essential for determining risk, evaluating maintenance, and improving future restoration projects.

Hypotheses and Objectives

The goal of this study is to obtain a quantitative understanding of the cross-sectional morphometric change of the river above a dynamic water level on a short-term temporal interval to evaluate current practices of stream modification. This goal can be summarized into the following research question: Does dynamic restoration (maintenance) enhance deposition in the Uncompahgre River? The following are hypotheses of the possible outcomes to that question:

H_0 = No, net erosion in restored area = net erosion downstream,

H_1 = Yes, net erosion in restored area < net erosion downstream, and

H_2 = No, net erosion in restored area > net erosion downstream.

The primary research objectives of this study are to:

1. Characterize the physical aspects of the Uncompahgre River north of Ouray, CO;
2. Quantify erosion and deposition of sediment at distinct locations;
3. Evaluate accuracy of photogrammetric vs. traditional methods; and
4. Identify depositional and erosional patterns related to location in stream (meander vs point bar), time of year, and discharge events.

Research Importance

The terrestrial photogrammetric techniques used in this research are on the forefront of new methods being developed for spatial analysis based on more traditional aerial remote sensing techniques. The successful and unsuccessful methods used in this research will help photogrammetry become more common for non-photogrammetrists.

Because funding for this project was not limited, the methodology for this research was developed such that a member of the public could perform this without spending large amounts of money. With the vast improvement of communication of a global scale and improvement of many remote-sensing technologies, public science communities are becoming more abundant. The Public Laboratory for Open Technology

and Science (PLOTS), a group made up of activists, educators, technologists, and community organizers, uses inexpensive do-it-yourself (DIY) techniques to seek to change how people observe the social, political, and environmental issues of today. As an open-source community, they promote action, intervention, and awareness by allowing anyone to participate in scientific research (2011).

The open-source community, specialized forums, and social media played a pivotal role in overcoming obstacles during data analysis. Likewise, I was able to respond to research questions from other individuals regarding remote sensing and photogrammetric techniques. Creating a public dialogue of methodologies between individuals located on different sides of the planet helps the individuals involved and provides a resource for those who are interested in learning more about science and performing their own research.

CHAPTER II

GEOMORPHIC CHANGES OF RIVER RESTORATION ON THE UNCOMPAHGRE RIVER IN OURAY, COLORADO, USA

Introduction

River restoration has been performed at a number of different locations in southwest Colorado (Elliott and Capesius, 2009; Wohl, 2006); however, the outcomes of restoration projects are often not assessed. This study provides a post analysis of a river restoration project in Ouray, CO, which is significant because it adds to the limited database of knowledge for the region concerning the character of rivers after restoration has been completed so that future projects can be designed more efficiently. Although river restoration, or river modification has become a very popular method of creating more buildable land on flood plains and aesthetically pleasing recreational areas, assessing the outcomes of engineering projects is essential for determining risks of natural hazards (Mathewson, 1992), evaluating maintenance, and improving future restoration projects by validating restoration methods.

A section of the Uncompahgre River in Ouray, CO, has been modified from a braided river system to a meandering river system through anthropogenic channel alteration. Riprap was installed to stabilize banks, prevent erosion, and maintain fixed meanders to increase usable land on the floodplain for building homes, hotels, and a riverwalk recreation area. In the modified section of the river, sediment is annually

dredged from newly created point bars, crushed, and sold as aggregate gravel to be used for construction. In 2010, the City of Ouray paid $15,000 to repair the channel from the erosion that had occurred from the spring runoff.

Unfortunately, knowledge of the rates of change and volume of material removed are unknown. This study will estimate the quantity of material deposited/eroded at specific sites within the modified channel and downstream in an unmodified portion of the channel using a series of traditional cross-sectional surveys. Photographs were collected primarily for photogrammetric analysis, but were also used to qualitatively identify temporal and spatial patterns of geomorphic changes.

The goal of this study is to obtain a quantitative understanding of the cross-sectional morphometric change of the river above a dynamic water level on a short-term temporal interval to evaluate current practices of stream modification. This goal can be summarized into the following research question: Does dynamic restoration (maintenance) enhance deposition in the Uncompahgre River? The following are hypotheses of the possible outcomes to that question:

H_0 = No, net deposition in restored area = net deposition downstream,

H_1 = No, net deposition in restored area < net deposition downstream, and

H_2 = Yes, net deposition in restored area > net deposition downstream.

The primary research objectives of this study are to:

1. Characterize the physical aspects of the Uncompahgre River north of Ouray, CO,

2. Quantify erosion and deposition of sediment at distinct locations, and
3. Identify depositional and erosional patterns related to location in stream channel.

Background for River Restoration

Introduction

River restoration can be broadly classified into five categories: (1) flow regulation, (2) biotic integrity, (3) water pollution, (4) channel alteration, and (5) land use (Wohl, 2006). This thesis focuses primarly on river geometry and sediment transport, which are included in the flow regulation and channel alteration categories, although land use may also provide insight about changes in river geometry and sediment transport.

Channel reconfiguration, often termed “restoration”, has recently become very popular in the western U.S., as people have become aware of the environmental benefits including: improved water “control” in flood-prone areas, enhancement of riparian areas, mitigation of unstable streambed/streambanks, and general improvement for recreational use (Elliott and Capesius, 2009). Although stream restoration has the potential to offer these improvements, unpredicted geomorphic changes can prohibit these improvements from being utilized, or destroy reconfiguration designs shortly after being completed.

Restoration failure can be attributed to a number of geomorphic processes, such as: bank erosion, high rates of sediment transport, streambed deposition/incision, floodplain deposition/scour, decreases in soil moisture, extended submergence, and loss of riparian vegetation. Assessment of restoration projects, which involves quantifying

the already mentioned processes, is also underfunded and overlooked when this final stage may provide the data needed to evaluate further restoration or maintenance options (Elliott and Capesius, 2009).

River restoration projects that fail often do so because of six primary design problems. Elliot and Capesius (2009) state that restoration techniques rely on: (1) the assumption that the reconfigured channel will follow its forced reconfigured channel form; (2) the use of fixed-location boulder, log, and rip-rap structures in a dynamic river channel; (3) the strict correlation of channel form (width, depth, meander wavelength, etc.) with a single discharge value usually estimated from a reference reach that is assumed to have the same characteristics of the redesigned channel; (4) the failure to account for natural variability of a stream with time; (5) the failure to account for the disproportion in driving and resisting forces or sediment supply and transport capacity of the stream; and (6) an assumed average stream condition at scales of reach. All problems in the design process can be summed into the following statement: Rivers are dynamic systems whereas restoration techniques attempt to force a single configuration on a natural system that is constantly changing.

Case Studies from Colorado

Uncompahgre River at Ridgeway

Elliot and Capesius (2009) provided a one-dimensional cross-sectional evaluation of three restoration sites in southwestern Colorado: (1) the Uncompahgre River at Ridgeway (approximately 15km NW of Ouray, CO); (2) the North Fork Gunnison River

at Hotchkiss; and (3) the Lake Fork at Gateview. Their goal was to evaluate the potential changes of the reconfigured channels in response to hypothetical flood discharges and the actual peak flood discharge from 2005. Q_2, Q_5, and Q_{10} represent the theoretical discharges for given reoccurrence flood intervals of 2, 5, and 10 years, respectively, which were all derived using previous USGS stream gauge records that use USIACWD (1982) methods (Flynn et al., 2006).

Data were obtained using traditional field methods, including measurements of sediment sizes for the streambed, banks, alluvial bars, and terraces, topographic surveys of cross-sections and longitudinal profiles, as well as oblique photography. Additional topographic data from DEMs and aerial photographs were used for more extensive geomorphic evaluations.

Stream restoration of the Uncompahgre River in Ridgeway, CO, was designed to confine a braided channel into a single channel by decreasing the width to depth ratio and increasing the sinuosity through channel excavation and grading bed material. Channel modification was undertaken to (1) create stable floodplain areas, (2) stabilize the streambed near the Highway 62 bridge, (3) create backwater habitat, (4) allow bed-material transport, (5) stabilize stream banks, and (6) to facilitate the development of a healthy riparian zone, recreational trail, and wetland area. To stabilize banks, boulders up to 1m or more in diameter and log banks were installed along channel edges (Elliott and Capesius, 2009). With the exception of creating a wetland area, stabilizing the streambed near Highway 62, and using log banks, the same methods and goals were performed for restoration in Ouray, CO.

By confining a braided stream into a single channel that meanders, an unnatural and potentially unstable state was created at this specific location. Unstable streams will adjust dimensions rapidly and progressively as they try to obtain a state of dynamic equilibrium (Schumm, 1977). The Uncompahgre River at Ridgeway amongst other braided channels in southwestern Colorado that have been "restored" were assessed, and it was determined that the steep slope and large magnitude of discharge with a two-year reoccurrence interval (Q_2) naturally forms braided channels with alluvial islands or midchannel bars (Elliott and Capesius, 2009).

After flooding in 2005, some artificially placed boulders were buried by laterally accreting bars, whereas other boulder structures had been moved and buried by sediment. Large boulders often obstructed downstream sediment transport instead of blocking bank erosion as originally intended. Restoration designs assume in-channel structures will remain stationary to provide some desired hydraulic function, unfortunately, this is often not the case. Although most boulders did not move, those that did altered the original intended flow path and created eddies, which encouraged further erosion of the opposite bank. Alluvial bars exhibited the same response. High rates of bank erosion occurred where bank material contained a larger variety of grain sizes because this material is more entrainable (Elliott and Capesius, 2009).

Examining these changes from a mathematical point-of-view can be expressed in terms of work performed by the stream. When calculating the total work performed by a stream, unless discharge changes, total work will remain constant. Work can be defined by a number of variables: velocity, depth, width, and slope. If discharge changes, it is

very unlikely that any one of these variables will change more than others unless physical conditions prohibit change (Langbein and Leopold, 1964). By importing riprap designed to maintain a constant channel width, it is likely that these other variables (velocity, depth, and slope) will exhibit larger changes with increases in discharge than if the stream were left unmodified.

The τ_o / τ_c ratio was calculated using equations 1 and 2 to predict sediment movement at individual sites (Fig 1.) and for sediment budgets to be compared from site-to-site (Elliott and Capesius, 2009). DuBoys equation assumes steady stream flow, which was assumed because no significant inflows or outflows were present. Channel instability was assumed to be a function of entrained sediment from the streambed, stream banks, and alluvial bars (Elliott and Capesius, 2009).

At all cross-sections, for all discharge values, sediment was moved with the most volume of sediment moving through XS-6, and the least volume through XS-1. Using this method of predicting sediment transport, the most volume of deposition should occur between XS-6 and XS-7, whereas rates of erosion would increase traveling downstream from XS-1 to XS-6.

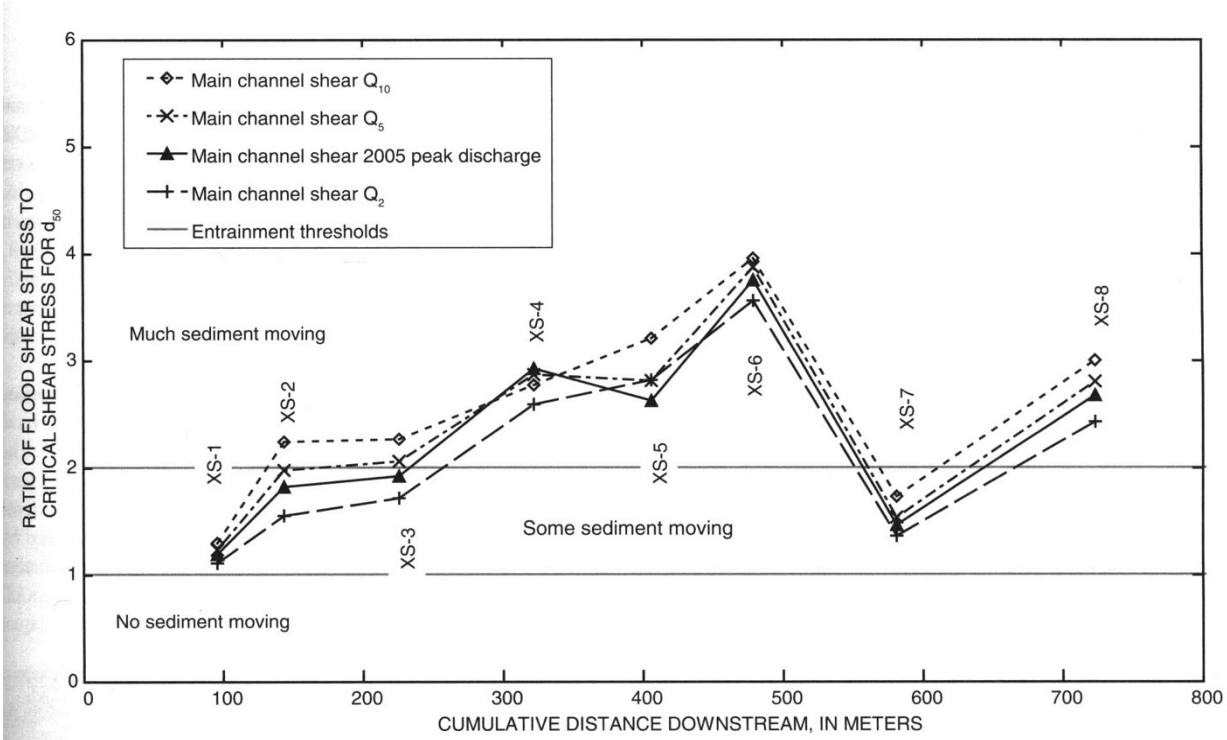

Figure 10. Uncompahgre River sediment-entrainment potential for the 2 yr, 5 yr, 10 yr, and May 2005 floods.

Fig. 1. The potential of entrainment of sediment in the Uncompahgre River at Ridgeway for calculated 2-year, 5-year, and 10-year floods, as well as the actual flood from May of 2005 (Elliott and Capesius, 2009).

Variations in cross-section morphology produce variable hydraulic conditions for sediment entrainment, sorting, and deposition at different locations within the streambed (Smith and Prestegaard, 2005). As a result, cross-section mean boundary shear stresses will vary with changes in hydraulic radius and energy gradient. Cross-channel boundary shear stresses, calculated using duBoys equation, account for changes in river geometry ((Chow, 1959) as cited by Elliott and Capesius (2009)):

$$\tau_o = \gamma RS \quad (1)$$

where

τ_o = cross-section mean boundary shear stress (N/m^2)
γ = specific weight of water (9807 N/m^3)
R = hydraulic radius (m)
S = energy gradient for a specific discharge (m/m)

The hydraulic radius (R) can be substituted for depth of flow, and the water surface slope can be substituted for the energy gradient, which was done for the Uncompahgre River assessment by Elliott and Capesius (2009) where the energy gradient was calculated using HEC-RAS, a procedure developed by the U.S. Army Corps of Engineers. D_{50} for the Uncompahgre River reach were 25 mm on average, but ranged from 14-48 mm at different cross-sections. The critical shear stress was calculated using Shields equation:

$$\tau_c = \tau_c^*(\gamma_s - \gamma)D_{50} \quad (2)$$

where

τ_c = critical shear stress (N/m^2)

τ_c^* = Shields parameter
γ_s = specific weight of sediment (assumed to be 2.65 times the specific weight of water)
γ = specific weight of water (9807 N/m^3)
D_{50} =median sediment-particle size (m).

A conservative value for the Shields parameter was used to determine the critical shear stress based on data from a previous study on the Gunnison River (Elliott and Hammack, 2000), so that critical shear stress is slightly underestimated. The critical shear stress for the sediment in the Uncompahgre River at Ridgeway ranged from 6.8 to 24 N/m^2 (Elliott and Capesius, 2009). The boundary shear stresses exceeded the critical shear stress at all cross-sections for all flood levels (Fig. 1).

East St. Louis Creek

East St. Louis Creek, located about 60km west of Denver near Fraser, CO, has a cold temperate climate where two-thirds of the annual mean precipitation (740 mm) is in the form of snow and 95% of the stream runoff is derived from snowmelt. Most of its flow occurs between April and October with peak discharge occurring in mid June followed by a rapid decrease. The widths of valley bottom ranges from 15-75 m, whereas the stream channel has an average width of 3.5 m. Unlike the Uncompahgre River, the riparian zone here was stabilized with trees, shrubs, and grasses, but evidence for periodic lateral channel migration was still observed (Adenlof and Wohl, 1994).

Because mountain streams have large particle-size, near-bed velocity should be measured at least two grain diameters above the bed to obtain a more accurate average velocity measurement rather than a large velocity gradient derived from these large grains (Middleton and Southard, 1984). Mean velocity was measured at 0.6 of the flow depth. Near-bed velocity for each cross-section was averaged from near-bed velocities taken at 0.06 m above the bed at three sampling points. Even though discharge and

sediment movement were highly correlated, sediment movement and mean channel velocity were very poorly correlated. Therefore, either mean velocity is not fully representative of the variations in velocity along cross-sections, or cross-sectional variations in velocity do not play such a significant role in sediment transport along a 1-1.5 km segment when compared to larger reach-scale variations (Adenlof and Wohl, 1994).

Sources of bedload sediment usually originate from either the valley bottom/channel boundaries or from neighboring slopes. Slopes tend to provide more material through episodic mass movements like landslides, whereas valley bottoms provide material located in a position that can be eroded with fluctuations in streamflow. Slopes can also contain higher frequency, slow moving processes like creep (Adenlof and Wohl, 1994), but overall, material provided by the valley bottom is provided as a function of streamflow, whereas slope material is independent of streamflow response. Slopes also provide coarse material to the valley bottom where it is stored and later the voids are filled in with finer sediments by floods. For the East St. Louis Creek, coarse sediment is primarily provided by valley bottom sources, with limited course sediments entering from nearby slopes. Creep and slope wash provide finer sediment into the channel, which was inferred because of exposed roots and bent tree trunks along the basin slopes (Adenlof and Wohl, 1994).

The subsurface of the valley floor, was primarily composed of coarse sand to cobble-sized grains with an underlying layer of unconsolidated clast-supported cobbles and boulders. Every site contained a very thin (≤2 cm) loamy soil on top, which may

have been provided by periodic flooding (Adenlof and Wohl, 1994). It is very likely that the primary source of coarse grains in the East St. Louis Creek is from this unconsolidated cobble and boulder layer.

Mountain streambeds often contain irregularly large individual clasts and poorly-sorted bed material. This factor makes predicting critical threshold conditions for entrainment of coarse bed sediments very difficult and can be quite a complex process (Griffiths, 1980). Limited sediment-sources, nonuniform flow conditions, and local in-channel storage are a few more conditions typically found in mountain streams that also make mountain streams very complex systems (Adenlof and Wohl, 1994).

Grain sheer stress using "Law of the Wall" (Dietrich and Whiting, 1989):

$$\tau_b = \frac{\rho(uk)^2}{(\ln({}^{z}/_{z_0})^2} \quad (3)$$

where

τ_b = bed sheer stress (N m^{-2})
ρ = water density (1000kg m^{-3})
u = bed velocity (m s^{-1})
k = Von Karman constant (0.4)
z = height above bed where velocity is measured (m)
z_0 = 0.1 of the bed D_{84} (m).

Total shear stress for a cross section:

$$\tau = \gamma h s \quad (4)$$

where

τ = total shear stress of cross section
γ = specific weight of water (9800 N m^{-3})
h = mean flow depth (m)

s = bed slope.

Critical shear stress for entrainment of channel-bed sediment (Komar, 1987):

$$\tau_i = 0.045(\rho_s - \rho)gD_{50}^{0.6}D_i^{0.4} \quad (5)$$

where

τ_i = critical shear stress (dynes cm^{-2})
ρ_s = grain density (2.65 g cm^{-3})
ρ = fluid density (1.0 g cm^{-3})
g = gravitational acceleration (980 cm s^{-2})
D_{50} = median diameter of mixed bed materials (cm)
$D_i = D_{84}$, the 84 percentile diameter of mixed bed material (cm).

The study of the East St Louis Creek revealed that critical shear stress (eq 5) was about the same as bed shear stress (eq 3) and uniformly lower than the total cross-sectional shear stress (eq 4) (Adenlof and Wohl, 1994). These results suggest that the bed surface is near the threshold between stability and instability, making it fairly easy for grains to become mobilized. Once these clasts are entrained, velocities provide the sufficient energy to keep grains mobile until they are blocked, which for this stream is most commonly some type of woody debris. Therefore, in step-pool/channel-unit scales, channel stability is controlled by grain size, the packing and sorting of grains, and the presence of woody debris (Adenlof and Wohl, 1994).

Study Area

Geology

The geology surrounding Ouray, CO, is very diverse and includes igneous, sedimentary, and metamorphic rocks all within very close proximity to the Uncompahgre River. The headwaters, which start south of downtown Ouray along Highway 550, also known as The Million Dollar Highway, flow on exposed limestone, quartzite, and slate. The surrounding sedimentary rocks vary from shales to sandstones with frequent conglomerate layers and lenses. Igneous rocks in the area come from the San Juan Tuff and several different dikes consist of diabase, porphyritic granodiorite, porphyritic andesite, and porphyritic quartz latite (Luedke, 1962).

From oldest to youngest, the Uncompahgre River most likely contains all the following strata in its riverbed: Uncompahgre Formation, Leadville Limestone, Hermosa Formation, Cutler Formation, Dolores, Morrison, Mancos, Granodiorite Porphyry, San Juan Tuff, and a variety of Quaternary deposits from alluvial fans, talus, landslides, and glacial till. Much of the gravels present in the stream are sub-rounded to very rounded quartzite and porphyritic volcanics. Cobbles tend to be more rounded and consist of quartzite, whereas smaller gravel pieces are sub-rounded volcanics and slate. The riverbed flows through Quaternary Alluvium deposits for all river sites, but in an area about 1 mile upstream of R1, very large red silt-sandstone boulders (>5m) may be large Quaternary talus or bedrock from the Cutler Formation. The Cutler formation is composed of red shales, siltstones, and sandstones interspersed with conglomerate lenses.

Discharge of the Uncompahgre River

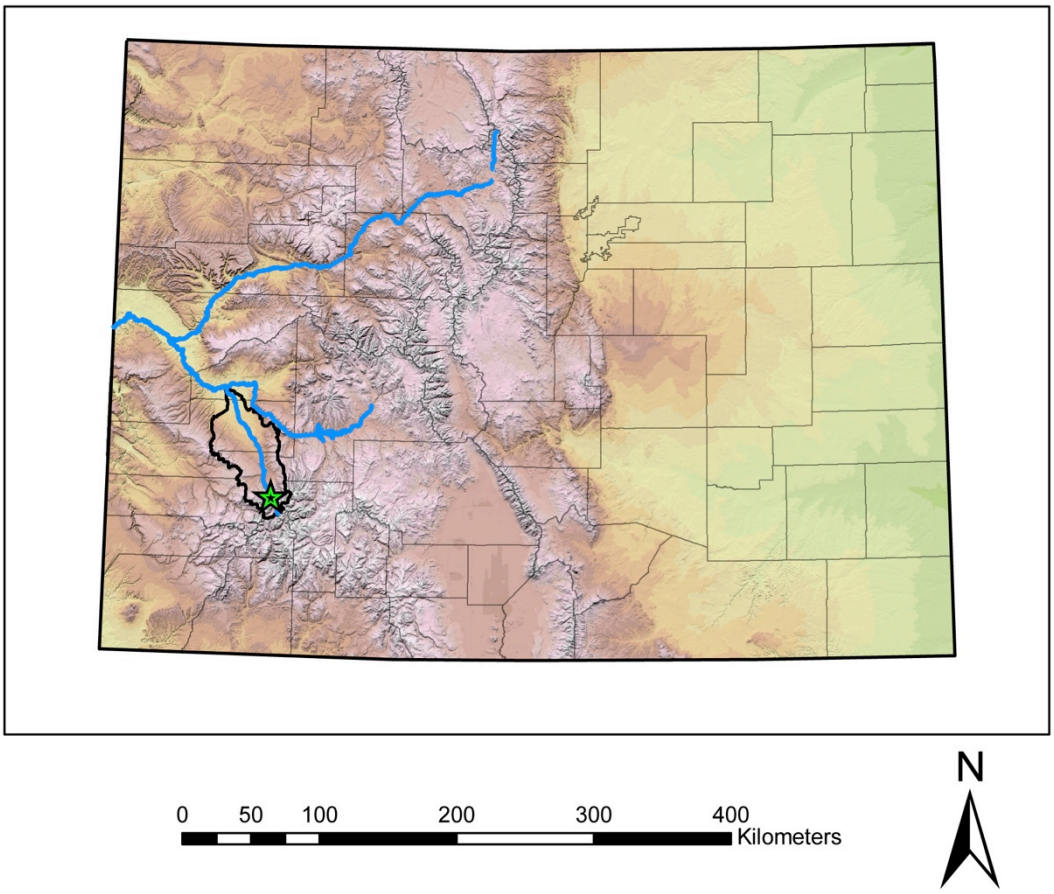

Fig. 2. Map showing the location of the Uncompahgre River in Colorado. The Uncompahgre River flows north into the Gunnison River, which flows into the Colorado River. Ouray is located at the headwaters of the Uncompahgre Drainage Basin.

The headwaters of the Uncompahgre River originate near Ouray, CO, located in the southwest corner of Colorado (Fig. 2.), and flow north into the Gunnison River near Delta, CO, and continue into the Colorado River (Fig. 3.). A drainage divide exists near Red Mountain Pass that is oriented approximately E-W, so that surface water drains either north into the Animas River starting near Silverton, or south into the Uncompahgre River, which then flows through Ouray. The Uncompahgre River in

Ouray flows through a “U”-shaped glacial valley that widens near Ridgeway. The USGS has five gauging stations located on the Uncompahgre River (Table 1) with Ouray being the closest to the headwaters and containing the smallest drainage basin of 199 km^2 .

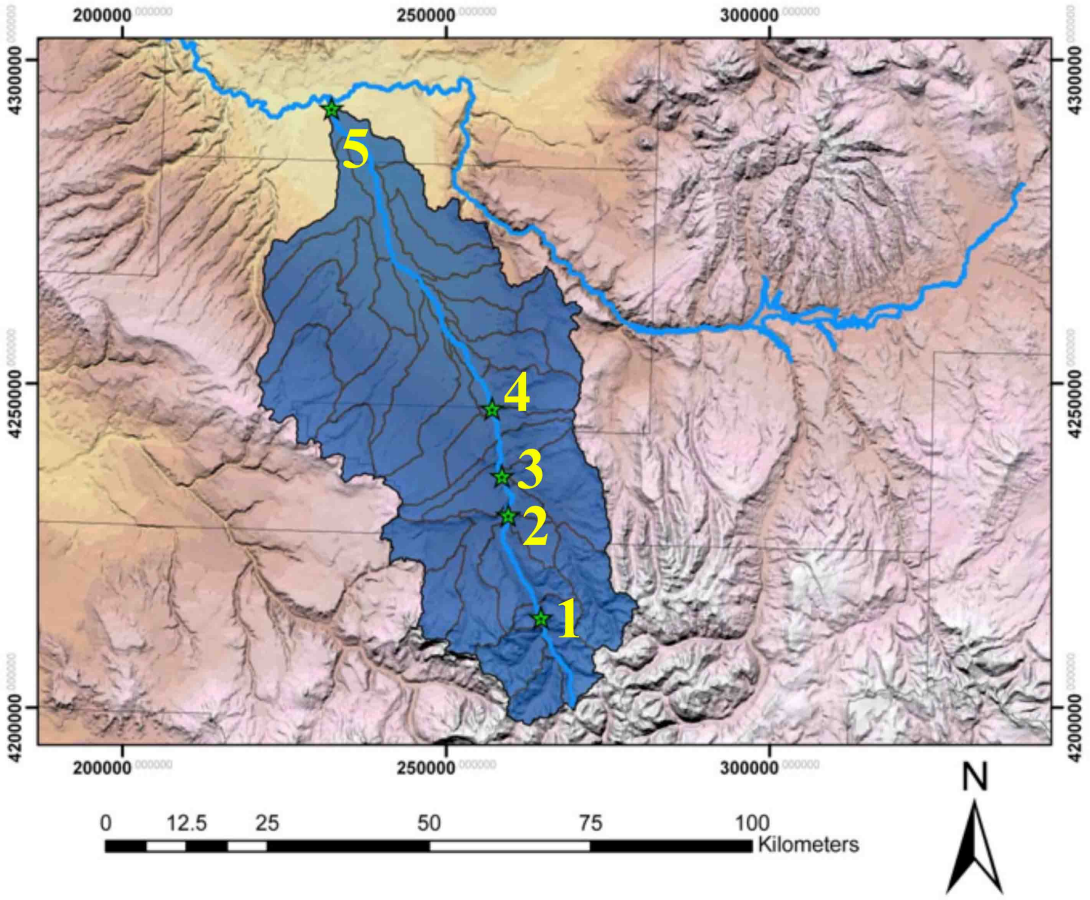

Fig. 3. Map of all five USGS gauging stations located on the Uncompahgre River.

Table 1
Details for each USGS gauging stations on the Uncompahgre River

# on Map	Location	Gauge #	Drainage Area (sq km)	Continuous Data on Record from present to
1	Ouray, CO	9146020	199	2001
2	Ridgeway, CO	9146200	386	1958
3	Ridgeway, CO below Dam	9147025	686	1988
4	Colona, CO	9147500	1160	1912
5	Delta, CO	9149500	2888	1938

The discharge of the Uncompahgre River is characteristic of a flashy alpine stream with low flows that occur throughout the winter months and large discharges during mid-summer from snowmelt and isolated thunderstorms (Figs. 4 and 5.).

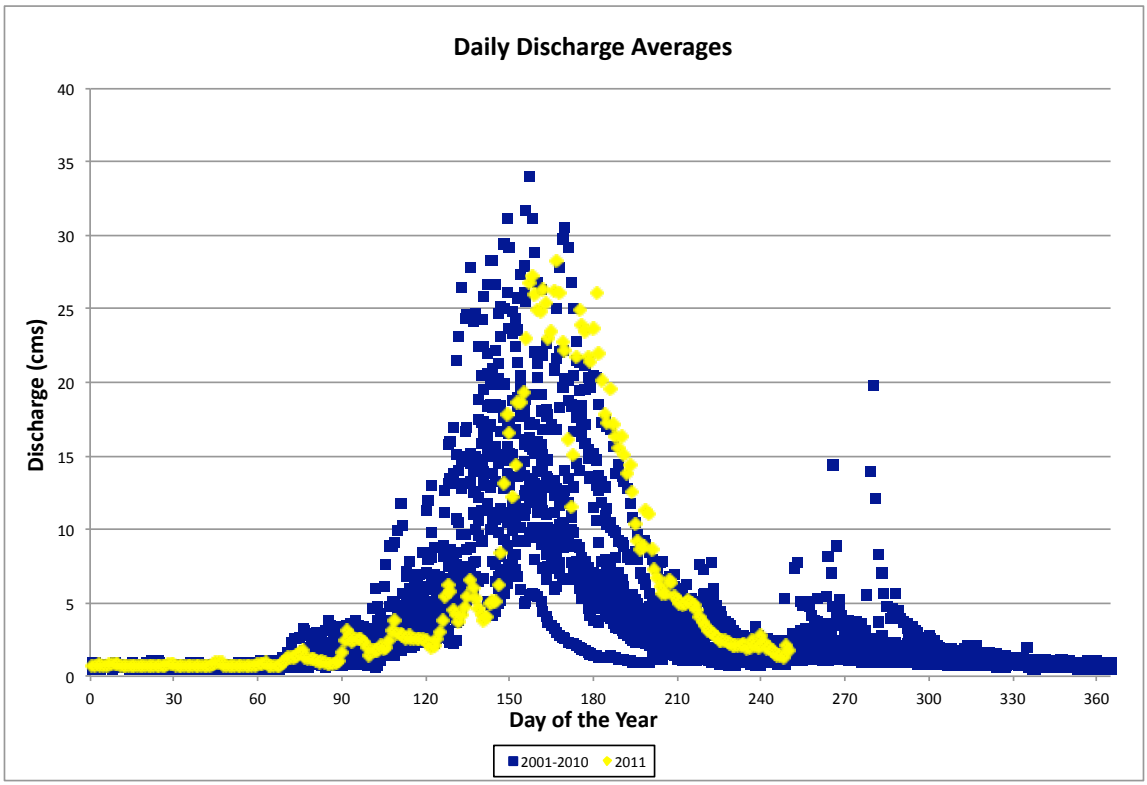

Fig. 4. Mean daily discharge values for all available data for the Uncompahgre River near Ouray, CO. Source: USGS Gauging Station # 09146020

Downstream from Ouray, flow between the peak summer months and the lower winter months is generally more intense and lasts for a longer portion of the year, whereas in Ouray, a low flow is maintained for a longer duration with a shorter, more rapid, but less intense peak that occurs around June. The average of the annual maximum of mean daily discharges from 2001-2011 is 24.8 cms. The annual maximum of mean daily discharges in 2011 was around 28.9 cms and instantaneous discharges reached around 32 cms (Table 2).

Table 2
Annual maximums of mean daily discharges for all gauge data in Ouray, CO

Year	Max Mean Daily Discharge (cms)	Max Mean Daily Discharge (cfs)
2001	18.4	649
2002	7.7	273
2003	31.1	1,100
2004	22.1	781
2005	28.3	1,000
2006	22.1	782
2007	22.2	783
2008	30.6	1,080
2009	27.8	983
2010	34.0	1,200
2011	28.9	1,020
Average	24.8	877

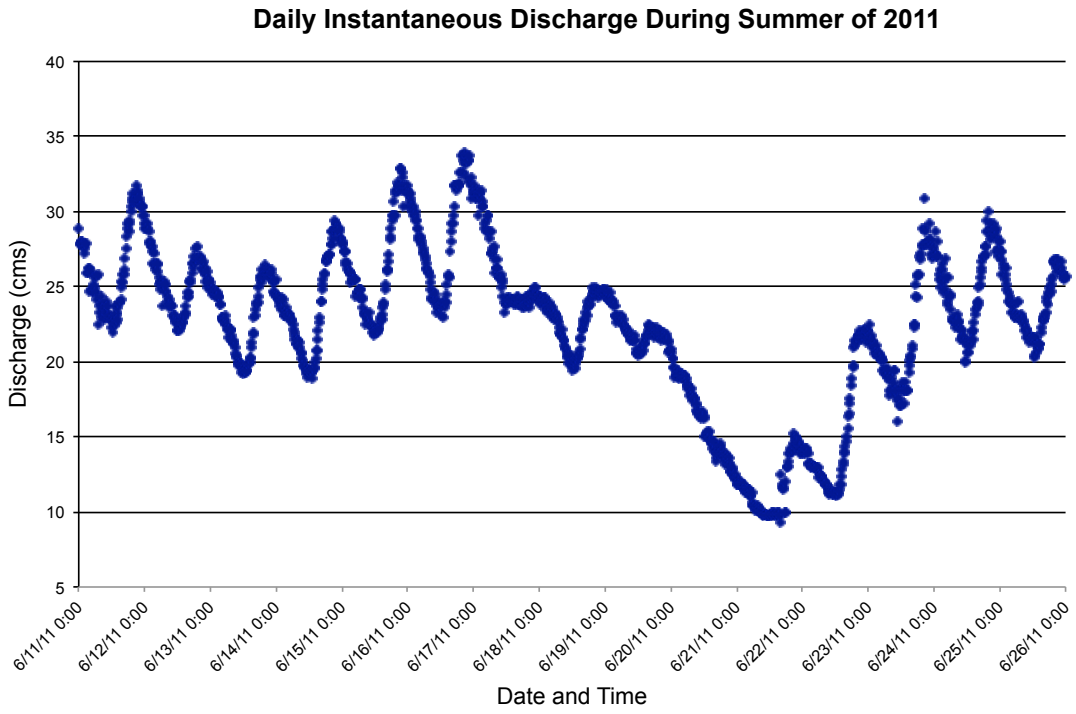

Fig. 5. Discharge values collected at 15-minute intervals for June 11- 26, 2011.

Daily discharges during the summer vary considerably because snowpack melt during daylight hours produce discharge peaks during mid to late afternoon. The lowest discharge throughout a one-day period will vary, but typically occurs before noon. These large changes in discharge and temperature are typical of an alpine environment and may contribute to stream bank erosion at night by freeze-thaw and erosion during afternoons and evenings of fall and early spring from increased stream power. Freeze-thaw processes are directly linked to air temperature, which is increasing in alpine areas, particularly in the winter because of snow-albedo feedback (Clow, 2010). The order and severity of freeze-thaw and streamflow events can have a dramatic impact on the net erosion that occurs on a streambank (Fig 6). If the temperature is cold enough to produce free-thaw, yet maintain high temperatures during the day to produce large quantities of snowmelt and large discharge, the overall net erosion has the potential to increase dramatically.

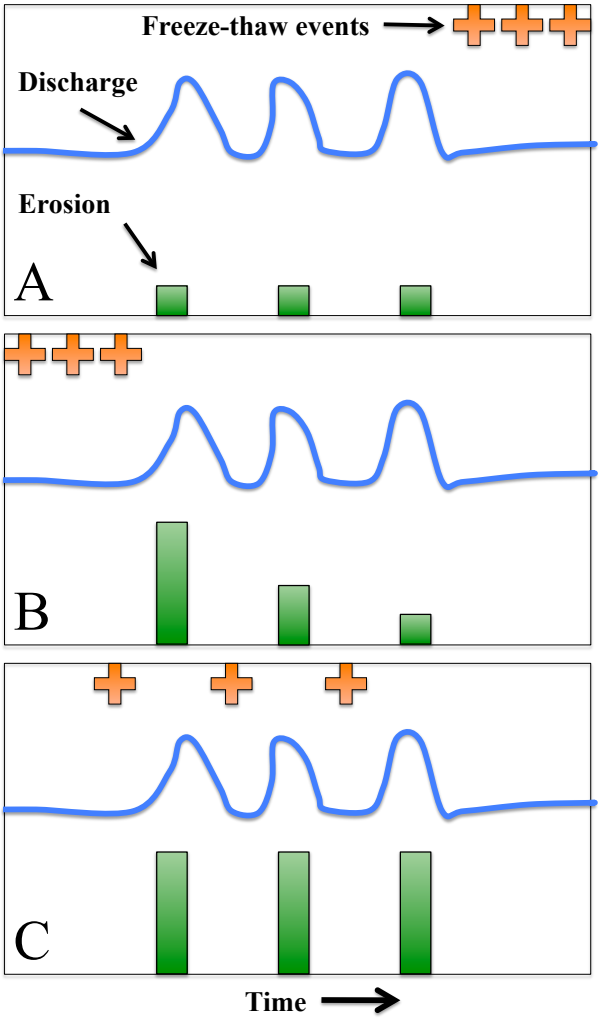

Fig. 6. A hypothetical example illustrating how the timing of freeze-thaw and peak streamflow can influence the timing and magnitude of erosion. A) All freeze-thaw events occur after three successive peak flows. B) All freeze-thaw events occur before the first peak flow. C) All freeze-thaw events occur just before the three peak flows. Figure modified from (Lawler, 2005).

River Modification

1996 During Modification

Winter 1999

Summer 2010

Fig.7. Repeat photographs looking south from the northern terminus of the modification project. The width of the stream channel has been decreased significantly and buildings have been constructed where the river previously existed. The star denotes the same location of a large house.

In the small tourist town of Ouray in southwestern Colorado, the Uncompahgre River was modified starting in 1996 so that a recreational area and more development could occur (Figs. 7-9). Much of the river channel has been modified from a wide braided stream into a confined meandering river channel using boulders. Areas immediately adjacent to the stream have been used for a recreational river walk that contains trails, picnic tables, prairie grasses, trees, and exercise equipment. Modification increased the sinuosity of the stream and decreased the overall slope, but no previous data were available before restoration to quantify the change.

Fig. 8. Looking northwest onto the Uncompahgre River on the southern side of Ouray, CO. Many permanent structures have been erected directly adjacent to the modified channel.

1996 During Modification

Summer 2010

Fig. 9. Repeat photographs located at about the midway point of the channel modification. Permanent structures are located adjacent the new meandering channel.

Each fall, the City of Ouray excavates the gravel point bars that have been deposited during the previous year and sells this material. The exact quantity that is deposited naturally and removed every year is unknown, but it is has been estimated to

be about 2,300-3,800 m^3 throughout the entirety of the restoration area (Rondinelli, 2011). On the other hand, if armoring (i.e. boulders) is eroded, the City of Ouray performs maintenance to maintain a specific channel configuration, which can cost tens of thousands of dollars (Rondinelli, 2011).

The modification project ends abruptly at the northernmost side of town where the city property ends. A pedestrian bridge marks the end of the restoration area, which is also where a USGS gauging station is located. Directly adjacent, the channel remains straight for a couple hundred meters and continues to meander downstream. The channel width in the modified stream is similar to the channel width in the natural channel downstream, although the modified channel width varies widely. The modified channel in most areas contains gravel bars on the opposite sides of meanders, but in some places, gravel bars have also formed in the middle of the stream, making small braids even though the overall channel is meandering (Fig. 10).

Fig. 10. Mid-channel bars have developed inside the modified “meandering” channel.

Methods of Study

Surveys of Cross-Sections

Locations of reach sites were based on optimal camera geometry because cross-sectional surveys were designed to be compared with photogrammetric models created from terrestrial photographs. In addition, optimal areas needed to show signs of significant erosion and deposition. R2 (Site 2) had favorable geometry for the use of oblique-aerial photography because its exposure to the eastern and western cliffs whereas all other sites were primarily photographed at a close range (25 m).

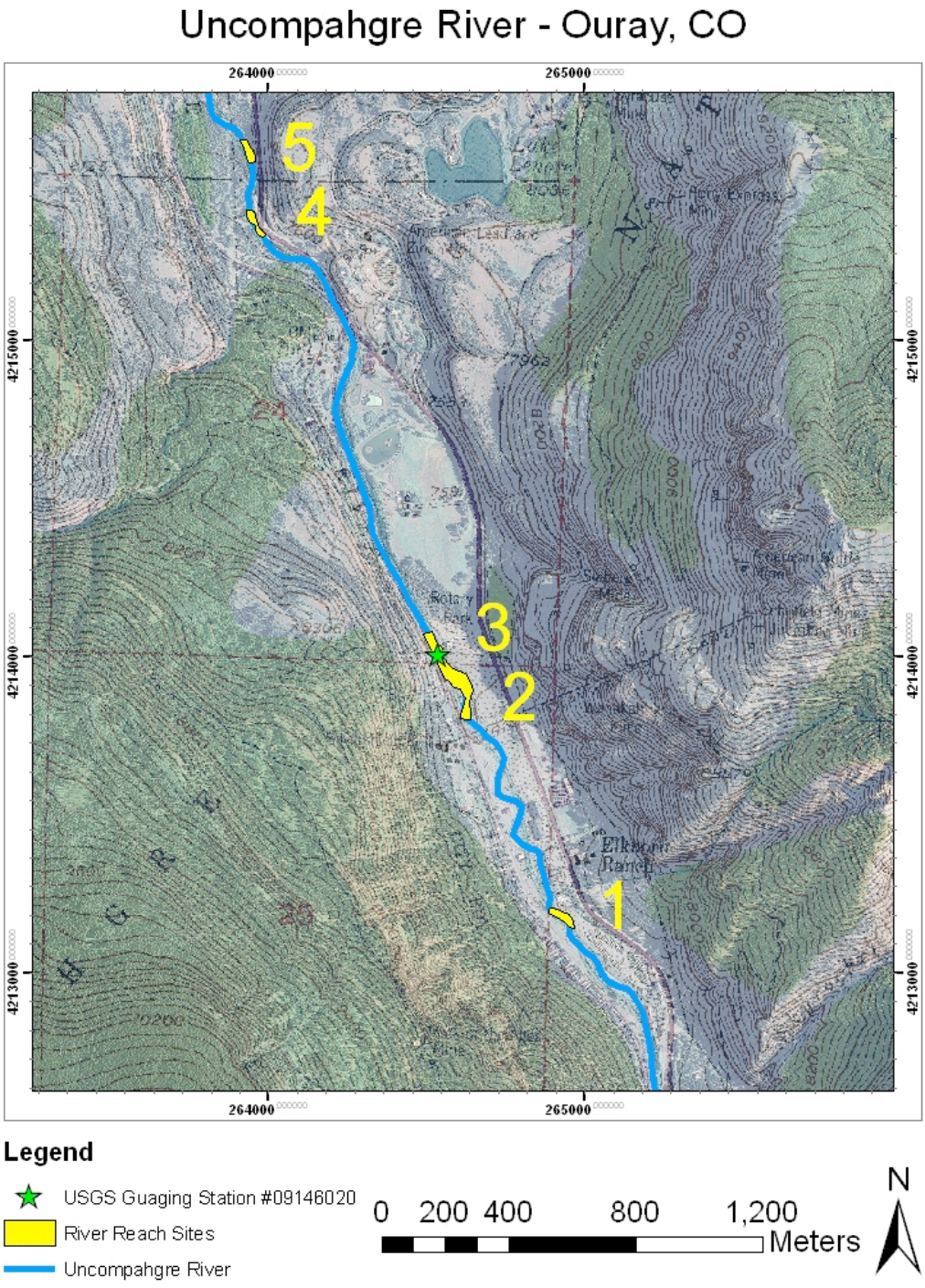

Fig. 11. Map of the Uncompahgre River Valley on the north side of Ouray, CO.

Traditional surveying techniques using a total station and reflector were used to determine cross-sections of the river at five different locations (Fig. 11). Long nails with painted washers were used as temporary benchmarks to mark exact cross-section locations on both sides of the stream. Cross-sectional data were collected using the (x, y, z) coordinates for each point. In the field, a constant interval of 0.5 m was estimated visually, and the exact horizontal distance of each point of cross-sections was calculated later using:

$$d_{interval} = \sqrt{(x_1 - x_2)^2 + (y_1 - y_2)^2} \quad (6)$$

Every stake was relocated and used for repeat measurements; however, some stakes moved slightly because of erosion. Because the horizontal distance between stakes changed, a ratio was used to shrink or expand horizontal measurements. The exact distance between the stakes on the east and west sides were calculated using:

$$d_{total\ XS} = \sqrt{(x_1 - x_2)^2 + (y_1 - y_2)^2 + (z_1 - z_2)^2} \quad (7)$$

where the locations of stake 1 and stake 2 were (x_1, y_1, z_1) and (x_2, y_2, z_2), respectively. Each horizontal point location at each cross-section was shrunk or expanded by multiplying the horizontal value by the ratio below:

$$\frac{d_{total\ XS\ May}}{d_{total\ XS\ Sept}} = Adjustment\ Ratio \quad (8)$$

To estimate the error associated with the total station and human error by not surveying a perfectly straight line, cross-section R1XS1 was measured consecutively to determine the difference in cross-sectional area (Fig. 12).

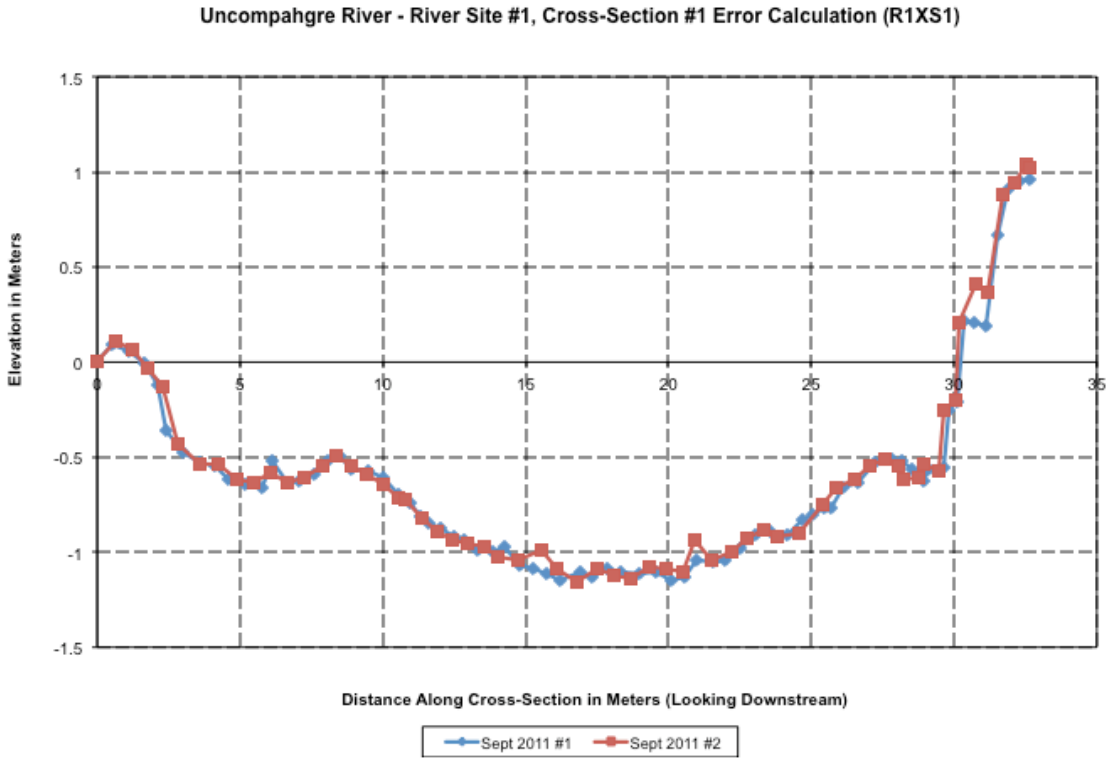

Fig. 12. Error determination of cross-sectional area via two consecutive surveys of the same cross-section.

Theoretically, if the exact same points were measured, the error and cross-sectional area would be zero. The cross-sectional area or difference between the same cross-section was -0.551m^2. This value was incorporated into the error of all other cross-sectional areas as +/- 0.551m^2.

Fig. 13. Map of cross-sections at R1.

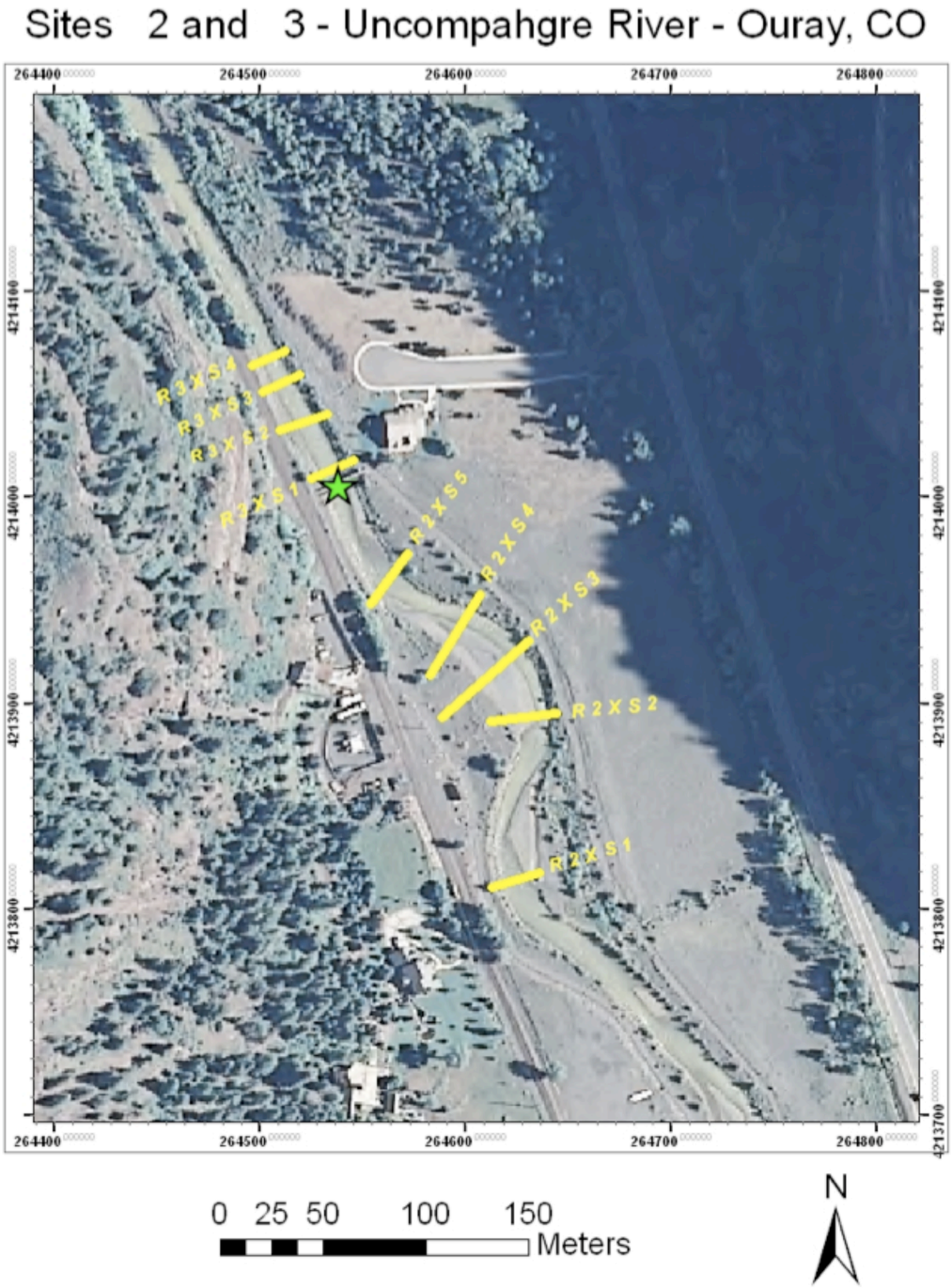

Fig. 14. Map of cross-sections at R2 and R3. The USGS gauging station is attached to a pedestrian bridge which, coincides with the end of the restoration project.

Fig. 15. Map of cross-sections at R4. Cross-sections are located adjacent to the Uncompahgre National Forest sign pullover on Highway 550.

A total of 13 different cross-sections were surveyed (Figs. 13-15). Most survey data were collected in early May 2011 and early September 2011, and some preliminary cross-sectional data were collected during September and October of 2010. Longitudinal profiles were surveyed by collecting points at the edge of the water for each site individually to get a better estimate of local slopes, which were then used for calculating the boundary shear stress at each cross-section.

Shear Stress

A sample of gravel was collected from R2 to determine the grain density of material in the river. Average gravel density was determined using a graduated cylinder and balance to be 2,585 kg m^{-3}. This density was used for all critical shear stress calculations. For each cross-section, the boundary shear stress and critical shear stress were calculated to produce a ratio τ_o / τ_i where the theoretical threshold of entrainment could be determined. Boundary shear stress was calculated using equation 1 (Chow, 1959), where local slope of the water surface was used rather than the actual slope within the stream channel for the energy gradient. Critical shear stress for entrainment of channel-bed sediment was calculated using equation 5 (Komar, 1987).

Analysis of Pebble Counts

Random pebble counts (Wolman, 1954) were performed on sites R1, R2, and R5 in early May 2011. Discharge levels made it difficult to enter the stream at all cross-sections safely, especially at R5. These data, therefore, might be more representative of

bar and shallow stream material rather than the overall stream channel. During September of 2011, pebble counts were collected for all sites (R1-R5). Where large boulders existed underwater, measurements were estimated by using the survey rod to determine the extent of the boulder. The outer boundary of the stream channel was determined by locating a steep increase in slope, as well as the presence of vegetation. Boulders used as armoring were not included in the pebble counts because they were imported for the modification project and were assumed not to have moved during the time intervals used in this study.

Geomorphic Analysis

Google Earth® was used to obtain rough values for the sinuosity index and slope of the modified channel and the unmodified channel directly downstream. Because Ouray is located in a mountain valley with very large relief (1,950 m in the surrounding area), image acquisition using a plane is difficult. Because of this, aerial photographs are obtained above the valley peaks (3,650 m) looking down over the valley (2,200 m) and surrounding mountains. This results in low ground resolution, which makes it difficult to provide sufficient data for detailed geomorphic applications. For sinuosity indexes of the river, however, the resolution is adequate over the large area of interest.

Longitudinal surveys were conducted using a total station at R1-R4 using the edge of the water as an indicator of water surface. The water surface was assumed to be a reliable equivalent to bed slope.

Results

Surveys of Cross-Sections

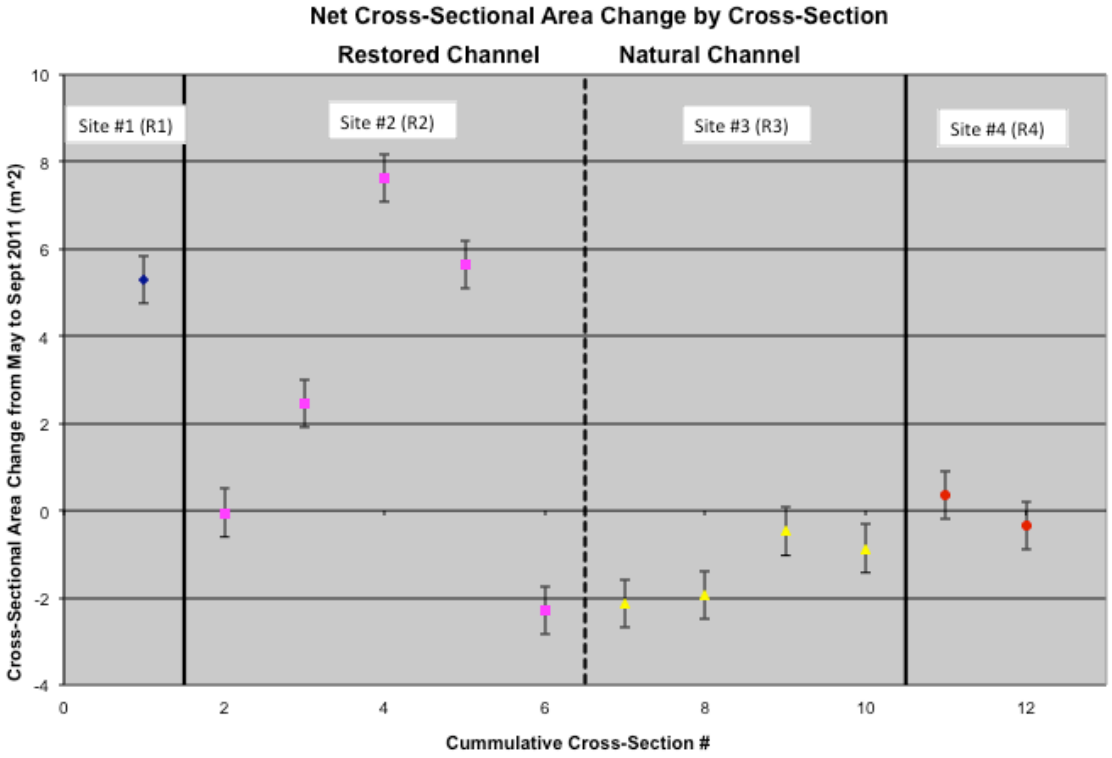

Fig. 16. The net area change of each cross-section measured from May 2011 to Sept 2011.

The cross-sectional area from May 2011 to Sept 2011 changed for seven of the twelve cross-sections that were collected (Fig. 16). With the exception of R2, cross-sections from the same sites displayed all deposition or all erosion. Cross-sections for R2 started with little to no change at the first cross-section and increased dramatically at the third cross-section, which showed the largest deposition of 8 m^2. This cross-section was located in the middle of a meander whereas the next two were on the downstream side of the same meander. The largest change in cross-sectional area of adjacent cross-sections

occurred between the fourth to the fifth cross-section where 4 m^2 of material was deposited at the fourth cross-section, whereas the fifth cross-section eroded $2m^2$. The fifth cross-section at R2 is the only cross-section in the restored channel that is eroding, and it is located 50 m from the end of the restored channel and 30m downstream from the previous cross-section.

Cross-sections outside of the modified channel either showed no net change or small quantities of erosion. Highest erosion occurred directly adjacent to the modified river channel at R3 whereas R4, located about 1.5 km downstream, showed no net erosion.

Shear Stress

The τ_o / τ_i ratio at each cross-section for May 2011 and Sept 2011 was used to estimate the stability of each cross-section (Fig. 17). If the τ_o / τ_i ratio is greater than 1, the cross-section is considered unstable and sediment has an easier potential to be eroded because the critical shear stress has been overcome by the boundary shear stress. If the τ_o / τ_i ratio is less than one, that cross-sectional area is considered stable, and no sediment becomes entrained.

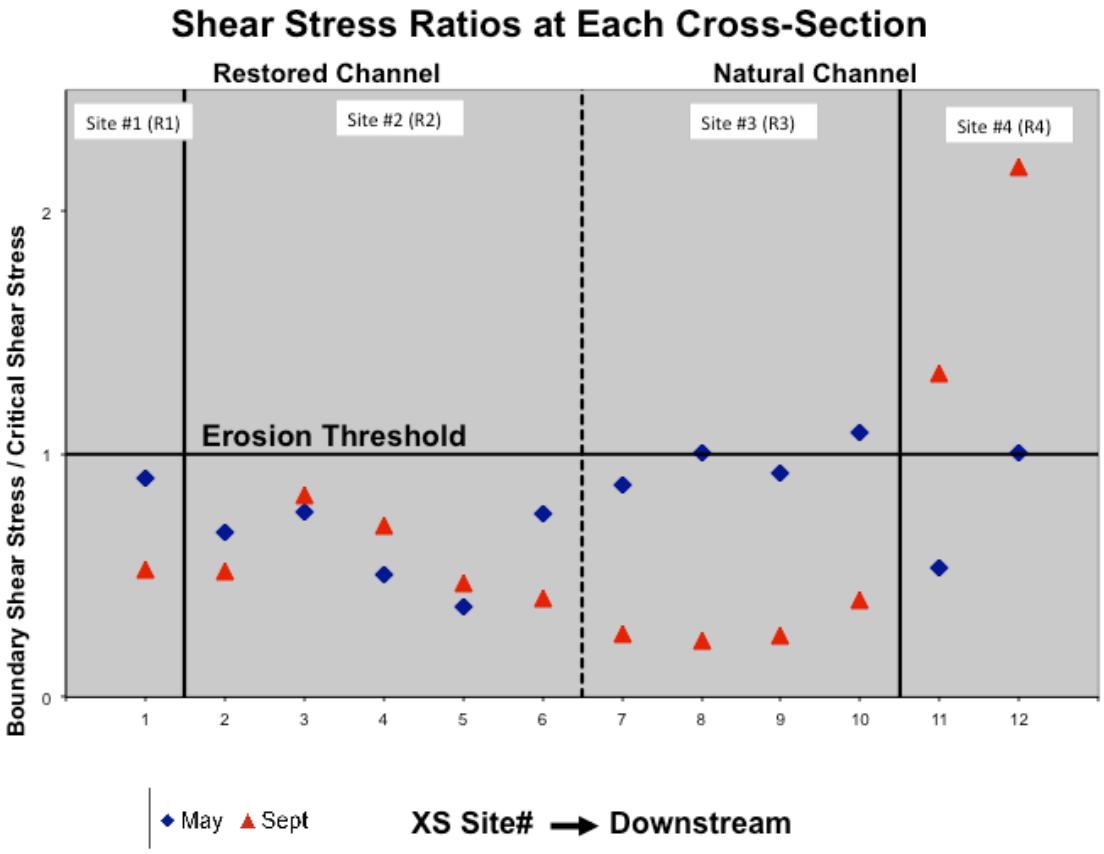

Fig. 17. Shear Stress Ratios of each Cross-Section for May and September 2011.

Shear stress ratios at all cross-sections decreased from May to September, indicating a change to more stable geometries, with the exception of cross-sections: R2XS2, R2XS3, R2XS4, R4XS2, and R4XS3. The change in τ_o / τ_i ratios from May to September reversed between R2XS4 and R2XS5, indicating that the geomorphic threshold is upstream of the actual transition from the modified channel to the natural channel. These two cross-sections also showed very different cross-sectional area changes (Fig 16). The sharp contrast in observations of these two cross-sections is

thought to be because R2XS5 does not include any part of the gravel bar that is part of R2XS2, R2XS3, and R2XS4. Therefore, even though large quantities of deposition still occurred at the most downstream portion of bars within the restored channel, scouring occurred immediately where the bar ends (Figs. 18 and 19).

Although shear stress ratios at R3 were below the theoretical entrainment threshold, erosion still occurred for all cross-sections at this location. The same characteristics were observed for cross-section R2XS5, which had a lower shear stress ratio than any cross-section at R3 in May. Erosion occurred and shear stress ratios also decreased for all cross-sections in R3. Thus, erosion may be linked with reducing shear stress ratios, which is generally associated with a stream that is approaching more stable conditions. Cross-sections at R4 may have shown small amounts of erosion, but error is too large to confirm. Both cross-sections at R4 underwent the largest increases in shear stress ratios, an indicator of destabilization.

Overall, the derivation of shear stress ratios are based on fundamental assumptions about the character of flow and grain-sorting that are not typically found in alpine streams with poorly-sorted grains and high heterogeneity flow regimes. In the restored portion of the stream, no clear pattern emerged between change in shear stress ratios and cross-sectional areas. The lack of a clear patter can be shown explained by comparing cross-sections R1XS1 and R2XS5, which had similar τ_o / τ_i ratios in May and September and changes in shear stress ratios; however, R1XS1 had ~3x the quantity of material deposited than the quantity of material eroded at R2XS5. For cross-sections in the natural channel, shear stress ratios were all close to 1, and all cross-sections either

experienced erosion or no definite net cross-sectional areas change occurred. It is possible that the theoretical erosion threshold, defined by the τ_o / τ_i ratio, is slightly lower than 1 for the natural channel. Also, the decrease in the τ_o / τ_i ratio, rather than the value itself could be used as an indicator of erosion in the natural channel of the Uncompahgre River whereas deposition and erosion inside the restored channel is more directly related to reach location rather than shear-stress ratio changes.

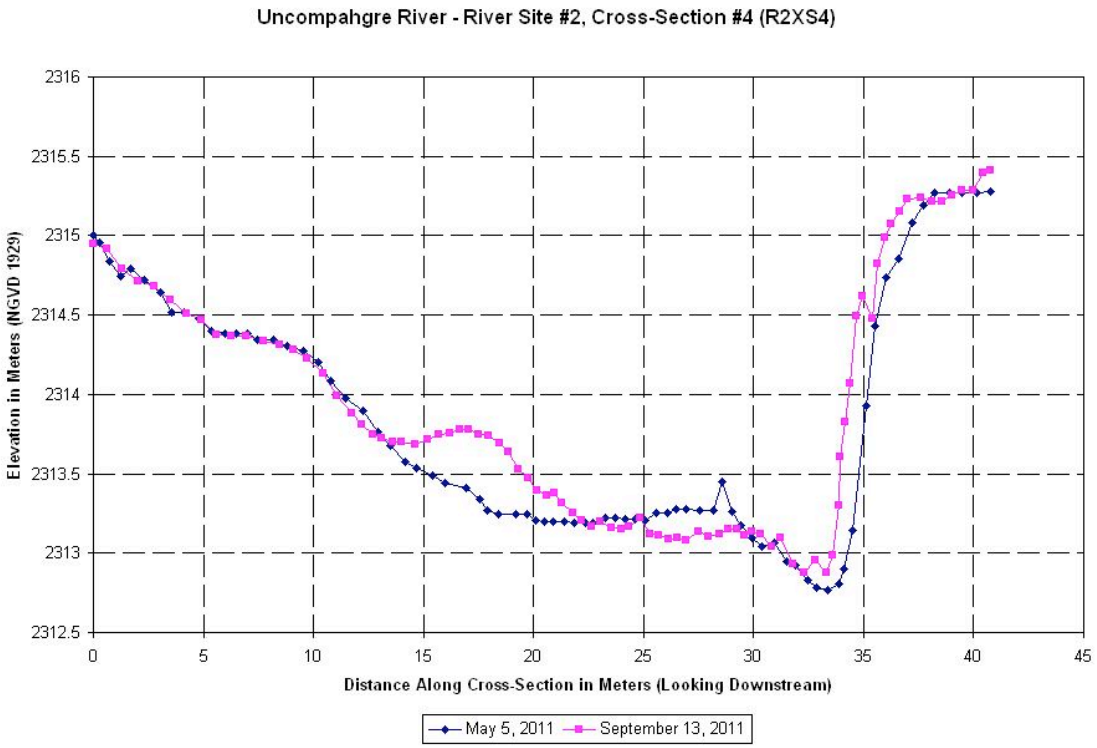

Fig. 18. Cross-section of R2XS4.

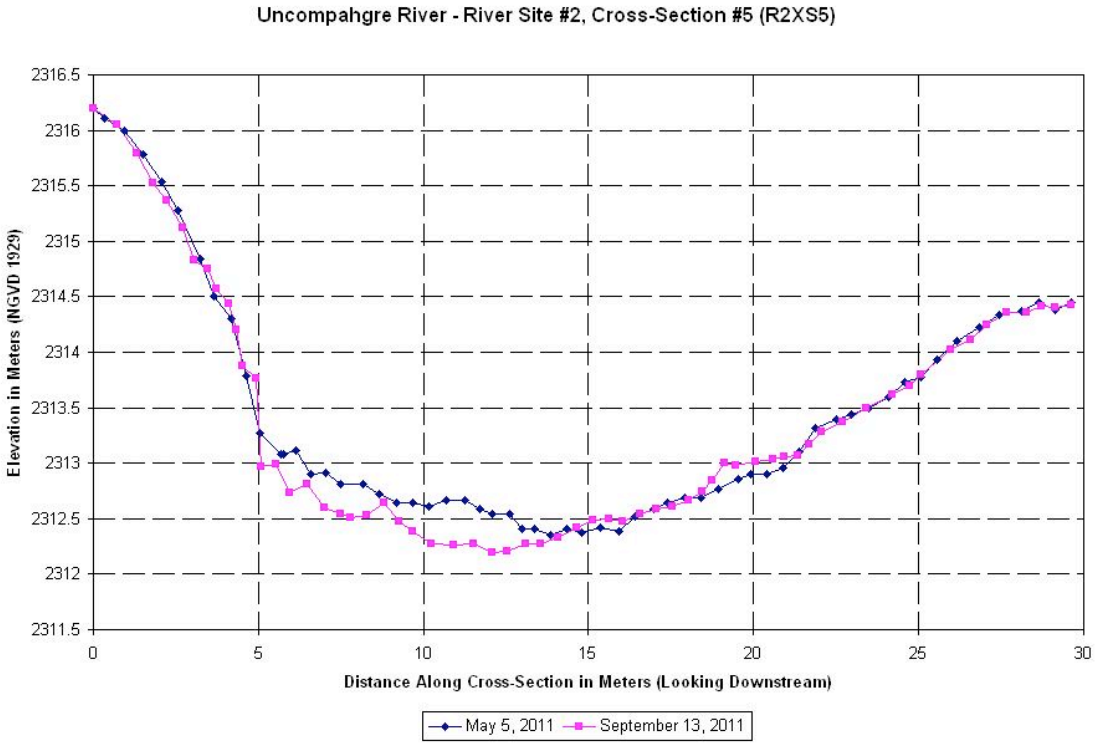

Fig. 19. Cross-section of R2XS5.

Analysis of Pebble Counts

Pebble counts were performed on May 2nd and 3rd of 2011 at two sites within the restored portion of the Uncompahgre River (R1 and R2) whereas R5 was selected to be representative of the natural state of the Uncompahgre River. Fig. 20. shows that the natural state of the stream has a significantly different grain-size distribution than the reaches in the modified channel. Clasts at the natural site are more poorly sorted, containing more very fines and large boulders whereas the clasts in the modified channel are more evenly dispersed as gravels. The clasts at R2, which is located at the most downstream portion of the modified channel, has more fines and large boulders than R1,

which is located at the ~midpoint of the modified channel. As the river flows downstream within the modified channel, clast sizes gradually become larger, but have a larger quantity of clasts 10mm or less. In the natural channel, a dramatic increase in boulders occurs along with a small increase of fines of 10mm or less.

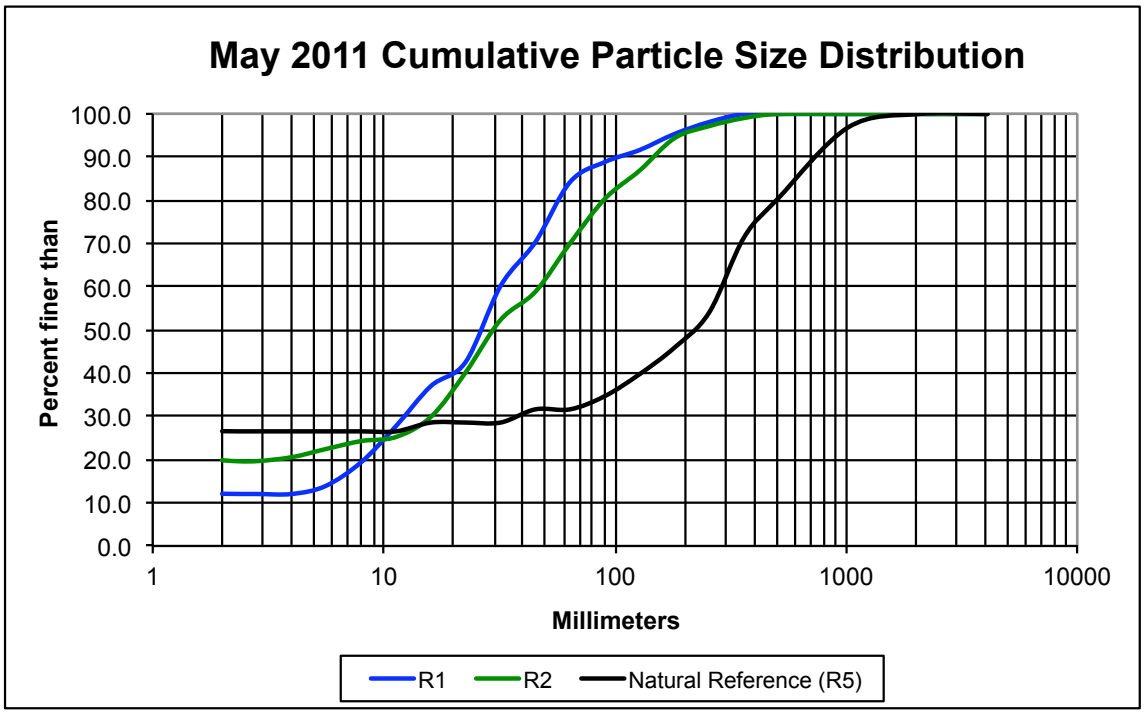

Fig. 20. Pebble counts from R1, R2, and R5 taken in early May 2011 shown as curves of cumulative size distributions.

Pebble counts were repeated for all river sites from September 11-14, 2011. Unlike the pebble counts performed in May 2011, fines become less abundant downstream with a large drop between R1 and R2 (Fig. 20.). Directly downstream from the modified channel is R3, which had a large concentration of larger cobbles and less gravel. R4, about a mile further downstream, contains a greater quantity of gravels, less

cobbles, and more boulders than R3. R5 has less fines and small cobbles than all other sites and also has more boulders over 0.5m than any other sites. R4 has similar amounts of large boulders, but they are slightly less abundant.

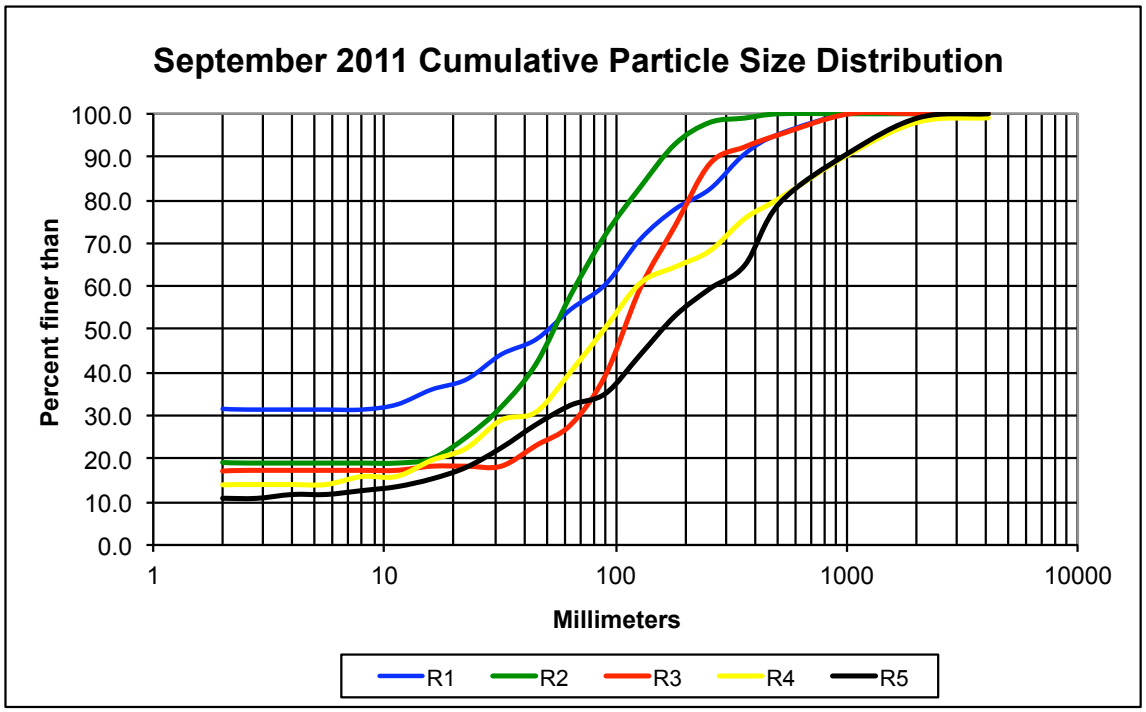

Fig. 21. Pebble counts from R1- R5 taken in mid September 2011 shown as curves of cumulative size distributions.

Comparing individual pebble counts at sites R1, R2, and R5 show that the distributions of clast sizes are very different at each site. From May to September, R1 becomes much more fine-grained and poorly sorted resembling a curve similar to the natural channel, but with more pebbles and cobbles and less boulders (Fig. 21).

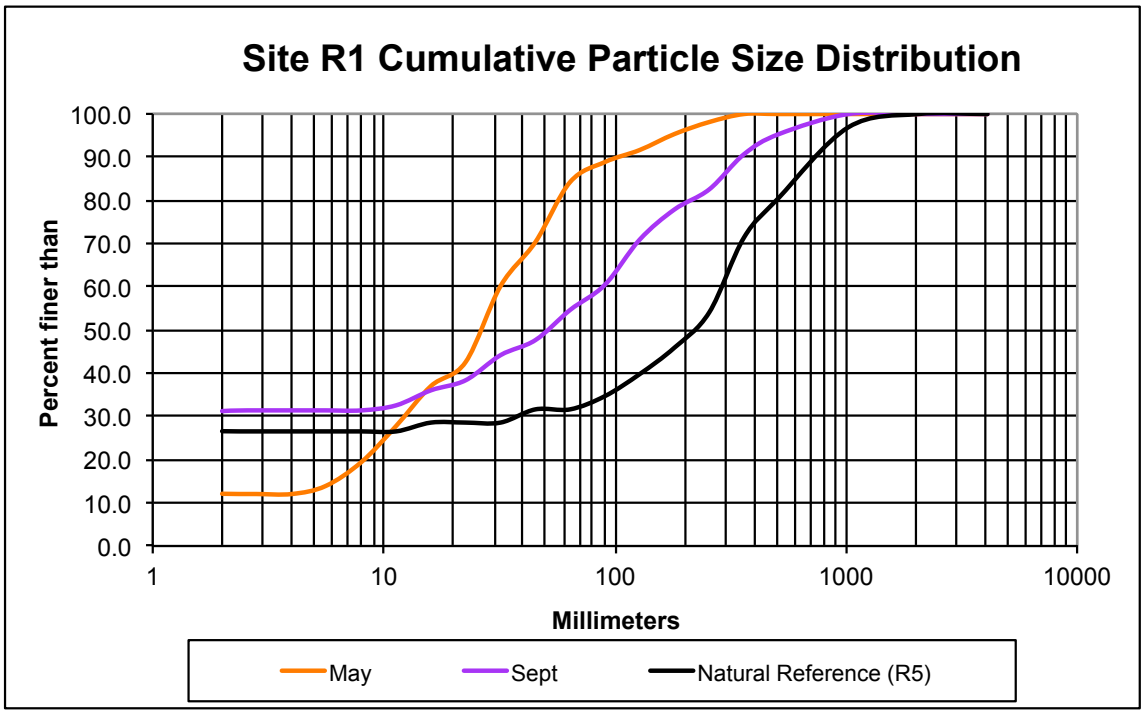

Fig. 22. Pebble counts at R1 taken in early May and mid September of 2011 shown as curves of cumulative size distributions compared against the natural channel.

R1, a site that underwent deposition during this time interval, became much more abundant in fine-grained sediment (~15mm or less) and gravel-sized clasts (Fig. 22).

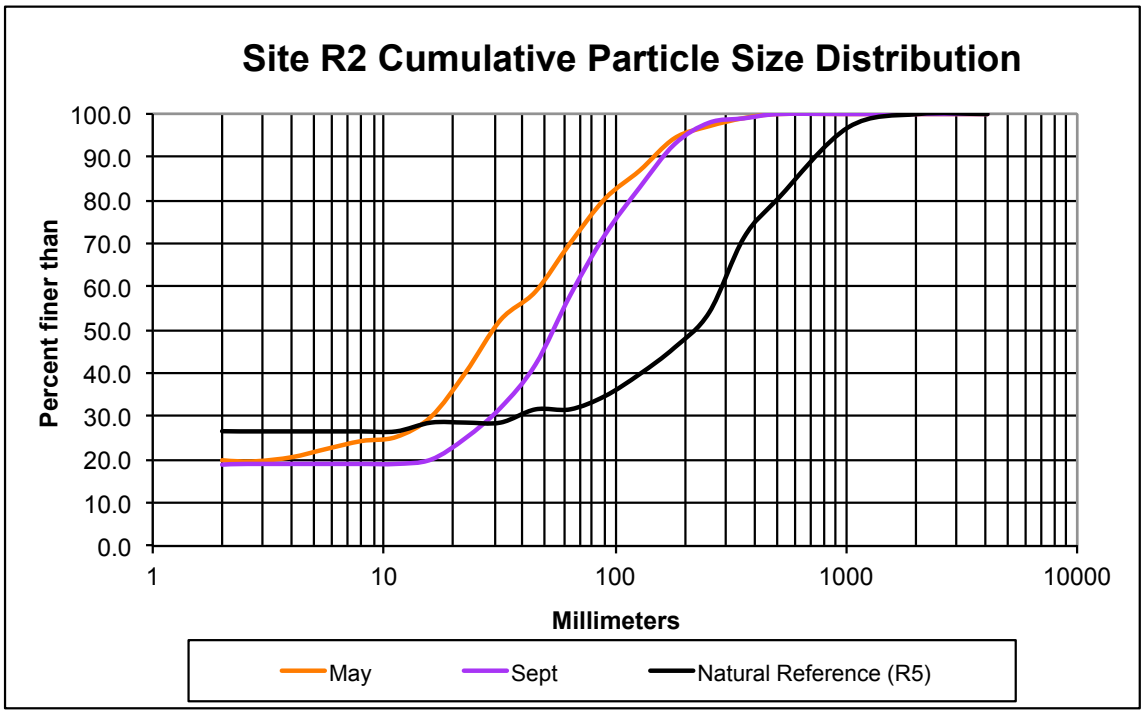

Fig. 23. Pebble counts at R2 taken in early May and mid September of 2011 shown as curves of cumulative size distributions compared against the natural channel.

Slightly larger gravels and cobbles at R2 become more abundant, but fines were about the same and small gravels and coarse sands became less abundant (Fig. 23).

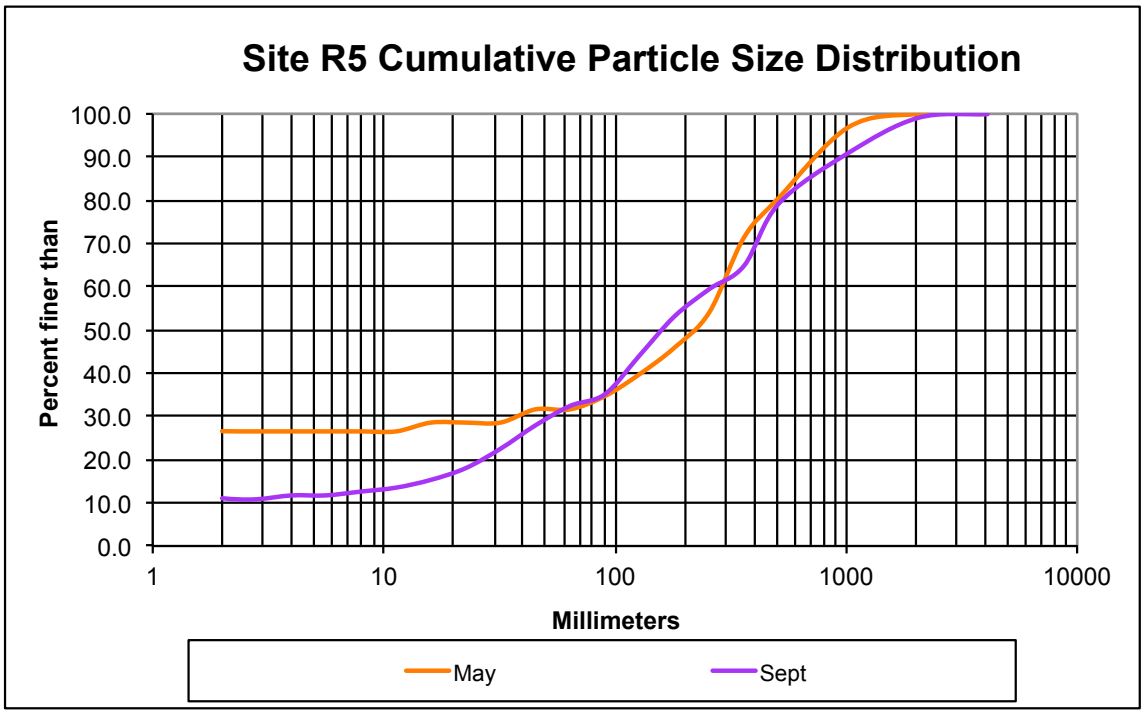

Fig. 24. Pebble counts at R5 taken in early May and mid September of 2011 shown as curves of cumulative size distributions.

Fines at R5 become significantly less abundant whereas large cobbles and very large boulders become slightly more abundant (Fig. 24). Clasts with diameters from ~1-50mm were most likely eroded at R5 by large discharges during the mid-summer peak flows, whereas fines (1-15mm) were deposited in the modified channel.

Geomorphic Analysis

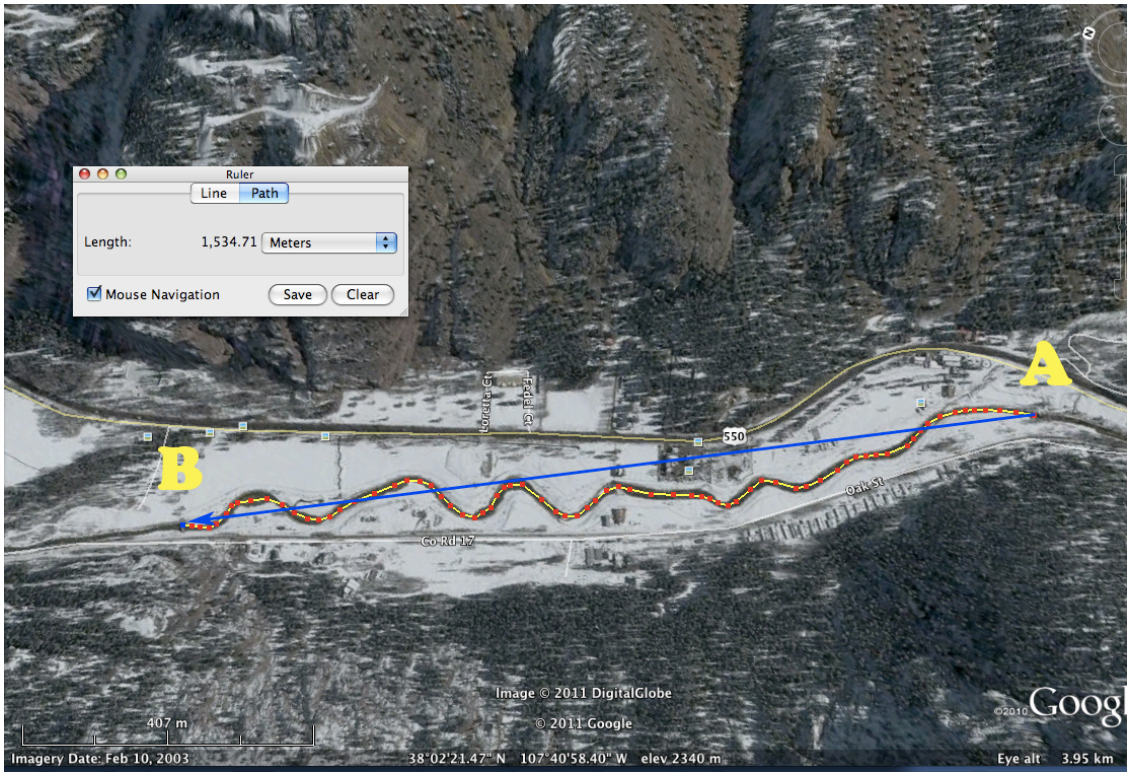

Fig. 25. Sinuosity and slope measurements for the modified portion of the Uncompahgre River made in Google Earth®.

Table 3
Sinuosity and slope values for the modified portion of the Uncompahgre River.

Image from 2/10/2003				
	Point A	Point B		
Elevation	2,336m	2,317m	19m	<---Elev Change
Distance Line A-B	1,374m			
Distance Stream Curve A-B	1,534m			
Sinuosity Index	1.1169			
Slope	0.0138			
Slope %	1.3827			

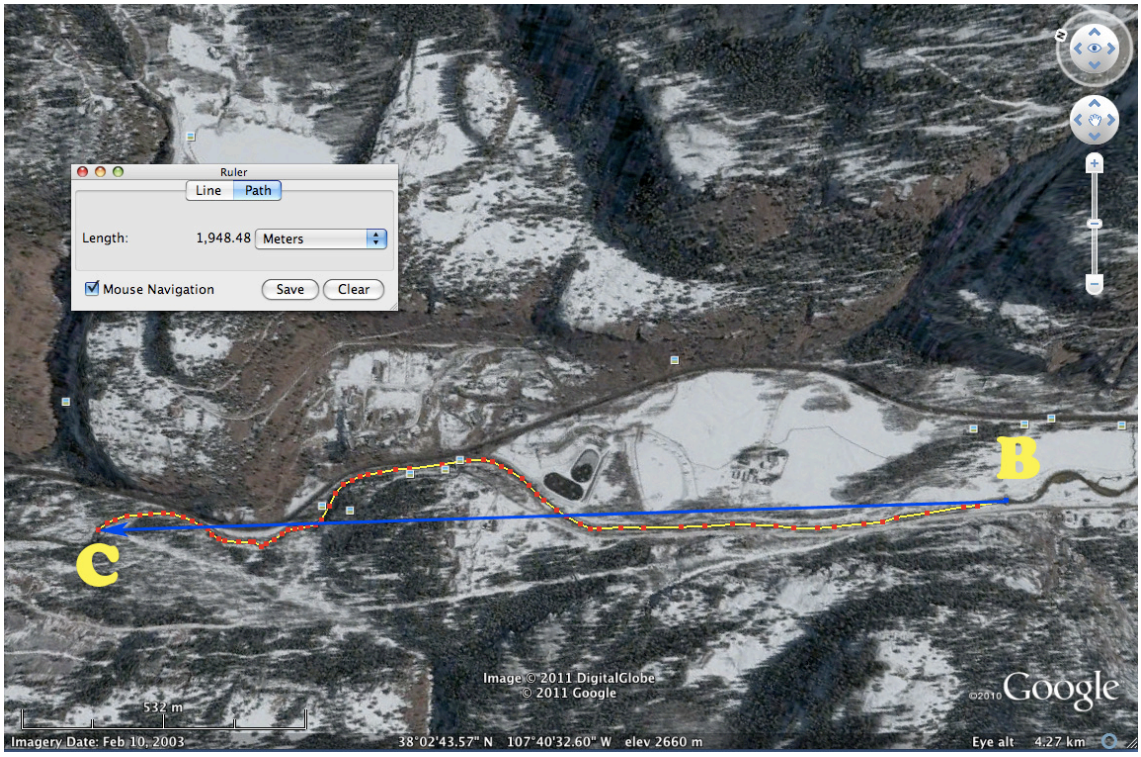

Fig. 26. Sinuosity and slope measurements made in Google Earth® for the natural portion of the Uncompahgre River directly downstream from the modified portion.

Table 4
Sinuosity and slope measurements values for the natural portion of the Uncompahgre River directly downstream from the modified portion

Image from 2/10/2003				
	Point B	Point C		
Elevation	2,316m	2,273m	43m	<---Elev Change
Dist Line B-C	1,814m			
Dist Stream Curve B-C	1,948m			
SINUOSITY INDEX	1.0740			
SLOPE	0.0237			
SLOPE %	2.3701			

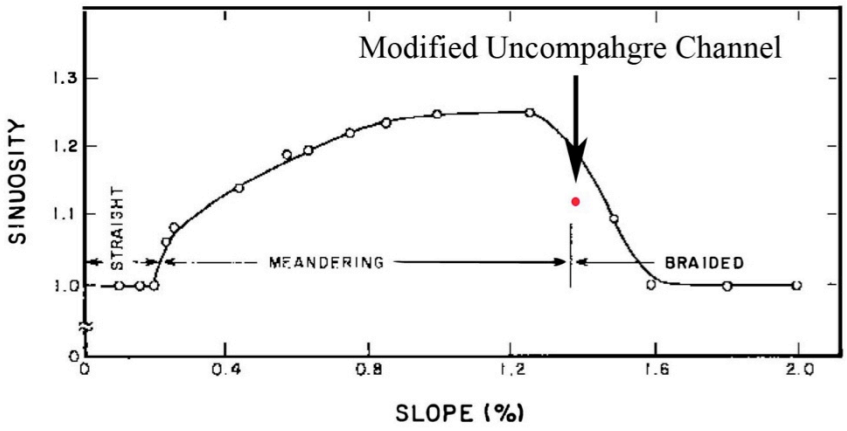

Fig. 27. Slope and sinuosity relationships based on experimental flume studies at constant discharge (Schumm and Khan, 1972). A single data point has been added to the original curve denoting the modified portion of the Uncompahgre River in Ouray, CO.

Comparing the slope and sinuosity of the Uncompahgre River, as determined using Google Earth® (Figs. 25 and 26 and Tables 3 and 4), with experimentally determined values (Schumm and Khan, 1972) shows that the modified channel is on the threshold between a braided and a meandering stream (Fig. 27.) whereas the natural channel has a slope of ~2.4, which classifies it as a braided stream. Because the slope of the channel has been significantly modified from its natural state, the stream will continue eroding and depositing material to form a steeper river channel closer to its previous form.

The slope values as determined for the overall natural and modified reaches were plotted against the 2-year flood discharge (Q_2), which was calculated using daily mean discharge averages from the USGS gauging station in Ouray. Comparing Q_2 and slope values to other rivers in southwest Colorado suggests that the Q_2 is similar to other rivers, but the slope for the Uncompahgre in Ouray for both sites is larger than similar

braided streams (Fig. 28). Slopes at each site measured using the water surface were all ~1%, except for R4, which had a significantly higher slope at ~4.7% (Fig. 29). At R2, where significant deposition occurred, the slope also increased significantly and at R3 where small quantities of erosion occurred, a decrease in slope occurred. Although no erosion occurred at R4, the slope significantly increased.

Examination of the longitudinal profile shapes for each site shows that most sites in both May and September have very small, short, localized drops in slope and other areas that are more flat (Figs. 30 and 31). All slopes except R4, which is much steeper, become less linear from May to September. This change in slope suggests that as discharge increases during the summer, the slope of the river becomes more heterogeneous. Slope is not a direct indicator of erosion or deposition either. At R2, where most deposition occurred, the slope increased, whereas all other sites slope decreased. Slope is not a direct indicator of erosion or deposition. However, at R4, the τ_o / τ_i ratio increased more than at any other site, which is also where the largest decrease in slope occurred and a slope that is ~4x steeper than any other site exists.

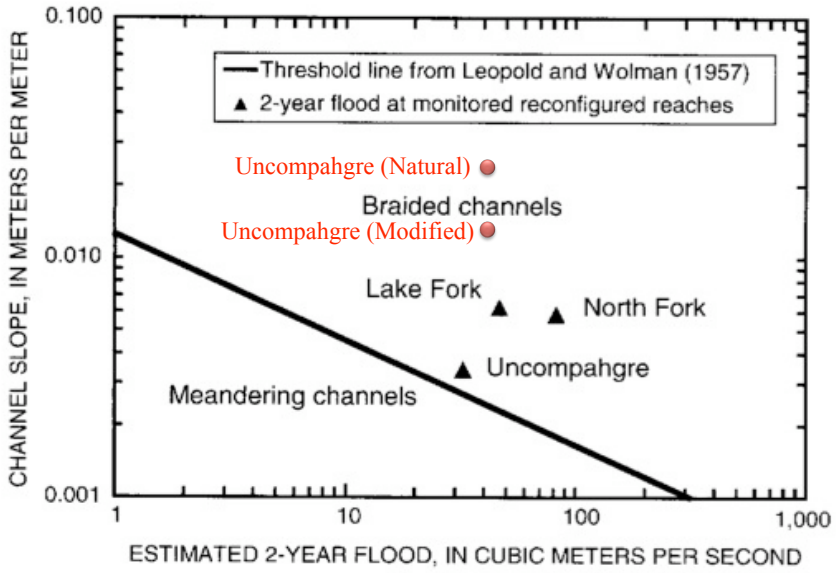

Fig. 28. Theoretical threshold between meandering and braided channels plotted using channel slope and estimated 2-year flood. All field sites from southwest Colorado were plotted above the threshold between meandering and braided channels (Elliott and Capesius, 2009).

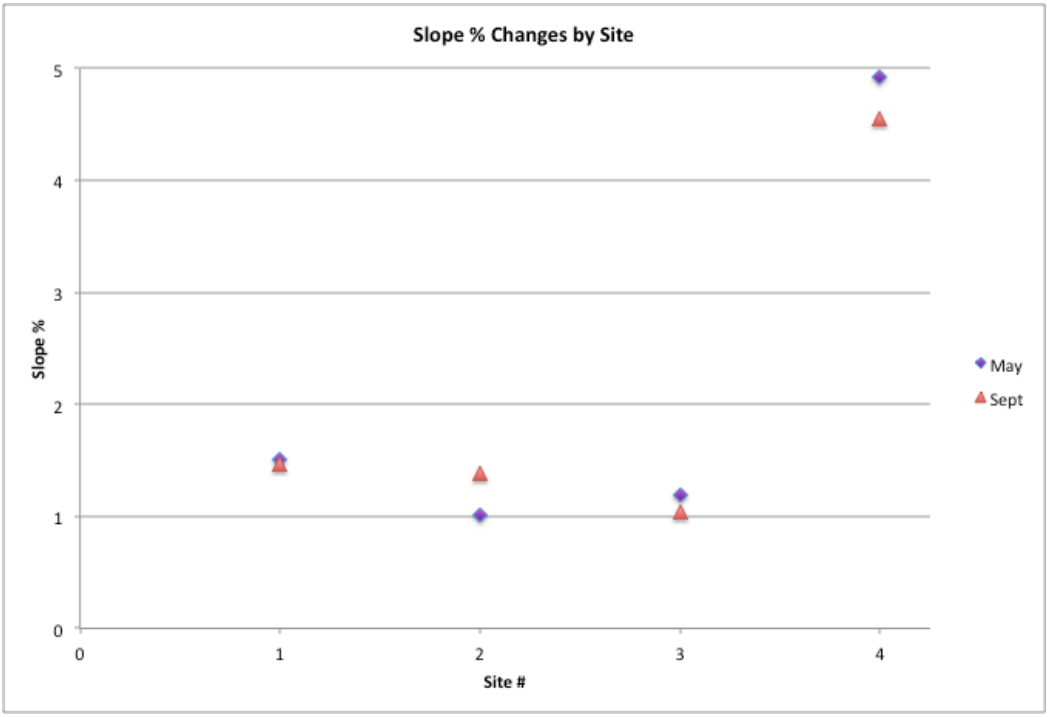

Fig. 29. Slope % values by site for May and September of 2011.

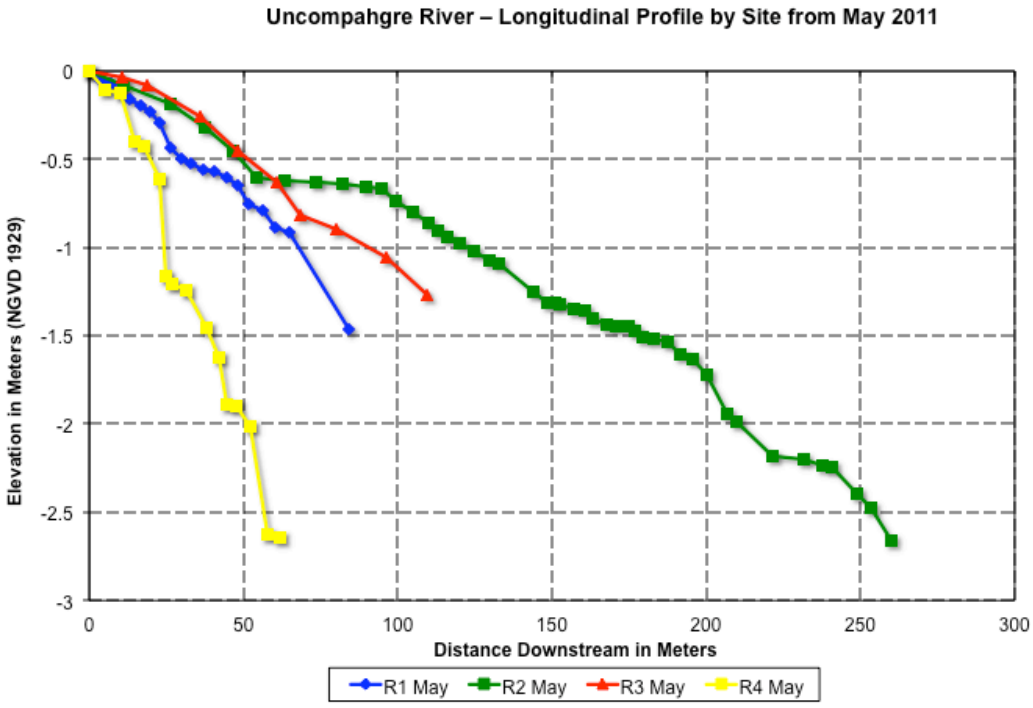

Fig. 30. Longitudinal profiles of the Uncompahgre River acquired from total station surveys of the water surface from May 2011.

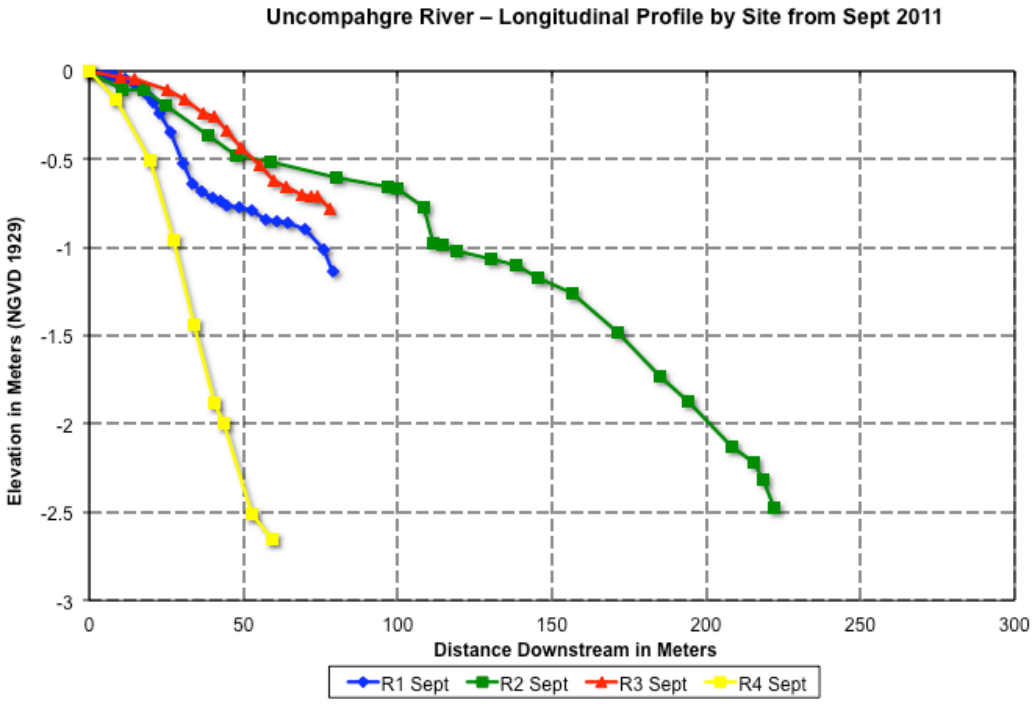

Fig. 31. Longitudinal profiles of the Uncompahgre River acquired from total station surveys of the water surface from September 2011.

Discussion

Limitations

The largest difficulty of fieldwork for this study was identifying and actually surveying cross-sections. Most areas in the modified stream were shallow enough to allow crossing with waders; however, the natural channel presented some challenges even during low flows around 1.42 m^3/s. In May, daily discharges started around 1.42 m^3/s in the morning and peaked around 5.66 m^3/s only hours later, making surveys impossible to perform without high risk of injury. Data collection for cross-sections was, therefore, limited to daylight hours in the early morning, which was also the time of the day that had the best lighting conditions for all terrestrial photographs (See Chapter III). In addition, dramatic shifts in weather patterns made fieldwork even more difficult to complete. For example, it snowed about 10 cm one day and the next day it was sunny and 21 ºC. The ability to perform more cross-sectional surveys directly upstream of the human-modified channel and at more locations within the modified channel could provide a better understanding between geomorphic changes, shear stress, and reach location.

Scientific studies can be performed at a wide variety of spatial scales, as well as temporal scales. In fluvial geomorphology especially, conclusions of a single case study may reveal results that are contrary to streams that have similar locations, environments, characteristics, etc. Therefore, the results of this study are not widely assumed to apply for stream studies at a different spatial scale. The data in this study were primarily collected at a cross-section to reach-scale and compared to other cross-sections or

reaches in other locations along the river. The conclusions of a fluvial geomorphology study on a reach-sized scale may agree and show trends with other rivers in a similar geographical context on a similar scales, but applying or assuming these conclusions to be true for rivers in different environments or over larger scales could be misleading. Alpine rivers, especially those near the headwaters are very heterogeneous. It should be noted that the equations that were used to calculate shear stress have underlying assumptions (Lorang and Hauer, 2003) such as uniform flow, that are not always valid for alpine streams.

Temporal Intervals

Temporal intervals for this study were primarily controlled by discharge of the Uncompahgre River and weather. It is only possible to survey when discharges are lower than 2.83 m^3/s, however, low discharges most often occur during the late fall, winter and early spring when temperatures are near or below freezing. Because optimum dates for surveys were dependent on discharge and weather, both of which can quickly change, only a small window of time in the early summer and early fall allowed surveys to be obtained safely. Also, intervals were needed to avoid annual dredging so as to avoid mixing dredging change with natural change. If time permitted, surveying cross-sections directly before and after dredging would help determine quantitative changes from dredging.

Temporal intervals only measure *net* change between surveys and not overall change. “In geomorphology, many competent events may have occurred in a single

measurement interval, so that we are actually measuring some aggregated, temporally lumped response (Lawler, 2005, p. 3).” Collecting streambank elevation data at “long” temporal intervals may reveal results that cannot be linked together with other processes; however, when the same measurements are undertaken with a shorter temporal interval, individual events can be isolated easier, correlations between elevation response and other processes like discharge can be made, and a more accurate geomorphological explanation can be determined (Lawler, 2005).

Conclusions

The overall research question of this study is: Does dynamic restoration (i.e., maintenance) enhance deposition in the Uncompahgre River? Traditional cross-sectional analysis suggests that H_2 is true because net deposition only occurred in the modified channel, and the net deposition in restored area was greater than net deposition downstream in the natural channel.

The river restoration project in Ouray, CO, decreased the overall slope of the river and increased the sinuosity of the river for the reach that was modified. The natural channel was originally a braided stream that was modified to an artificial meandering shape. Nevertheless, today it can be described as a braided stream within a meandering channel. The slope, sinuosity, Q_2, existence of midchannel bars, and cumulative grain-size distribution all show that the channel should be characterized as a braided stream. If the slope was decreased slightly, the combination of slope and sinuosity could be

classified as a meandering stream based on previous flume studies (Schumm and Khan, 1972).

Meandering streams typically deposit large quantities of fine-grained material that has traveled long distances from its source. Creating an artificial meandering stream in an alpine environment resulted in deposition of bars consisting of large gravel and cobbles. However, deposition of material in the modified channel reduced the quantity of bedload material and suspended sediment, which could potentially increase erosion downstream because water that was once carrying sediment now has more power to erode and transport sediment.

Pebble counts revealed a clear difference between grain-size distribution in the restored channel (R1 and R2) and sites in the natural channel that are located over 1.5 km downstream of restoration (R4 and R5). A large increase in the abundance of fine-grained sediment (<4mm) at R1 from May to September occurred, whereas all sites in September showed a decrease in the abundance of fine-grained sediment further downstream. The decrease in abundance of fine-grained sediments at R5 from May to September also supports the possibility of suspended sediment decreasing from deposition in the modified channel, which would increase the potential suspended sediment capacity downstream. Although this process may be occurring in the Uncompahgre River, tracking individual clasts and taking samples to measure suspended sediment should confirm this. If the modified channel is not dredged annually, deposition in the modified channel may decrease, which may decrease erosion downstream.

For river modification, or restoration projects, in alpine areas that are designed to imitate a meandering stream, it may be beneficial to design the channel slope and sinuosity near previously determined thresholds (Schumm and Khan, 1972). This approach would limit deposition in the modified channel, which reduces the potential for erosion downstream. This approach however, would decrease the potential for communities to "mine" gravel bars for raw material to process into construction materials.

River restoration with regards to altering river geometry is often a difficult process to maintain because the design goal is a "static" condition, which is inherently different from the dynamics of a river system. The designed goal is often altered by sediment transport, a complex and heterogeneous process. Sediment transport can be predicted based on the channel geometry and given discharge; however, these variables also change quickly. This and other case studies in southwest Colorado show the detail required in analyzing stream geometry, which can be a timely and expensive process, making it even less of a priority for the original restoration plan.

Restoration designers have to design for a specific maximum discharge and maximum duration of high discharge, but these values are both driven by variable climatic conditions (Elliott and Capesius, 2009). Although the influence of climatic systems on discharge is beyond the scope of this paper, it is a fundamental driver for engineering projects that must be able to survive within natural systems.

CHAPTER III

TERRESTRIAL PHOTOGRAMMETRY USING CONSUMER-GRADE CAMERAS TO STUDY SHORT-TERM TEMPORAL CHANGE: UNCOMPAHGRE RIVER, COLORADO, USA

Introduction

Photogrammetry is often used where ground surveying is not economically or physically practical (Baily et al., 2003). In addition, photographs obtained on the ground are almost always cheaper to acquire than those obtained from an airborne platform (Birch, 2009a). Terrestrial photogrammetry remains one of the most financially economical mapping methods that offers quick data acquisition and accurate mapping results because photographs can be obtained quickly with consumer-grade cameras without the need of extensive field surveying. In addition, photogrammetry is a non-invasive procedure that has the potential for high accuracy, which makes it a convenient option for laboratory simulations on very small scales as well (Brasington and Smart, 2003; Butler et al., 2002; Thomas and Cantré, 2009).

Independent photographs are often used in fluvial geomorphology for qualitative analysis and to preserve a record of an area-of-interest (AOI) by visually documenting a certain “look” or “feel” of the landscape from the ground. These photographs can be used in presentations to show interested parties before and after conditions, potential problems, and current progress for current projects. In photogrammetry, however,

photographs are used to obtain quantitative spatial data. Photogrammetry applied to fluvial geomorphology has the ability to provide large quantities of good quality data (Lane and Chandler, 2003) to measure change of a landscape. Although "raw" photographs from the field can be obtained quickly, methods in "cleaning" photographs and DEMs may require advanced remote sensing and post-processing experience (Marcus and Fonstad, 2008). Still, preprocessed photographs can provide qualitative information that is useful for non-experts in public meetings or situations where rapid responses may dictate future research plans (Marcus and Fonstad, 2008), and can later be used for quantitative analysis.

Remote sensing and photogrammetric techniques have been used to estimate sediment budgets for natural braided gravel streams (Brasington et al., 2003; Lane et al., 2003; Marcus and Fonstad, 2008; Westaway et al., 2003); however, this method is rarely used with terrestrial photogrammetry (Chandler et al., 2002; Pyle et al., 1997) and has not been used to assess river restoration projects. This study is part of an evaluation of a river restoration project in Ouray, CO, using terrestrial photogrammetry techniques as a means of estimating erosion and deposition of a gravel bar in a modified alpine stream. Knowing the quantity of erosion and deposition in a restored channel and directly downstream will help assess the stability of the restored channel and the success of the restoration project.

The goal of this study is to obtain a quantitative understanding of geomorphic change of the river channel above a dynamic water level on a short-term temporal interval to evaluate current practices of stream modification.

The primary research ***objectives*** of this study are to:

1. Quantify erosion and deposition using photogrammetric models generated using extreme oblique photographs and close-range photographs,
2. Evaluate accuracy of photogrammetric vs. traditional methods, and
3. Identify depositional and erosional patterns related to location in stream (meander vs point bar), time of year, and discharge events.

Background on Photogrammetry

Terrestrial and Close-Range Photogrammetry (CRP)

Small-format cameras are often used in geologic/geomorphic studies because they are cheap and provide a non-invasive and accurate method of 3D mapping (Thomas and Cantré, 2009). Lidar is another remote sensing technology that has become very popular for obtaining 3D data in recent years because of its superior accuracy (Adams and Chandler, 2002), however, photogrammetry still provides adequate accuracies at a significantly cheaper cost.

In the past, photogrammetry was limited to aerial photographs because poor setup of terrestrial camera stations and poor photograph quality created identification errors during image point matching (Brecher and Thompson, 1993), making the use of close-range photographs difficult. Today, researchers and management agencies have developed many creative methods for obtaining imagery.

Another reason terrestrial photogrammetry is rarely used in geomorphology is because most studies analyze large spatial areas. Glacial studies for instance, typically use aerial photography or satellite imagery to evaluate long-term changes rather than short-term changes using terrestrial photography (Ceballos et al., 2006; Coudrain et al., 2005; Rignot et al., 2003) because the spatial scale is very large and the rate of change that is being studied is relatively small.

Orthorectified photographs obtained from oblique angles on the ground have been used for short-term monitoring on the order of weeks or even for hourly comparisons of stream flow in a braided river system (Ashmore and Sauks, 2006). Terrestrial photography is best applied to studies that require short, temporal intervals because obtaining data is easier and cheaper; permanent systems can be installed to consistently monitor rivers (Ashmore and Sauks, 2006; Chandler et al., 2002).

Although analytical photogrammetric methods provide more accurate measurements than most digital photogrammetric methods, improvements have been made so that digital methods can outcompete older analytical methods. Traditional photogrammetric methods require many repetitive manual measurements by photogrammetry specialists to acquire data whereas recent software programs automate much of this process and allow non-specialists to acquire the same data with minimal labor (Baily et al., 2003). In addition, large data sets can be analyzed in short periods of time without the need of large computer processing power (Birch, 2009b). This new technology enables researchers to efficiently generate 3D data quickly, which would

make the analysis of time-lapse photographs a realistic option for studies that collect many measurements at short temporal intervals.

Once DEMs representative of different time periods are created, they can be compared and overlapped to determine temporal patterns of volumetric deposition and erosion. Accurate measurements of volumetric change are important to understand process rates, which are difficult to obtain by direct measurement in gravel streams (Lane et al., 2003). When comparing any two models, the initial error associated with each data set must be known because the final observation will also contain those errors. Volumetric sediment budgets will be twice as sensitive because two DEMs are used and each model will incorporate its own error into the final quantities measured (Brasington et al., 2003).

Some geomorphic processes are still very difficult to measure using photogrammetry. During floods, for example, thin layers of silt and clays are often deposited in flood plains across very expansive areas. For comparing DEMs, this can present problems because the Z-axis may not be sensitive enough to detect this thin depositional layer of silts and clays. Therefore, the topographic structure of erosion and deposition must be considered when evaluating sediment budgets (Brasington et al., 2003), which will depend on the geomorphic process inducing change.

Camera Calibration

In any remote sensing application, data collection techniques and sensor properties need to be known so the appropriate adjustments can be made to eliminate

interference and distortions associated with the specific method of collection. With consumer-grade cameras, lens calibration needs to be performed to remove distortions caused by the projection of incoming light from many directions onto a flat image sensor. This ensures that each pixel in a single image is geometrically accurate. Knowing different parameters of the camera at the time when images were acquired may determine how 3D data are calculated.

Camera calibration involves two separate calculations or processes, internal orientation calibration (IO) and external orientation calibration (EO). These calculations are necessary for translating 2D coordinates (x, y) in image space from two or more images to 3D object space coordinates (X, Y, Z). Mathematically, this translation from (x, y) image coordinates to real-world 3D coordinates (X, Y, Z) can be represented by the extended collinearity equation model (Fraser, 1998):

$$x - x_0 + \Delta x = -c\frac{R_1}{R_3} \tag{9}$$

$$y - y_0 + \Delta y = -c\frac{R_2}{R_3} \tag{10}$$

where:

$$\begin{pmatrix} R_1 \\ R_2 \\ R_3 \end{pmatrix} = R\begin{pmatrix} X - X^0 \\ Y - Y^0 \\ Z - Z^0 \end{pmatrix} \tag{11}$$

(X^0, Y^0, Z^0) = Perspective Center

R = Rotation

(x_0, y_o) = principal point

c = focal length

IO involves determining the parameters of the lens and the digital image sensor. Sensor dimensions and image dimensions are needed to calculate the principal point (x_0, y_o), or optical center of photographs being used. The focal length (c) of the lens is often recorded in metadata of digital photographs and is also needed for calculations to approximate distortions created in images. Using these known variables, equations 10 and 11 can approximate all types of lens distortion (Fraser, 1998):

$$\Delta x = -x_0 - \frac{\overline{x}}{c}\Delta c + \overline{x}r^2K_1 + \overline{x}r^4K_2 + \overline{x}r^6K_3 + (2\overline{x}^2 + r^2)P_1 + 2\overline{x}\overline{y}P_2 + b_1\overline{x} + b_2\overline{y} \quad (12)$$

$$\Delta y = -y_0 - \frac{\overline{y}}{c}\Delta c + \overline{y}r^2K_1 + \overline{y}r^4K_2 + \overline{y}r^6K_3 + 2\overline{x}\overline{y}P_1 + (2\overline{y}^2 + r^2)P_2 \quad (13)$$

where:

$\underline{x} = x - x^0$,

(Δx, Δy) = image coordinate perturbations, or overall image distortion distance,

c = principal distance (focal length),

(x, y) = image space in 2D,

(x_0, y_o) = principal point ,

K_1, K_2, and K_3 = radial distortion coefficients,

P_1 and P_2 = decentering distortion coefficients, and

b_1 and b_2 = affinity and nonorthogonality terms.

In high accuracy photogrammetric applications, all ten parameters (x_0, y_o, Δc, K_1, K_2, K_3, P_1, P_2, b_1, and b_2) of the lens/camera are recommended to calibrate the camera (Fraser, 1998). For this study, calibration was performed using Brown's lens distortion model (Pasumansky, 2011):

$$x' = x(1 + K_1r^2 + K_2r^4 + K_3r^6) + P_2(r^2 + 2x^2) + 2P_1xy \quad (14)$$

$$y' = y(1 + K_1r^2 + K_2r^4 + K_3r^6) + P_2(r^2 + 2y^2) + 2P_2xy \quad (15)$$

$$u = c_x + x'f_x + y'skew \quad (16)$$

$$v = c_y + y'f_y \quad (17)$$

where:

x = X / Z,

y = Y / Z,

$r = \sqrt{x^2 + y^2}$,

(X, Y, Z) – point coordinates of local camera coordinate system,

(u, v) – projected point coordinates in the image coordinate system (pixels),

(f_x, f_y) – focal lengths,

(c_x, c_y) – principal point coordinates,

K_1, K_2, K_3 – radial distortion coefficients,

P_1, P_2 – tangential (decentering) distortion coefficients, and

Skew - skew coefficient between the x and y-axis.

Simpler mathematical methods exist for transforming 2D coordinates into 3D coordinates, however, these introduces linear dependencies between parameters that can result in errors that do not represent actual object space (Fraser, 1998). This method, however, allows photogrammetric models to be created with more flexibility because this equation does not require approximate values of IO and EO parameters, making it possible to obtain 3D data without pre-existing knowledge of the camera lens/sensor or its geographical location. The lens distortion variables are refined using linear least-squares estimation, which is called a bundle adjustment represented by equation 10 below (Fraser, 1998):

$$A_1X_1 + A_2X_2 + A_3X_3 + w = 0 \quad (18)$$

where:

X_1 = EO parameters,

X_2 = object point coordinates,

X_3 = self-calibration parameters,

A_i = configuration matrices, and

w = image coordinate discrepancy vector.

For a successful model to be created, the IO parameters for the camera and a minimum of three object space control-point coordinates must be available for each image to calculate the EO. At least two images are required, although many ambiguities can be

eliminated if three images are used (Fraser, 1998). In addition, the accuracy of models will increase as the quantity of photographs increase, but only as long as these photographs are acquired from different positions and still include the same control points.

Overall, creating 3D object-space coordinates from 2D image-space coordinates can be accomplished with two primary methods. If no information about the IO or the EO is known, then a more complicated collinearity equation model (equations 10-15) can be used to calculate camera parameters and the object-space coordinates. If the IO and the EO of the camera are known, then the linear least-squares estimation, or bundle adjustment (eq 16) can be used to estimate object-space coordinates. Equation 16 can be rewritten, however, to calculate IO and EO by using multiple photographs with at least three object control points to create a system of equations, eliminating the need for EO and IO to be determined by complex equations. The use of equation 16 in terrestrial photogrammetric applications has the potential to introduce linear errors, but also allows users a much greater flexibility for creating photogrammetric models.

Analytical and Digital Photogrammetry

The primary difference between analytical (i.e. analog/manual) photogrammetry and digital photogrammetric methods exists in image point matching. In analytical methods, image point matching is performed by a specialist by manually measuring distances on physical images and can yield approximately 5,000-6,000 points a day. Using a more advanced string and point data collection technique, this data collection

rate can be increased to 42,415 points in sixteen hours (Baily et al., 2003). Whereas this may seem like a significant number of points, digital analysis for the entire DTM creation process that yielded ~2 million points can be completed in about twenty minutes (Birch, 2009a).

Acquiring points in the field is also required for digital photogrammetry, but these points are generally used as control points for internal experimental validation. Brasington et al., (2000) used a global positioning system (GPS) to accumulate about 2,000 points per day for creating a DEM with a point density of 1.2-1.7pts m^{-2}. The model covered a 300 m x 80 m reach of a river and was sufficiently precise to detect changes as small as 10 cm at 95% confidence. Even though these measurements cover an expansive area and are very accurate, it took seven, eight-hour days to collect field observations. DEM generation with automated digital photogrammetry requires a minimum of three surveyed control points (Fraser, 1998) and digital photographs can be acquired in a matter of minutes. The key, however, is not simply generating more points with new methods, but quickly generating accurate points.

Photograph Acquisition

Because obtaining high-resolution imagery at sub-meter pixel resolutions is a difficult task and is not cheaply available from government agencies or commercial companies, researchers have developed many creative methods for obtaining such imagery. Plan-view images have been obtained using private aircraft, unmanned air vehicles (UAV) (Birch, 2009a), balloons (Dosemagen, 2010), among other methods.

Depending on the object of study, plan-view images are not necessarily ideal. Some fluvial geomorphology studies have taken advantage of the high relief of nearby cliffs to obtain terrestrial oblique photography (Ashmore and Sauks, 2006; Chandler et al., 2002). Other studies measuring volumes of small hills or mining walls obtain photographs while standing (Yilmaz, 2010), or when minimizing field time is a major priority, photographs can be obtained from a moving vehicle (Birch, 2009a).

For photographs to be transformed into accurate DEMs, it is imperative that photographs are obtained properly. In other words, the stereo pair, or any number of overlapped images must take into account object scale, base spacing, and overlap. With aerial platforms, camera position is rarely a problematic issue, but terrestrial photogrammetry presents new challenges.

Because all calculated 3D data are obtained from areas of overlap in adjacent images, obtaining multiple clear images with sufficient overlap of the AOI is the primary goal. Traditionally, aerial photographs used for photogrammetric analysis are expected to contain 60% lateral area overlap and 20% sidelap (Jensen, 2007). When photographs are taken, the lens is usually directly perpendicular to the land surface and pictures are taken on a given time interval while the aircraft maintains a constant velocity to retain 60% overlap in adjacent images.

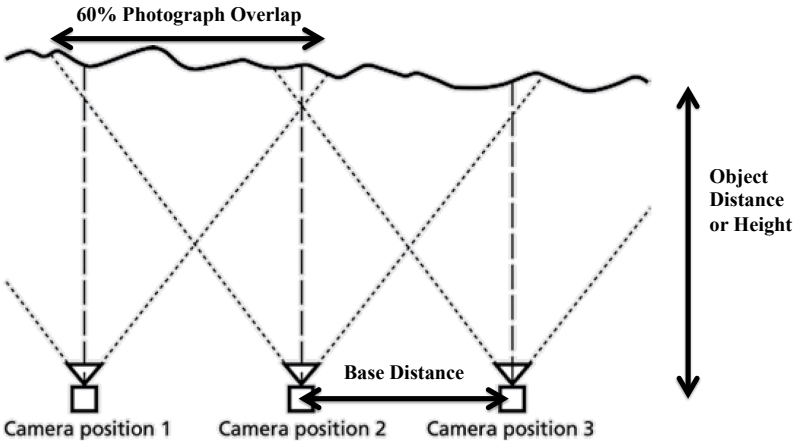

Fig. 32. Optimal camera station setup for terrestrial photogrammetry of a vertical planar object. Modified from (Matthews, 2008).

The distance between each camera position is referred to the base height (B), while height (H) is the distance from the AOI to the camera (Fig. 32.). When taking terrestrial photographs, obtaining 60% overlap and the optimum B/H ratio may not always be feasible. In some instances, changing topography and obstructions may prohibit images from being captured without the use of a sub-aerial or aerial platform. In addition, landscapes may limit the convergence angle between photographs. In aerial photography, this intersection angle is around 0° because lens direction is perpendicular to the land surface. Often times this geometry cannot be achieved in a terrestrial setting, therefore; camera angles must converge on the area of interest to obtain the necessary image overlap (Fig. 33). By following these basic photogrammetric techniques, image quality will increase, which increases the quality of the generated DTM.

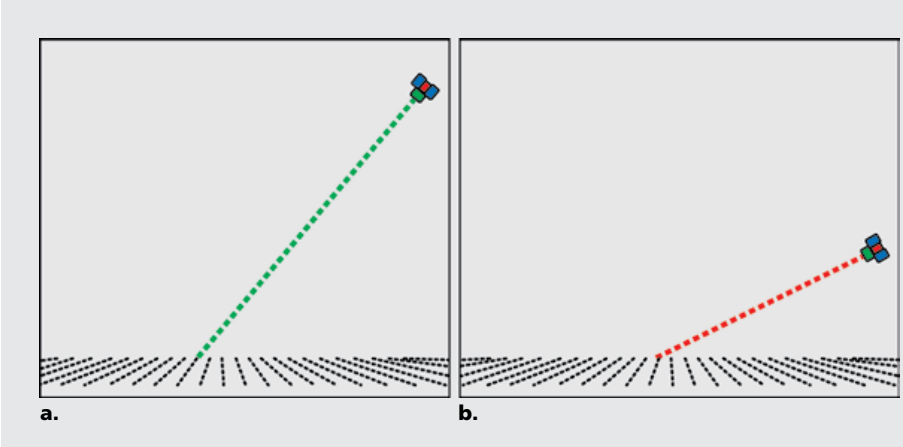

Fig. 33. (A) Acceptable oblique camera position in relation to land surface. (B) Low-angle or extreme oblique camera position is not optimal, and should be avoided if possible, but still can be used to collect data if no other options exist (Matthews, 2008).

Image Sensors for Consumer Cameras and Spatial Scales

Geomorphologists use a diverse set of information to study the response of rivers that often can be classified on different spatial scales. For example, turbulence would be measured on a smaller scale (cm or m) as opposed to discharge, which is often measured in tens and hundreds of kilometers. Depth and bed sediment size are other common characteristics that would be measured on a meter scale. Knowing the spatial scale of the features of interest is imperative for remote sensing as this determines what type of images or photographs are used. Whereas satellite images may provide sufficient information to calculate sinuosity indexes within a watershed, it probably will not provide useful information about turbidity or sediment size.

Images need to capture the entire AOI and pixel resolutions need to be smaller than the spatial feature that is being studied . For example, determining gravel and sand distributions of a gravel bar would require an image covering the entire gravel bar with

pixels that are smaller than the smallest sand grain intended to be analyzed. Quite often, obtaining the proper photographs requires aircraft, a costly expense for limited research budgets (Marcus and Fonstad, 2008), but because image sensors have undergone dramatic increases in the ability to capture high-resolution images while maintaining small-sensor dimensions in the last few decades, more accurate spatial data can be obtained while keeping cameras at a convenient size (Petrie and Walker, 2007).

In this research project, the Canon Rebel T2i DSLR camera was used, which has an 18MP CMOS sensor. Sensor Pixel Size (SPS) is calculated using the actual dimensions of the sensor and the resolution of photographs that the sensor can obtain (Matthews, 2008). For example, a 5184px (width) x 3456px (height) photograph obtained with a sensor with dimensions of 22.3mm x 14.9mm will have a SPS of 4.30μm and 4.31μm, respectively.

$$GSD = SPS * H / f \quad (19)$$

where:

GSD = Ground Sample Distance,
SPS = Sensor Pixel Size,
H = Height or Object Distance, and
f = Focal Length.

Using equation 17 (Matthews, 2008) for a photograph acquired using a 70 mm lens ~30 m away from an object, the GSD of that photograph would be ~0.01843 mm. The spatial resolution of a photograph with this GSD would be sufficient to provide information about gravel and cobble-sized clasts, provided it is acquired at the proper

orientation and under optimal lighting conditions. Although this study will not examine clast sizes using photographs, the photographs that were obtained have the potential to be used for such a purpose.

Temporal Intervals

With recent technological advances, studies are now being undertaken with temporal resolutions in the ranges of weeks, days, hours, to minutes (Lawler, 2005). Collecting data on shorter temporal resolutions may yield more accurate results, but does not necessarily mean that it is appropriate for all studies. Measuring changes requires an approximate estimate of the time required for the process or geomorphic change to take place. Even though the ability to record shorter temporal resolutions has increased as a result of new technology, many potential process-response effects are unknown.

Time is a key factor in process response (Wolman and Miller, 1960), which is the core of all geomorphic change. Landform change will occur when a threshold has been crossed, but thresholds vary depending on the system being observed (Schumm, 1979). In the case of river banks, when gravity overcomes the force holding up sand particles, cobbles, or consolidated soil, change will occur. The primary processes responsible for this intrinsic threshold being surpassed are expansion-contraction (i.e. freeze-thaw) and gravity. During times of high discharge, the stream, which is considered an external force to the system, is likely to overcome extrinsic thresholds, which would not have otherwise been overcome. For example, one portion of the riverbank had failed creating a large deposit of material at the base of the bank. During low discharge, the material in

this pile is influenced by gravity, whereas in the summer during high discharge this deposit is easily transported downstream, which could not have occurred from gravity alone.

Applications of Photogrammetry in Geomorphology

Remote sensing of rivers is a task that is often performed by remote sensors or geomorphologists, but to obtain meaningful results and take advantage of recent technological improvements, research needs to be undertaken by remote sensors *and* geomorphologists together in a collaborative setting (Marcus and Fonstad, 2008). Many stream studies involve mapping reaches in a small portion of a watershed or sporadically and discontinuously throughout the watershed. Rivers are very continuous, however, which makes this approach seem incomplete. Most often, the resources and time required to map comprehensively a river throughout a watershed are limited, making it impossible to obtain completely continuous maps (Marcus and Fonstad, 2008). Photogrammetry allows more extensive mapping while maintaining accurate DEMs.

DEMs are often used in geomorphology research to obtain a large number of cross-sections over a small area. In fluvial research, cross-sections are used to characterize the geometry of the stream, which determines flow properties of the stream. The accuracy of overall stream geometry can be affected by the cross-section spacing along the streambed (Lane et al., 2003). In a study of a glacial braided gravel stream, mean bed levels were averaged using cross-sections that were digitally calculated based on a minimum spacing value for the entire length of a the 3.5 km long stream. The

relative error of the mean bed levels became significant when cross-sectional spacing increased over 100m (Lane et al., 2003). As a result, the error for any geomorphic study involving cross-sections will depend on the frequency in which cross-sections are obtained, and, therefore, the field time available.

DEMs offer the possibility of obtaining an infinite number of cross-sections on streams, by sacrificing the accuracy of individual points. Still, DEMs are often used for 4D analysis by comparing two DEMs from different time periods.

Optical imagery has the advantage over other remote sensing sensors because sunlight can penetrate water (Brasington et al., 2003). Capturing data about the surface of water and the water column can provide information on river characteristics such as: depth, turbidity, algae, substrate, etc (Marcus and Fonstad, 2008). These data must be calculated based on assumptions that are based on characteristics of, and the relationship between the image sensor and the target that are more familiar to remote sensors rather than geomorphologists. The results can then be used by geomorphologists to characterize the river in greater detail (Marcus and Fonstad, 2008).

It is possible to obtain river morphodynamics data and discharge data from images simultaneously, so that images provide the ability to relate changes in morphology with discharge conditions (Ashmore and Sauks, 2006). For discharge prediction from images to be accurate, the mean water surface width and instantaneous discharge of a river reach must be known. In general, previous studies using satellite imagery have not been able to monitor continuously rivers during the year, but only during distinct events. Terrestrial oblique orthorectified photographs can be used for

short-term monitoring on the order of weeks or even for hourly comparisons of streamflow in a braided river system (Ashmore and Sauks, 2006).

One study used water width (the length of the water surface) to determine discharge. It was determined that this relationship was best represented as a linear function although for one year it was better represented as a polynomial (Ashmore and Sauks, 2006). When water rises above the banks or is at high flow, river width can increase dramatically without significant increases in discharge. The opposite is true during low flow stages because discharge can dramatically decrease while the water width does not show significant changes. Both extremes can be represented graphically as a polynomial approaching an asymptote, whereas the middle values are better represented as a linear function.

This concept also can create problems when estimating sediment budgets using DEMs. During floods, thin layers of silt and clays are often deposited in flood plains across very expansive areas. When comparing DEMs, this can present problems because data on the Z-axis (elevation) may not be sensitive enough to detect this thin depositional layer of silts and clays. Therefore, the topographic structure of erosion and deposition is important to consider when evaluating sediment budgets (Brasington et al., 2003).

Study Area

Site Geometry

On the northern side of Ouray, CO, a recreational river walk has been created along the Uncompahgre River. The river, which has been confined to a single meandering channel, is located in a "U"-shaped glacial valley with steep cliffs on both sides. This unique landscape facilitated oblique-aerial photos to be captured on both sides of the valley. Oblique photography, however, was only limited to the modified portion of the Uncompahgre River because cliffs become less steep downstream. Acceptable terrestrial photographs were also limited by interference with vegetation or other structures, which was the primary control of camera positions along cliffs. Access to cliffs is limited to public and private trails as the terrain off of these trails has dense vegetation, or dangerously steep faces.

Areas of change in the modified channel are primarily limited to the river channel. Small localities on banks showed signs of erosion, but were impossible to access for setting up and surveying control points. Most other banks were composed of riprap, which is designed to stay in place and would be difficult to predict when movement is likely to occur. The modified channel has large gravel bars 5-70 m long, most of which are present on the inside of meanders, but some of which migrate like bars in braided streams. One bar in particular was the primary focus of photogrammetric modeling because of its location relative to positions on cliffs with the least unobstructed view (Figs. 34 and 35.).

Directly downstream, outside of the modified channel, R3 was surveyed using a total station, but CRP was not used because no visual evidence of erosion or deposition above water levels was present (Fig. 36.). Further downstream, however, areas where quantifiable change could be visually identified were used for CRP. Photographs were captured of nearly vertical banks from a distance of ~10 m at sites R4 and R5 (Figs. 37 and 38.). The bank at R4 is composed of large boulders, soil, and many free-hanging roots dangling from the soil. R5 is composed primarily of boulders and cobbles, but also contains the root structure of a medium-sized tree.

Time-lapse camera capsules were originally setup at R4 from September 2010 to May 2011 because it has the best geometric setting for cameras to be permanently fixed with the least disturbance. These cameras were moved, however, to R5 from May 2011 to September 2011 because it was determined that the base-to-height ratio at R4 was too low to achieve acceptable photogrammetric spacing.

Fig. 34. R2 during late September 2010. The gravel bar has been prepared for excavation by bulldozing a large pile.

Fig. 35. Oblique close-up of the gravel bar at R2. Targets shown in the circles are 30 cm x 30 cm.

Fig. 36. Looking west at R3 in September 2011.

Fig. 37. Looking west at R4 in September 2011 (Note survey rod for scale).

Fig. 38. Looking west at R5 in September 2011.

Methodology

Oblique Photogrammetry

Photographs of R2 were obtained of the Uncompahgre River from nearby cliffs using a Canon Rebel T2i with several different types of lenses. Camera stations from the cliffs on the east side averaged a distance of ~295 m from the gravel bar being photographed, whereas photographs from the west side averaged a distance of ~232 m.

Table 5 Oblique photograph camera positions from cliffs. Distances and oblique angles are measured in relation to the gravel bar from R2. Oblique angles represent the angle from the line perpendicular to the plane of the land surface to the camera angle.

Camera Station	UTM Lat	UTM Long	Elevation (m)	Object Distance (m)	Oblique Angle (º)
EM1	264,929	4,213,964	2,470	352	63
EM2	264,644	4,214,053	2,457	219	49
EM3	264,834	4,214,074	2,452	314	64
WM1	264,440	4,213,821	2,412	217	63
WM2	264,415	4,213,953	2,433	248	61

The obliqueness of all images is extreme (Table 5), as most aerial photographs are taken near nadir with an oblique angle of 0º, or perpendicular to the land surface. The oblique angle can vary largely within an image depending on where the object or ROI is located.

Fig. 39. Oblique aerial image of R2 captured in September 2010 just before artificial bar was removed by the City of Ouray.

With aerial photography, a single pixel can represent the exact same square dimensions of the land surface whereas oblique images will introduce land-surface compression in each pixel in the viewing direction of the image. The pixels located at the top of Fig. 39 are more vertically compressed than pixels located at the bottom of the image.

Close-Range Photogrammetry (CRP)

Photographs were acquired of a cut bank ~one km downstream of the northern terminus of the modified channel. Photographs of a cut bank of the stream were acquired on the opposing bank located ~10 m apart. This cut bank was nearly vertical, had evidence of creep on the top, and had large boulders embedded in loose soil overhanging the bottom of the cut bank. These factors all made acquisition of the control points difficult, but not impossible. Small painted blocks, approximately 7cm x 7cm were placed in the most stable locations, which mostly occurred along the bottom of the cut bank under the overhand. In May, photographs were acquired using panoramic-image fans at four separate camera stations whereas photographs in September were acquired using only two image fans (Figs. 40 and 41). Although this technique was used, it was later determined that it is not recommended because photographs are too similar. Thus, this technique is not recommended if less than three camera stations are used.

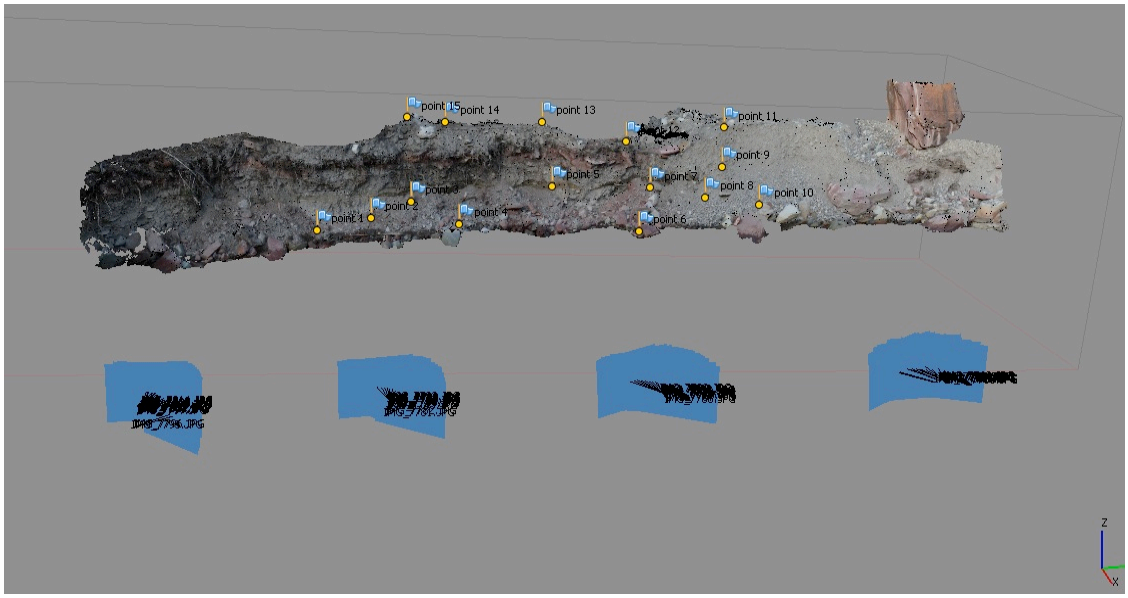

Fig. 40. DTM of R4 in May 2011.

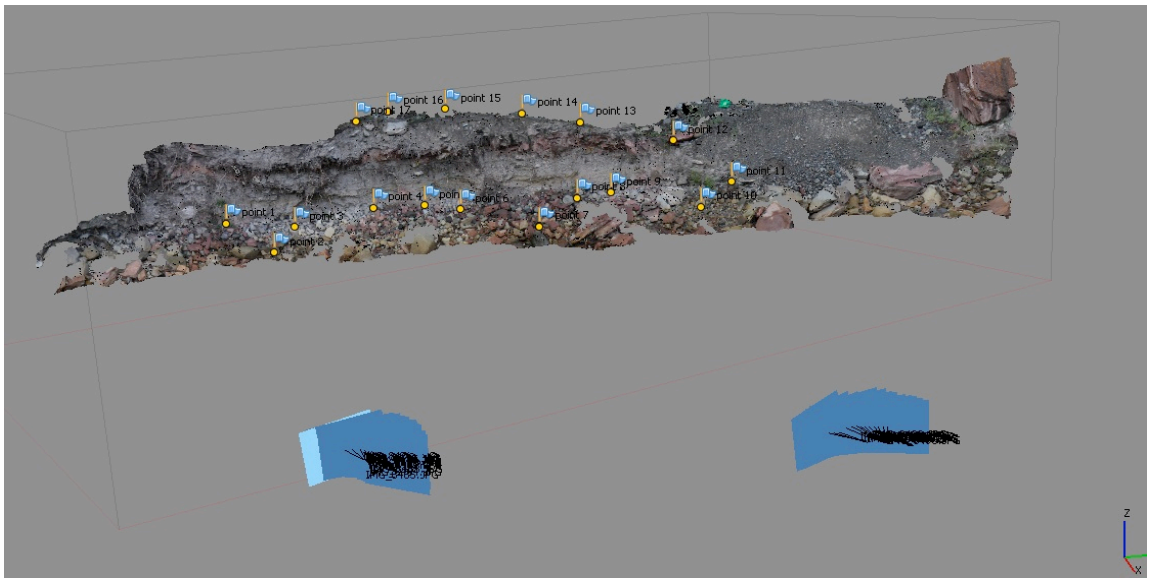

Fig. 41. DTM of R4 in September 2011.

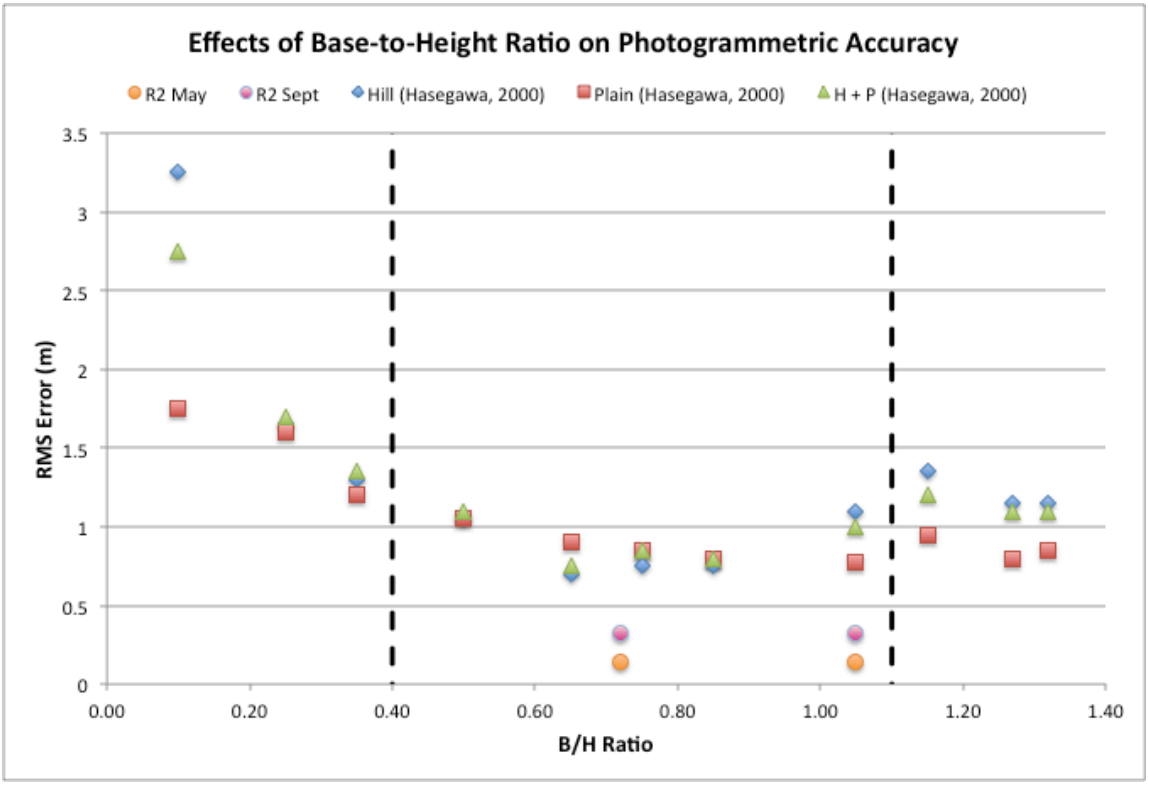

Fig. 42. The relationship between the base-to-height ratio and DEM accuracy for different terrain classified by local slopes. Data from the photogrammetric results at R2 have been added. Vertical dotted lines mark the upper and lower thresholds of optimal B/H ratios. Modified from (Hasegawa, 2000).

Optimal base-to-height ratios range from about 0.4 to 1.1, with values of less than 0.2 creating large errors in DEM generation (Fig. 42). Using image fans with many camera stations with predetermined base-to-height ratios allows base-to-height ratios to be controlled while capturing large numbers of photographs to provide greater detail in a single DEM.

Time-Lapse Photography

Time-lapse capsules were permanently installed to large trees to obtain photographs of the stream bank. These cameras were designed to capture data at a higher

temporal resolution and lower spatial resolution. Two time-lapse cameras were originally installed at Site R4 in October 2010 and collected daily photographs until the internal batteries died during mid November 2010. In May 2011, new batteries were installed and the cameras were moved to Site R5 to obtain a larger base-to-height ratio so that photographs could be used for photogrammetric analysis. The cameras were programmed to take photographs at 10-minute intervals from 6:40AM-2:30PM MST and 6:40PM-9:00PM MST each day. These times were chosen because these periods of the day had the most optimal sunlight.

The temporal interval of these cameras was designed around the quantity of memory that could be stored on a local memory card (2GB), which provided an adequate interval to capture individual discharges. Unfortunately, the stream bank that was monitored at R5 during the summer of 2011 did not show sufficient visual signs of deposition or erosion even though large changes in discharge occurred.

Camera Calibration

For each unique lens focal length and sensor/camera combination that captures an image, a set of interior parameters must be calculated, so that focal distortions can be removed for photogrammetric analysis. Even if the same camera/sensor is used, if the focal distance or zoom is changed, this alteration will change the focal length and a new calibration is needed. A free software application, Agisoft Lens, which uses Brown's lens distortion model (Pasumansky, 2011), was used for all camera calibrations. This program enables very simple calibration and can be completed in minutes.

For a single calibration, a set of images that contain a planar surface displaying an equidistant black-and-white checkerboard pattern must be captured. Because a lens will introduce distortion, the pixel distance between intersections of white and black squares will vary throughout an image depending on its location within that image. These distances are subsequently used to calculate radial distortion coefficients (k1, k2, k3) and tangential distortion coefficients (p1 and p2) following Brown's lens distortion model. The black-and-white checkerboard pattern can be displayed on an LCD monitor; however, for wide-angle lenses and lenses that need to focus at infinity, LCD monitors present challenges in proper image acquisition because of its small size. Instead, photographs of the checkerboard design from a projector were used because a projector can produce images much larger than smaller LCD monitors. Because it is assumed that a planar surface is used to display this checkerboard pattern, and that the true value of the spacing between squares is equal, the projector must be aligned perpendicular to the planar surface it is projecting onto. This is probably not 100% accurate, but calibration parameters only need to be estimated to proceed with photogrammetric measurements because they are automatically readjusted during photogrammetric analysis.

Total Station Surveys

A Topcon® GPT-3000 total station was used in all photogrammetric and geomorphic surveys. It uses a laser and a reflector to calculate N, E, and Z coordinates for every surveyed point. Precision of all points reached 1 mm, but the accuracy of surveyed points was difficult to calculate. When local benchmarks were surveyed in

May and September, the horizontal distance between two particular benchmarks changed ~11 cm. No visual evidence suggests that the benchmarks were actually disrupted. As the distance from the total station to the reflector increased, inaccuracies became more common; therefore, surveys were conducted with the total station as close as possible to cross-sections, which was usually a greater distance from benchmarks. Locating the total station in this manner resulted in a higher relative accuracy but a poorer absolute accuracy to real-world coordinates.

Benchmarks had been installed during the construction of the modified river channel, which conveniently provided accurate real-world coordinates for all coordinates surveyed at R1, R2, and R3. For R4, an NOAA benchmark was used, but coordinates for R4 were not converted to real-world coordinates. R4 and R5 were primarily controlled using nails with painted washers that were driven into the ground.

Initially, control points for images were created from rebar that was painted alternating colors with punctured tennis balls attached to the top so that targets could remain in place year-round for time-lapse cameras. A local person volunteered to take pictures, which negated the need for re-surveying targets. Unfortunately, these targets failed to provide adequate accuracy for manually identifying control point pixels within photographs, as they did not remain stationary throughout the year. Instead, square pieces of plywood with lengths of 7.6 cm (3”), 30.5 cm (12”), and 61.0 cm (24”) were painted with a black-and-white triangle design to minimize error between actual points surveyed and the actual pixel representing that control point. These targets were removed after image acquisition. Natural targets (fence posts, signs, sidewalk corners,

etc.) were also surveyed to help validate photogrammetric models, but were not used because the DTMs produced did not include these locations.

Data and Results

Calibration

Although all lenses generally follow the same pattern with more distortion further from the principal point of the lens, this distortion will be much larger for lenses with shorter focal lengths, which is why they are often avoided in photogrammetric studies. The lens and sensor configuration for the Reconyx time-lapse capsule was completely unknown from EXIF metadata that is usually produced with digital photographs from consumer cameras. Because these images have post-processed borders that are branded into each individual image containing date, time, temperature, etc., even the original image resolution could not be properly determined. Despite this, the manufacturer quoted the lens having a focal length of 8.5 mm and although the sensor size was only 3.1MP (VanderZee, 2010), a successful calibration was created. Distortion graphs for each lens are in the appendix.

Images used for calibration must include camera rotations along the axis in which the photograph is being captured, so that the horizontal and vertical distortions can be more accurately determined. Figs. 43-46 show how the results of a bad calibration from images that were only captured while oriented horizontally would underestimate radial distortion and overestimate tangential distortion.

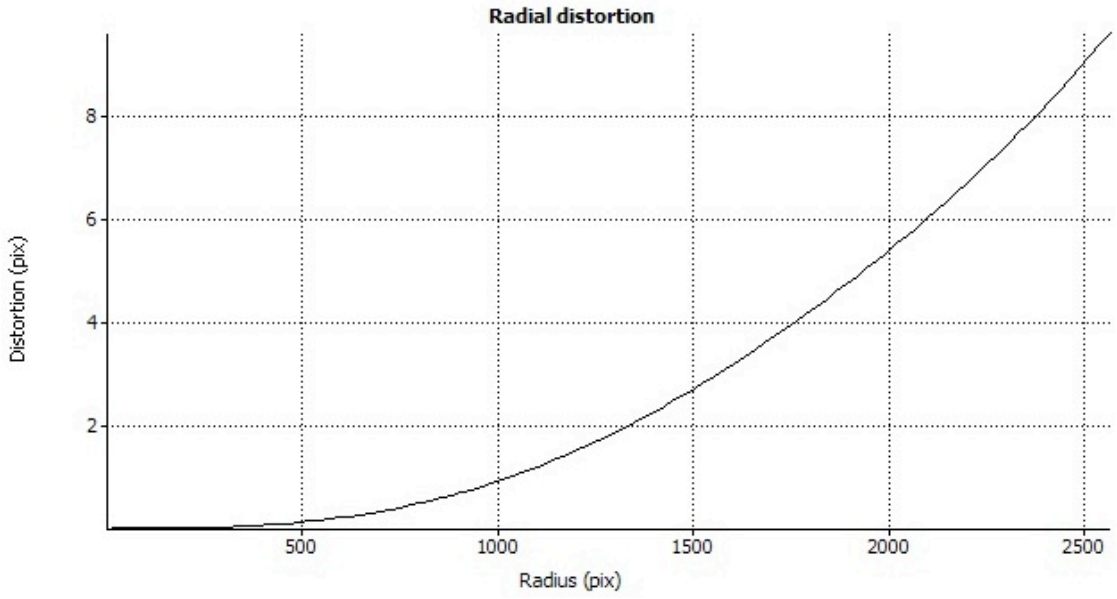

Fig. 43. Proper predicted radial distortion for 70mm lens from images rotated approximately 180º images from one vertical side to another vertical side.

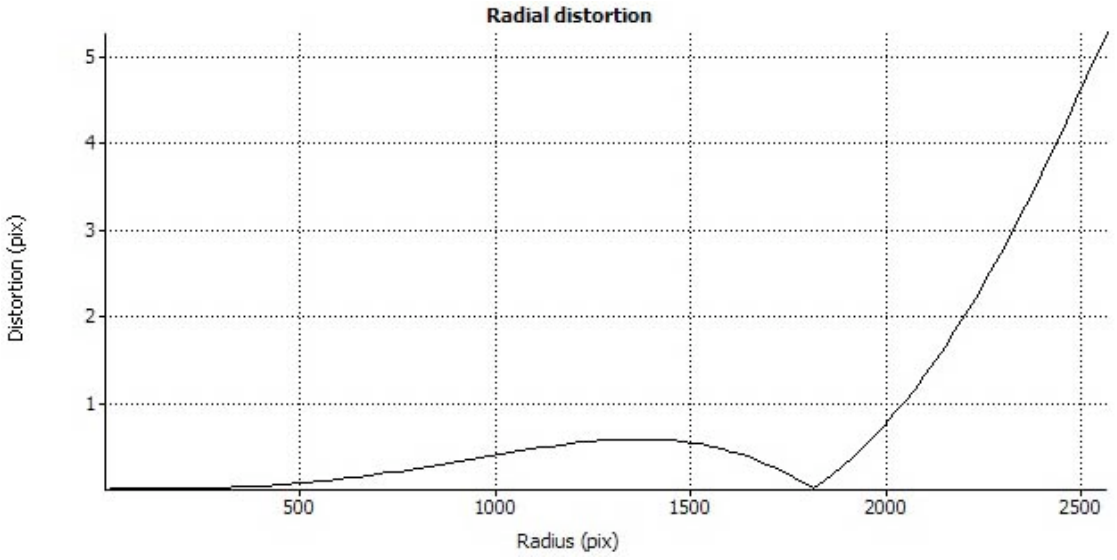

Fig. 44. Improper predicted of radial distortion for 70mm lens from images that were only taken in a horizontal position.

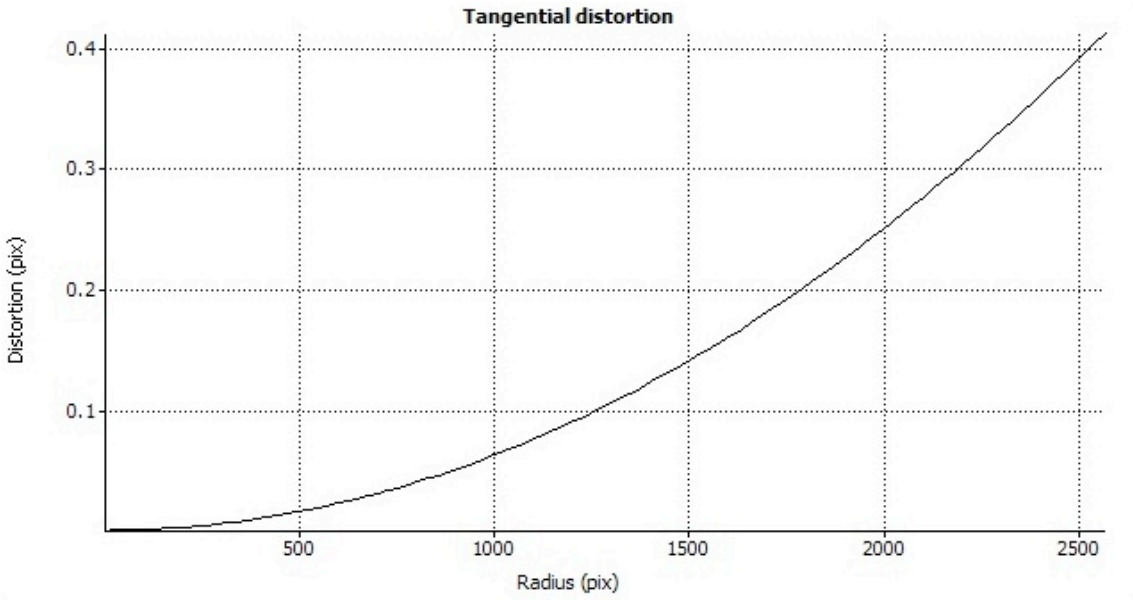

Fig. 45. Proper predicted tangential distortion for 70mm lens from images rotated approximately 180º images from one vertical side to another vertical side.

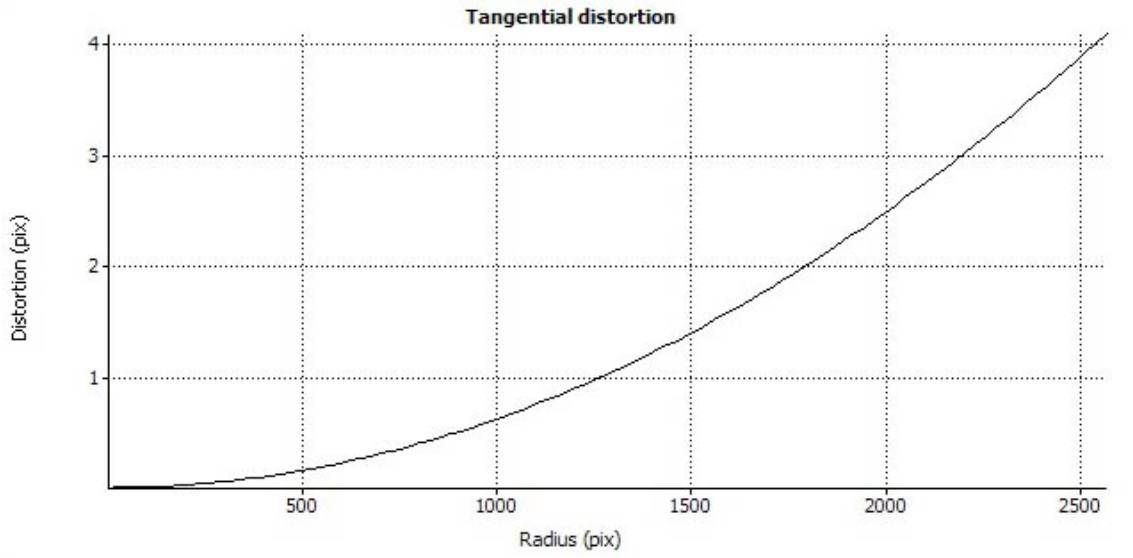

Fig. 46. Improper predicted of tangential distortion for 70mm lens from images that were only taken in a horizontal position.

DEM Generation and Accuracy Assessments

DEMs were generated for R2, R4, and R5 using a variety of lens configurations and widely varying camera positions. For R2, the DEMs were created of a single gravel bar in May 2011 and September 2011using six and nine photos, respectively, from a 70 mm lens. Twenty-nine GCPs were surveyed at R2 with ~fifteen GCPs covering each image. Initially, about fifteen images were setup for DTM processing, but these failed to create a DTM on multiple threshold settings. The number of images was reduced and image masks were introduced, eliminating a majority of each image from actual DTM processing (Fig. 47). This step provided much quicker processing and more accurate results during DTM generation despite the reduction to nine GCPs.

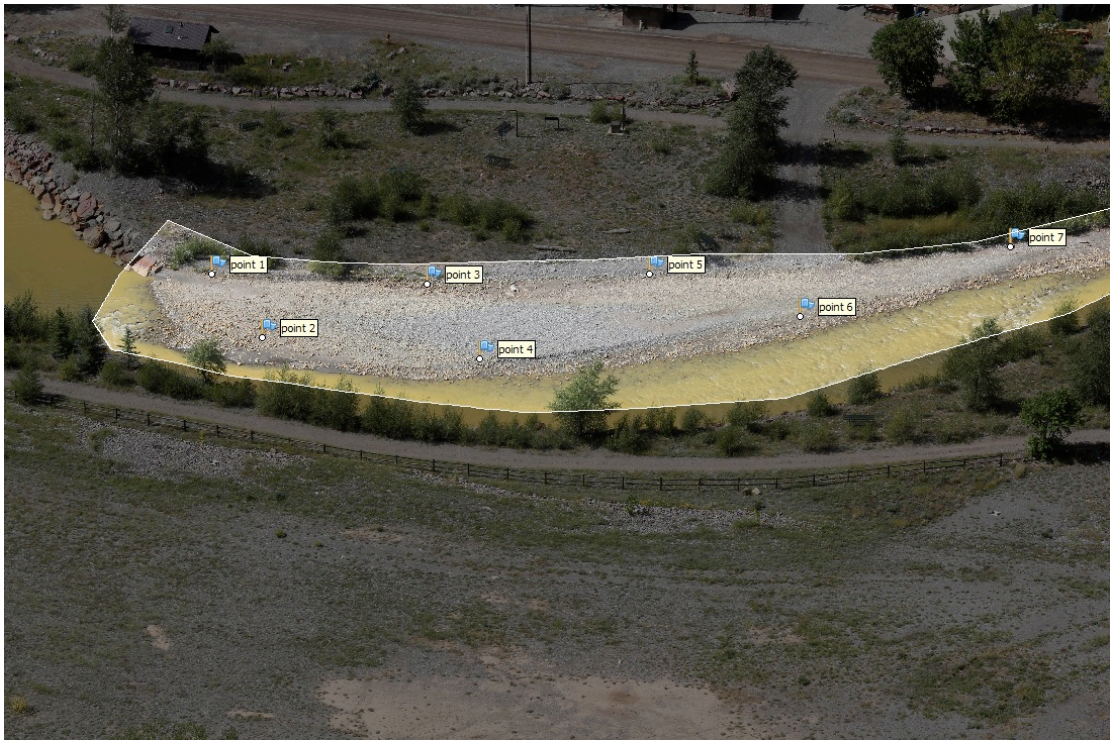

Fig. 47. Screen shot of image used in DTM processing with an image mask only covering the gravel bar. Nine ground control points (GCPs) in total were located on the gravel bar in September.

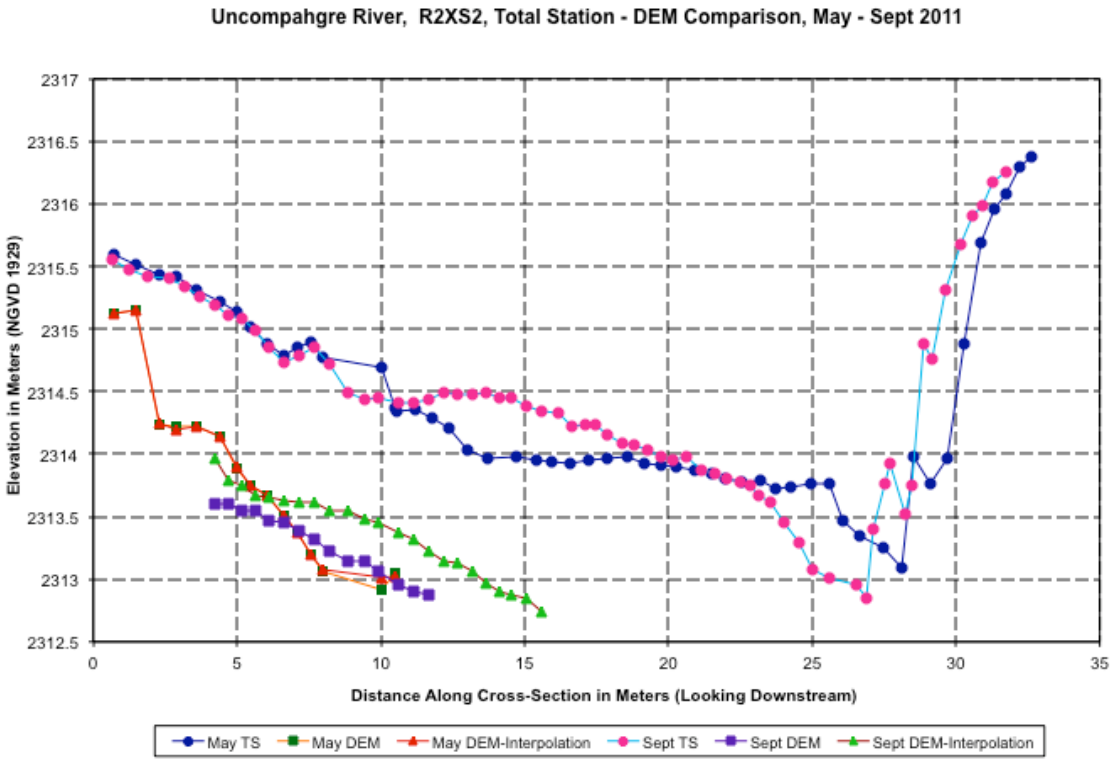

Fig. 48. Repeat cross-sectional data for R2XS2 from May 2011 and September 2011 acquired from total station surveys and DEMs produced using photogrammetric analysis.

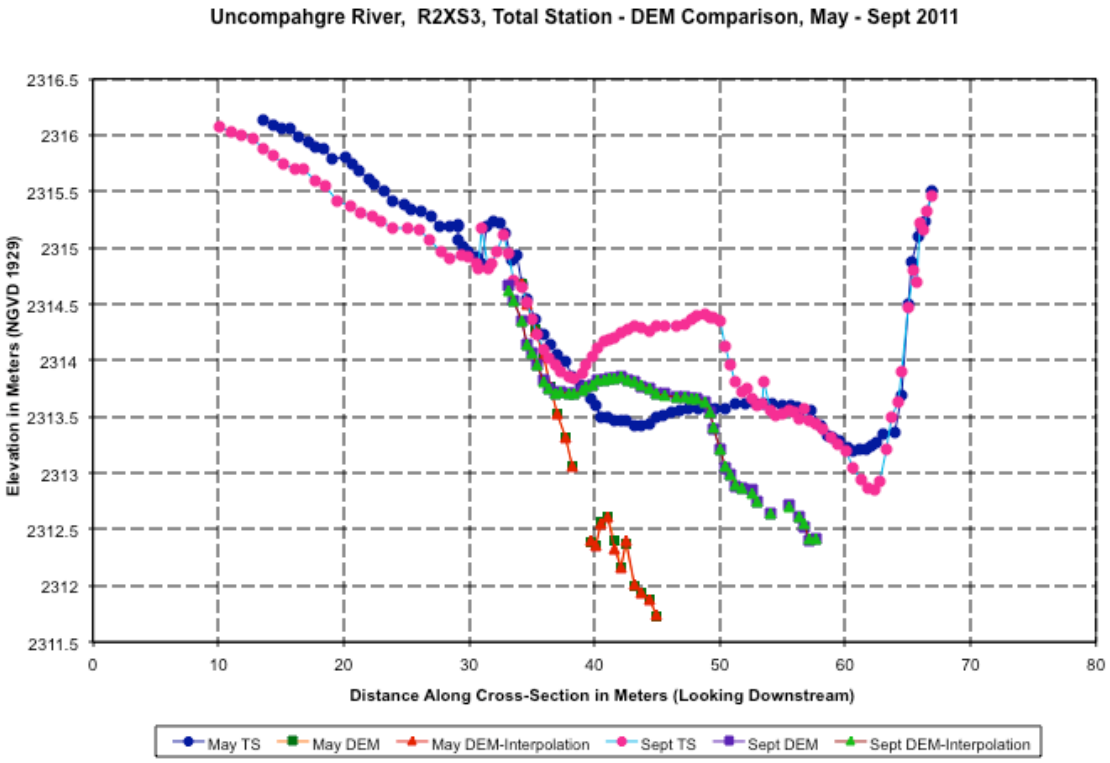

Fig. 49. Repeat cross-sectional data for R2XS3 from May 2011 and September 2011 acquired from total station surveys and DEMs produced using photogrammetric analysis.

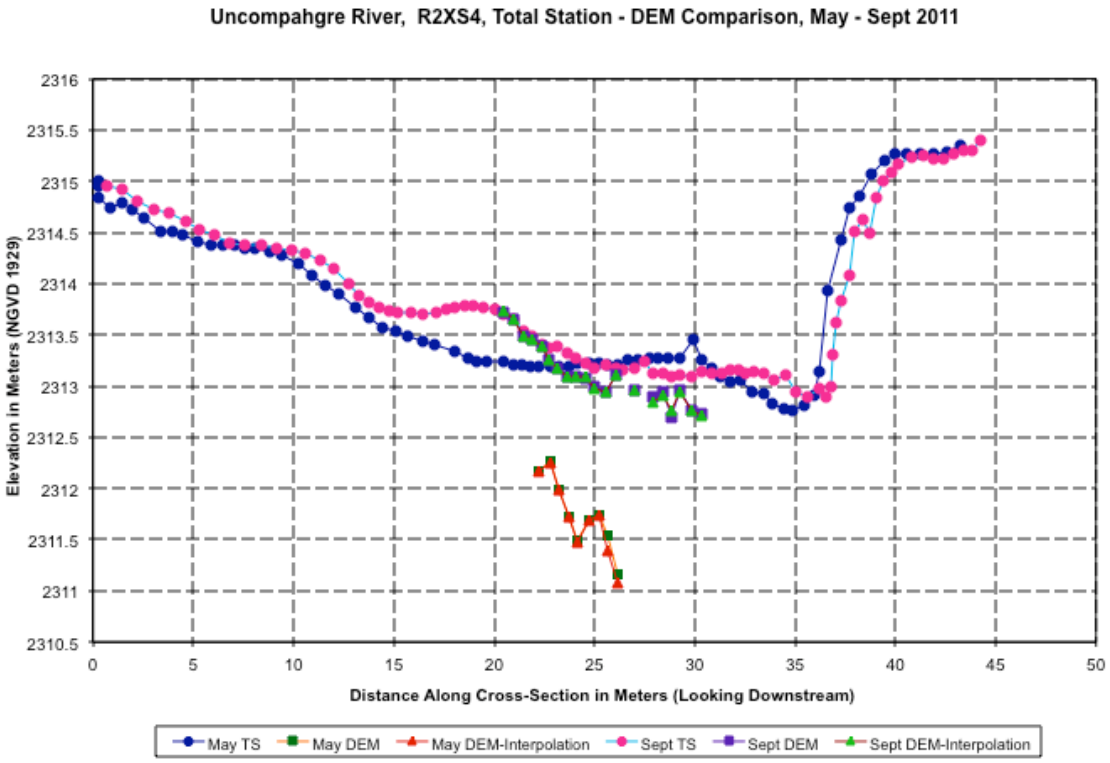

Fig. 50. Repeat cross-sectional data for R2XS4 from May 2011 and September 2011 acquired from total station surveys and DEMs produced using photogrammetric analysis.

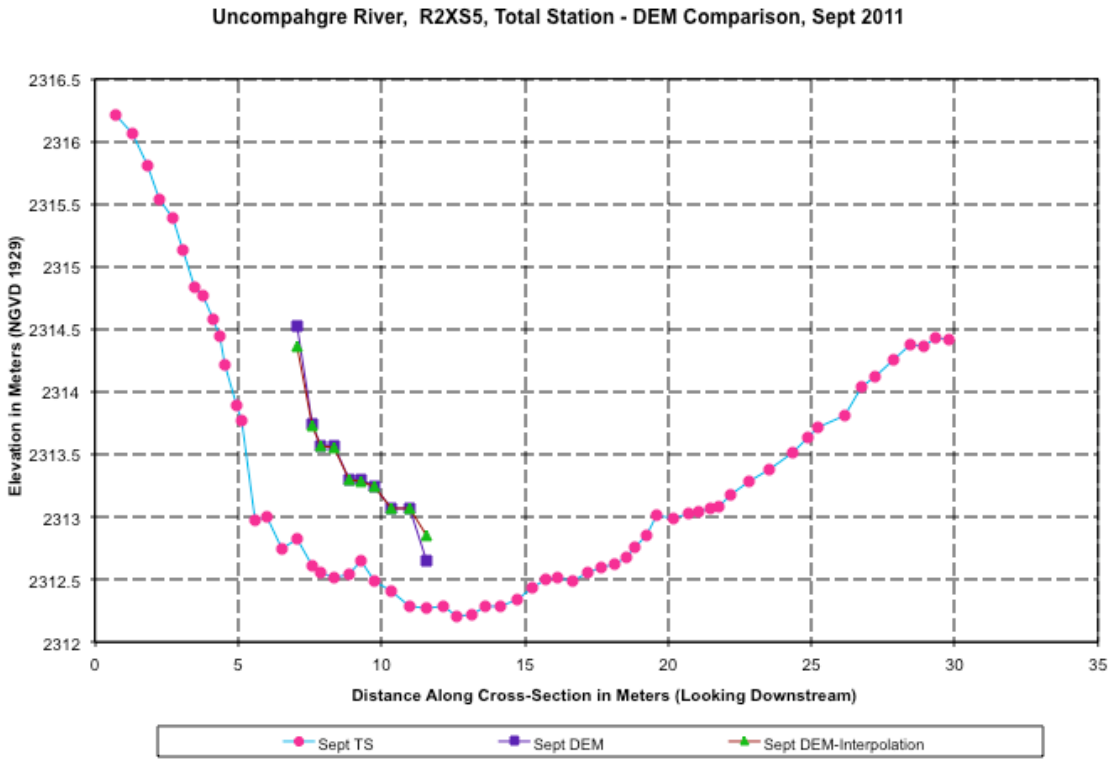

Fig. 51. Repeat cross-sectional data for R2XS5 from May 2011 and September 2011 acquired from total station surveys and DEMs produced using photogrammetric analysis.

Visual inspection of the cross-sections of the DEMs show that R2XS2 (Fig. 48.) has systematic error with elevations below true values for both DEMs whereas R2XS3 (Fig. 49.) and R2XS4 (Fig. 50.) show large errors for the DEM from May 2011 and smaller errors for the DEM from September 2011, which results in an overestimation of deposition. The gravel bar at R2 intersected R2XS5 in September 2011, but did not exist at that location in May 2011 (Fig. 51.).

Table 6 RMSE values for DTMs of R2. Averages were calculated only using the |RMSE| of control points that were actually used for DTM adjustment. These values are in bold.

		RMSE (m)			
Model Name	Point #	Total	X	Y	Z
R2 70mm May High	**point 11**	**0.171**	**0.081**	**0.026**	**0.148**
	point 12	**0.204**	**-0.125**	**-0.031**	**-0.157**
	point 13	1.180	-0.827	-0.668	-0.513
	point 14	**0.093**	**0.044**	**-0.011**	**-0.081**
	point 15	**0.092**	**0.000**	**0.017**	**0.090**
	point 16	1.930	1.421	0.966	0.879
	point 17	5.601	4.221	2.670	2.536
	Average	0.140	0.063	0.021	0.119
R2 70mm Sept High					
	point 1	6.156	-6.062	0.624	-0.871
	point 2	**0.148**	**0.088**	**0.116**	**-0.024**
	point 3	1.866	-1.848	0.151	-0.213
	point 4	5.295	5.135	-1.150	0.595
	point 5	**0.203**	**-0.081**	**-0.182**	**0.039**
	point 6	4.746	4.522	-1.384	0.406
	point 7	**0.480**	**-0.470**	**0.097**	**-0.001**
	point 8	**0.464**	**0.462**	**-0.031**	**-0.014**
	Average	0.324	0.275	0.107	0.020

The average RMSE value for the DEM in May 2011 was lower than the DEM in September 2011 (Table 6), despite the fact that fewer images were used. Redundancy in images acquired too close together could have reduced model accuracy in September 2011. Also, a single image that was acquired from a different camera station located at a much higher elevation was used for processing in the DTM in May 2011. The area where this image was acquired was not accessible in September 2011.

The average RMSE for values on the X-axis are 2-3x higher than those on the Y-axis. Because images were taken at a high oblique angle facing parallel to the X-axis, these pixels will be compressed along the X-axis whereas the horizontal Y-axis will maintain its spatial data more accurately.

DEMs created from automated image matching often contain linearly correlated and systematic errors, allowing errors to propagate easily throughout an entire DEM (Gong et al., 2000; Westaway et al., 2003). Therefore, DEMs are edited to account for these systematic errors (Gong et al., 2000). DEMs also frequently contain densely-spaced areas that contain large gross errors (Lane et al., 2003). These regions occur where complex topography, high relief, or odd textural features exist (Baily et al., 2003; Brasington et al., 2003; Gong et al., 2000). If these large gross errors are not removed when comparing DEMs, they are often assumed to be areas where large volumes of erosion or deposition occurred when they are actually the result of large gross errors (Lane et al., 2003). Large gross errors were visible outside of the bar mainly because of vegetation or shadows. DEMs were cropped to capture only the gravel bar of interest to avoid these large gross errors. In the DEM of May 2011, low-water levels and wet gravels made visual separation between water and sediment difficult. This model was cropped more carefully to avoid including large gross errors created by the water surface; however, much of the shallow water surface remains in the DEM.

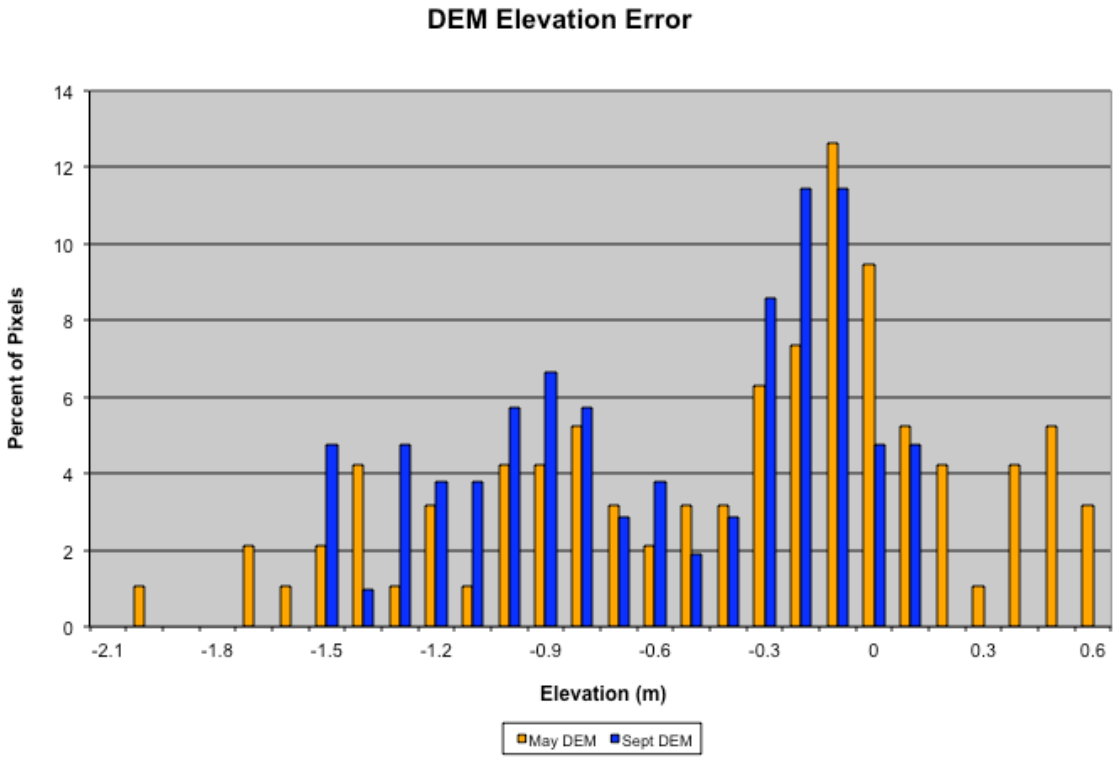

Fig. 52. Histogram of the 200 checkpoints used to determine elevation errors produced on DEMs.

Table 7
Summary of DEM error from total station checkpoints

	n	Mean error (m)	Standard deviation of errors (m)	Max absolute error (m)
May 2011	95	-0.431	0.620	2.055
Sept 2011	105	-0.519	0.553	1.592

A total of 200 checkpoints from cross-sectional surveys obtained using a total station were used to calculate errors between DEM elevation values and true elevations (Fig. 52 and Table 7). Systematic error in both DEMs has placed DEM elevation values lower than true values and has created a bimodal distribution of error values. One peak of both curves occurs just under 0 at ~-0.15 m, whereas the systematic error in both

models peaks around -1.0m, but is distributed broader throughout the DEM of May 2011. In addition, the error from the DEM of May 2011 includes large frequencies of error from 0.15 m to 0.6 m whereas the DEM of September 2011 does not include error with these values. The broader distribution of error for the DEM of May 2011 is likely a result of a shallow water surface creating localized gross errors, which is common in DTM generation near water surfaces (Westaway et al., 2003). Because water levels were higher and less gravel material was present, larger areas of water existed in May 2011 that had been replaced with gravel in September 2011, resulting in less gross errors in the DEM of September 2011.

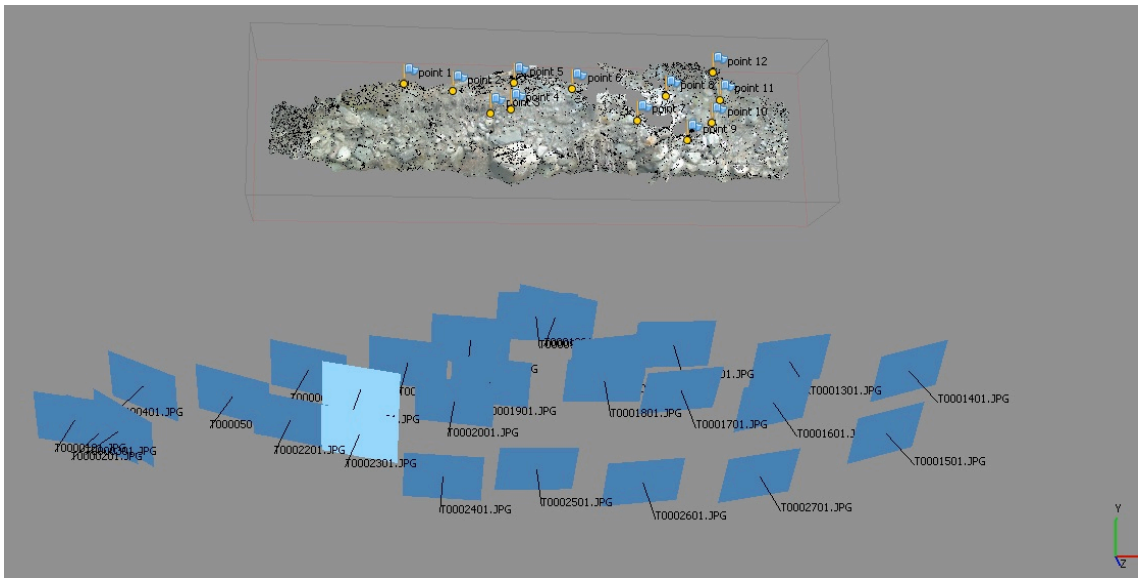

Fig. 53. Photogrammetric scene of R5 showing the riverbank and camera positions taken with a Reconyx time-lapse capsule.

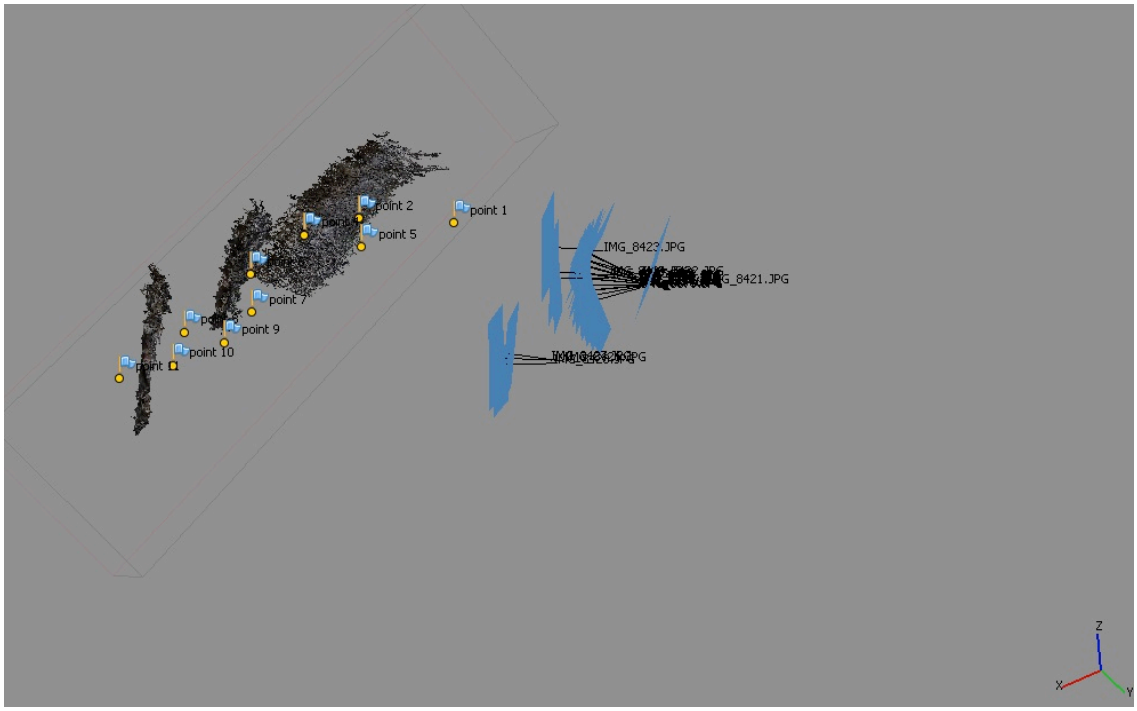

Fig. 54. Photogrammetric scene of R5 showing the riverbank and camera positions taken with a 50mm lens.

Figs. 53 and 54 show the dramatic difference in DEM quality produced from highly varied camera locations and a small number of image fans, respectively. The DEM created from image fans is composed of three separate curved planes with abundant localized gross errors. RMSE values (Table 8) were similar from both techniques, but visual inspection of the DTM created from the 50 mm lens clearly reveals incorrect terrain.

Table 8 RMSE values for both the DEM created from the Recoynx time-lapse capsule and the point cloud data generated from the 50mm lens at R5. Averages were calculated only using the |RMSE| of control points that were actually used for DTM adjustment. These values are in bold.

		RMSE (m)			
Model Name	Point #	Total	X	Y	Z
R5 Reconyx Low	**point 1**	**0.217**	**0.006**	**0.166**	**-0.139**
	point 10	2.445	0.713	-1.967	1.265
	point 11	**0.166**	**-0.094**	**-0.048**	**0.129**
	point 12	**0.228**	**0.121**	**0.004**	**-0.193**
	point 2	**0.194**	**0.019**	**-0.163**	**0.103**
	point 3	1.260	0.015	-1.033	0.721
	point 4	1.205	-0.004	-0.988	0.690
	point 5	0.499	0.020	0.426	-0.259
	point 6	**0.201**	**-0.007**	**-0.143**	**0.141**
	point 7	2.102	-0.070	-1.713	1.216
	point 8	**0.194**	**-0.044**	**0.184**	**-0.041**
	point 9	1.279	-1.096	-0.132	0.647
	Average	0.200	0.049	0.118	0.124
R5 50mm Sept Low	**point 1**	**0.371**	**0.346**	**0.130**	**-0.039**
	point 10	0.938	0.061	-0.604	0.715
	point 11	**0.242**	**0.171**	**0.110**	**-0.131**
	point 2	1.708	1.075	-1.222	0.518
	point 4	2.109	0.881	-1.641	0.988
	point 5	**0.507**	**-0.466**	**-0.199**	**0.025**
	point 6	1.618	0.676	-1.464	-0.131
	point 7	1.261	-0.734	-0.986	0.280
	point 8	**0.159**	**-0.051**	**-0.041**	**0.145**
	point 9	2.963	-2.260	1.912	-0.132
	Average	0.259	0.120	0.085	0.085

DEM Differencing

DEMs representative of time periods can be compared/overlapped to determine temporal patterns of volumetric deposition and/or erosion. Accurate measurements of volumetric change are important to understand rates of processes, which are difficult to obtain by direct measurement in gravel streams (Lane et al., 2003). When comparing any two models, the initial error associated with each data set must be known because the final observation will also contain those errors. Volumetric sediment budgets will be

twice as sensitive because two DEMs are used and each model will incorporate its own error into the final quantities measured (Brasington et al., 2003).

A primary goal for any 4-dimensional geomorphic study is to appropriately identify a statistically, reliable threshold of change detection for assessing the geomorphologic process of interest because this threshold will determine the precision and accuracy of the process being measured (Brasington et al., 2003). Random error exists in all experimental studies and is usually eliminated by obtaining a high signal to noise ratio. For DEM-volume calculations, random error associated with any two given points generated in a DEM can be calculated using equation 18 (Lane et al., 2003):

$$\sigma_c = \sqrt{(\sigma_1^2 + \sigma_2^2)} \tag{20}$$

where:

σ_c = Uncertainty in Magnitude of Change,
σ_1 = Uncertainty in point 1 of DEM, and
σ_2 = Uncertainty in point 2 of DEM.

Equation 18 is most often used to identify background noise in DEMs, so that random error can be removed by eliminating all values above a selected threshold. The value of this threshold can be chosen using the t-statistic in equation 19 (Lane et al., 2003), which shows if a single point within a DEM is statistically significant by creating a ratio between the value of change and the error associated with that change:

$$t = \frac{z_1 - z_2}{\sqrt{\sigma_1^2 + \sigma_2^2}} \tag{21}$$

where:

t = t statistic,
$z_1 - z_2$ = Difference in Elevation,
σ_1 = Uncertainty in point 1 of DEM, and
σ_2 = Uncertainty in point 2 of DEM.

Equation 19 was applied to sixty pixels from DEMs using uncertainties derived from actual elevations as determined by points from cross-sections that had been surveyed in both May 2011 and Sept 2011. Of the sixty pixels, eleven pixels had t-statistics lower than one, making 81% of the pixels statistically significant.

Without uncertainties of the exact same location on both DEMs, the actual t-statistic for that pixel cannot be determined. Instead, an approximation was calculated using the mean uncertainties from all 200 checkpoints to create an entire t-statistic filter across the entire DEM of change, which resulted in a t-statistic raster from equation 20. This resulted in only 51% of pixels being statistically significant, which suggests that applying the mean error to an entire data set exclude pixels that are actually statistically significant because when this was tested on sixty pixels using the unique error value of each pixels for the same location, 81% of the pixels were statistically significant.

$$t_{Raster} = \frac{z_{DEMSept} - z_{DEMMay}}{\sqrt{(\sigma_{meanSept})^2 + (\sigma_{meanMay})^2}} \quad (22)$$

Pixels with values from -1 to 1 were used as a filter on the DEM of change to calculate a statistically significant DEM of change.

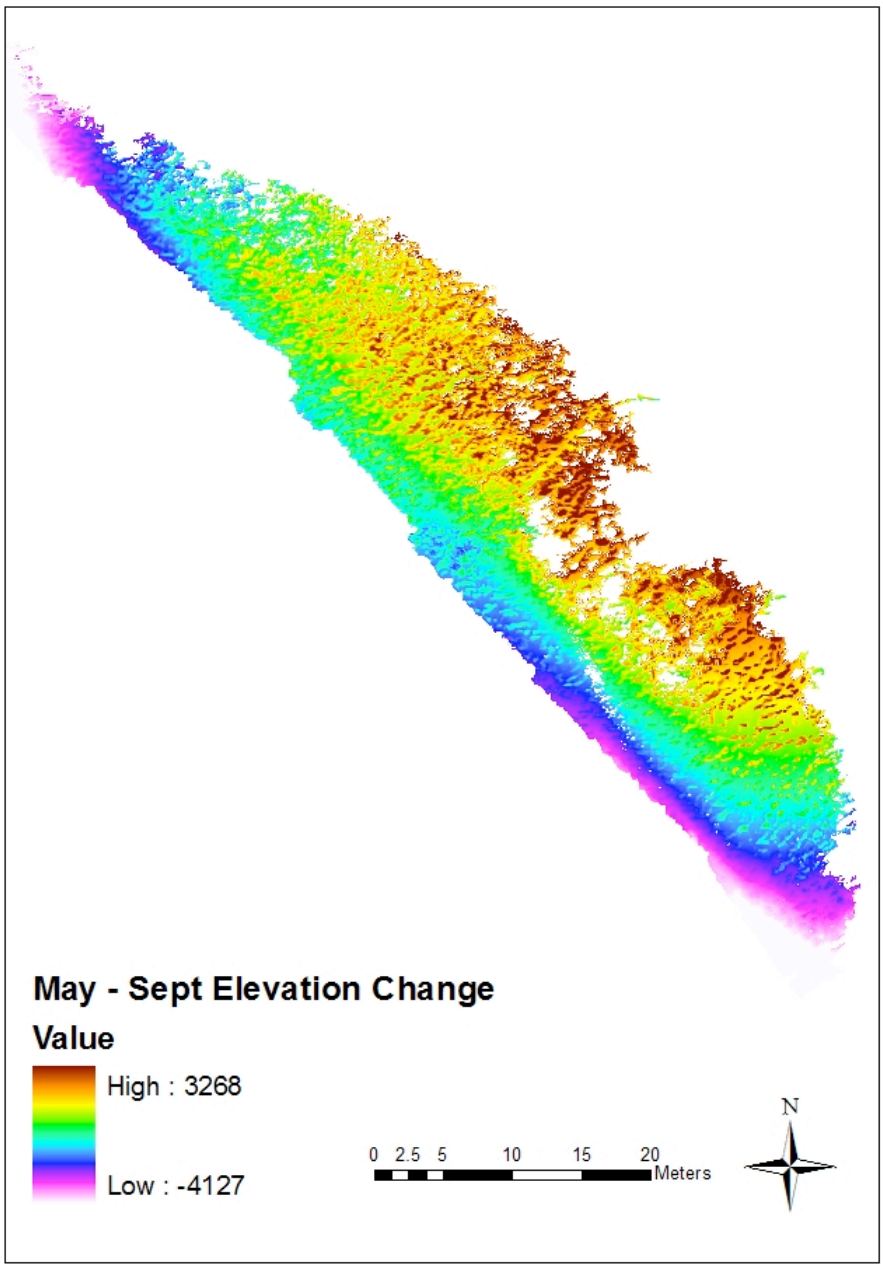

Fig. 55. Raw DEM of difference from May 2011 to Sept 2011.

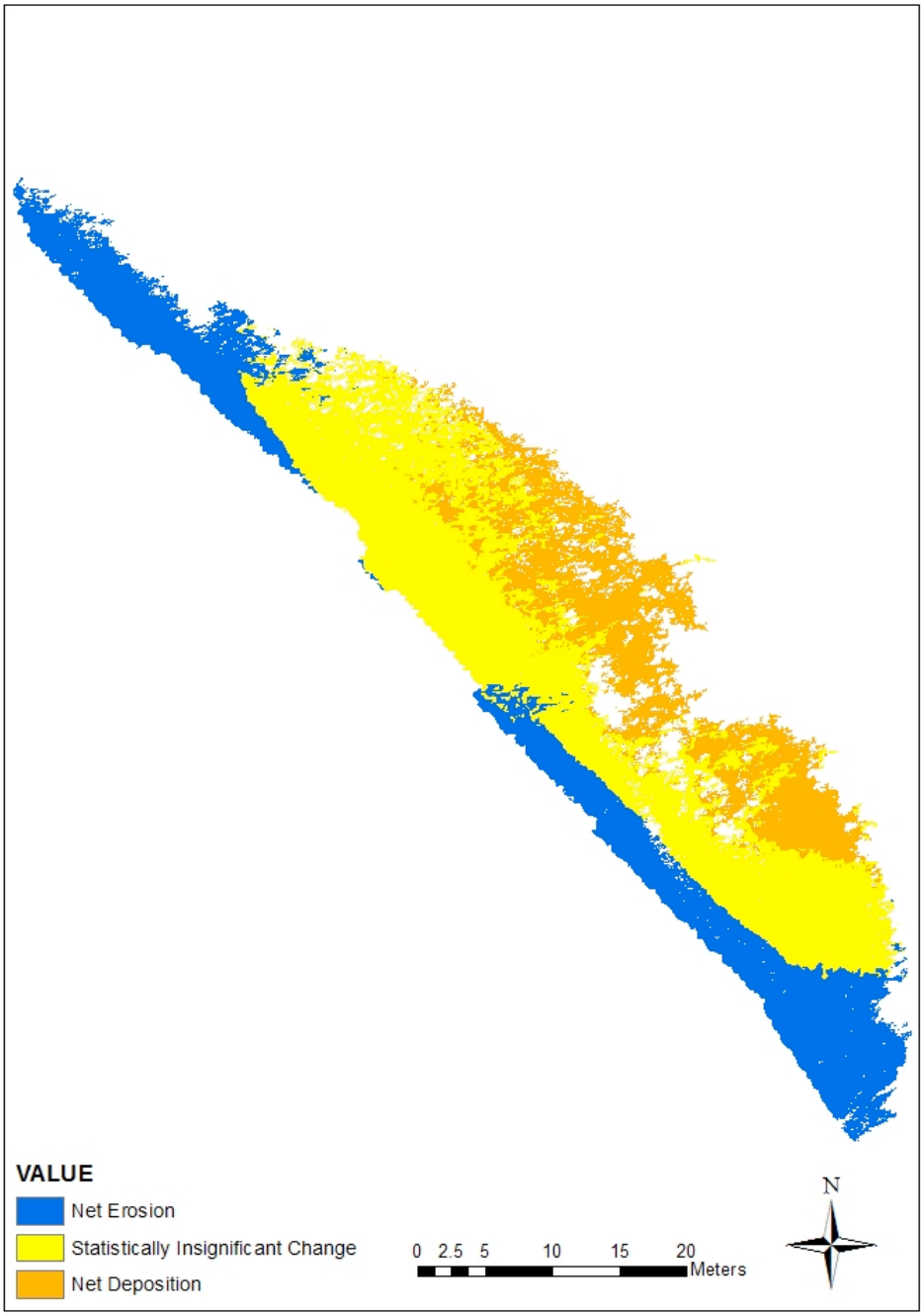

Fig. 56. Classifications of the t-statistic filter created from equation 20.

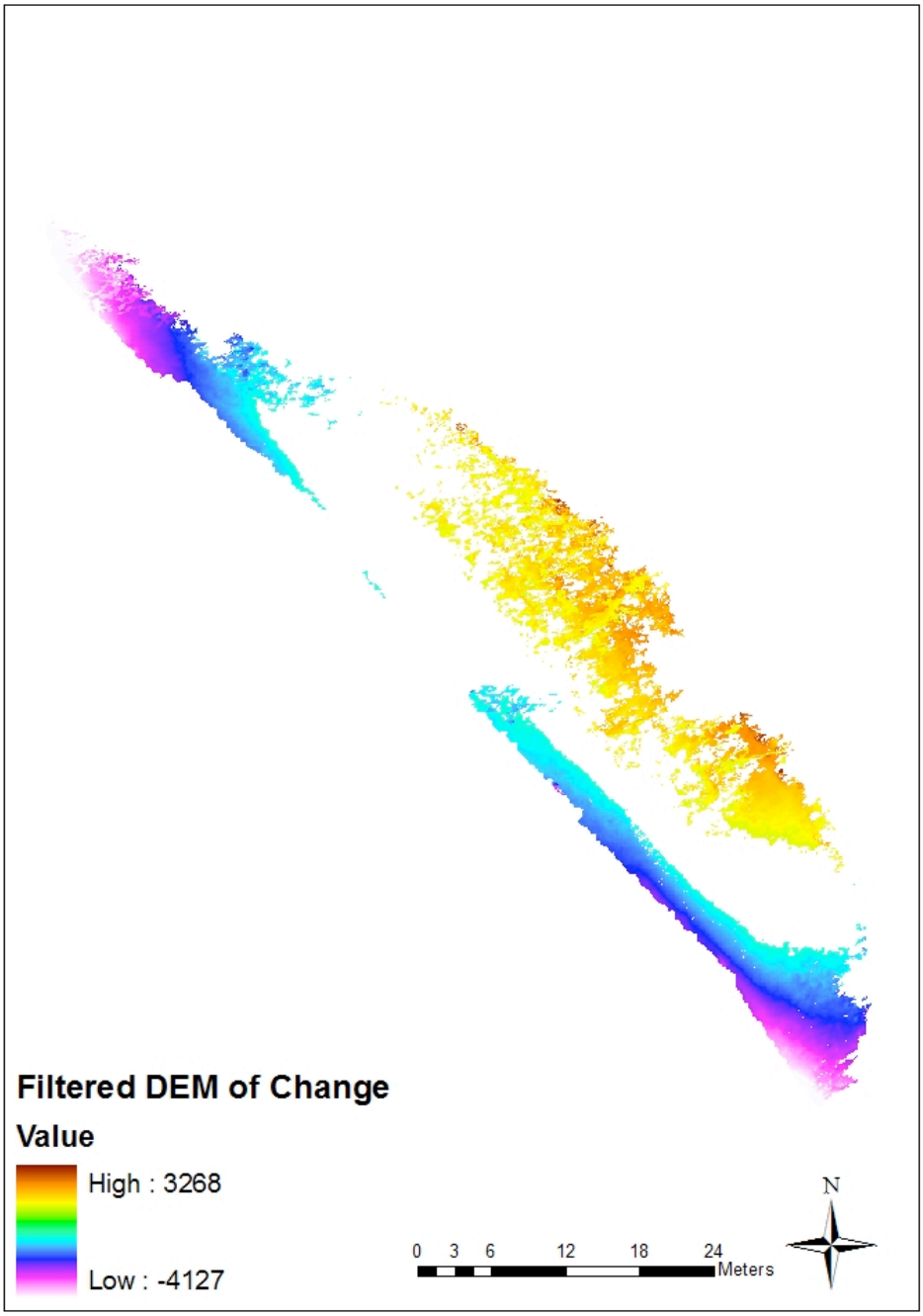

Fig. 57. DEM of difference from May 2011 to Sept 2011 after applying the t-statistic filter in Fig. 56.

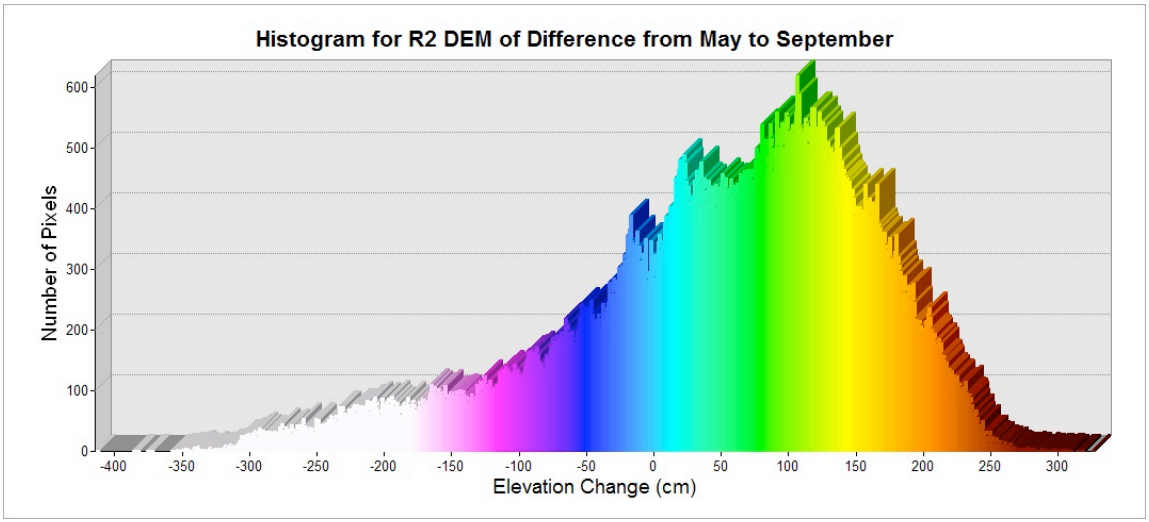

Fig. 58. Histogram of DEM of change at R2 showing the distribution a pixel values in terms of frequency and elevation.

Pixel values of the unedited DEM of change (Fig. 55) were summed to determine the net volume change, which was determined to be 440m^3. After applying the t-statistic threshold filter (Fig. 56) to the DEM of change, a statistically significant DEM of change was created (Fig. 57), which yielded a net deposition of 115m^3. In addition, the distribution of elevation changes across the gravel bar was determined from the filtered DEM of change showing that an area of 272m^2 contained erosion and an area of 215m^2 contained deposition. These values show that although the material deposited was greater in quantity, it was distributed around a smaller area and erosion occurred across a larger area in smaller quantities. This distribution is present in the histogram of the DEM of difference (Fig. 58).

As predicted, systematic errors in DEMs from May 2011 and September 2011 although similar, exaggerated net deposition. Regardless, a DEM of change containing statistically insignificant data can still provide an extensive map that identifies the spatial distribution of elevation change.

DEMs were also created at R4 to gather a better estimate of erosion and deposition of a vertical stream bank. Photographs were obtained using a fixed 50 mm lens and a 70 mm lens in May 2011 and September 2011, however, control points that were surveyed for both locations were not synchronized efficiently. The benchmarks used were located at a large distance from the actual control points used in the images, which introduced significant amounts of error during DEM alignment. Despite having two unsynchronized coordinate systems, DEMs of change were created for models of the same time period using the fixed 50mm and 70mm lenses. Although quantitative results of erosion and deposition cannot be measured, DEMs of change can still reveal where models are more likely to exhibit errors (Fig. 59.).

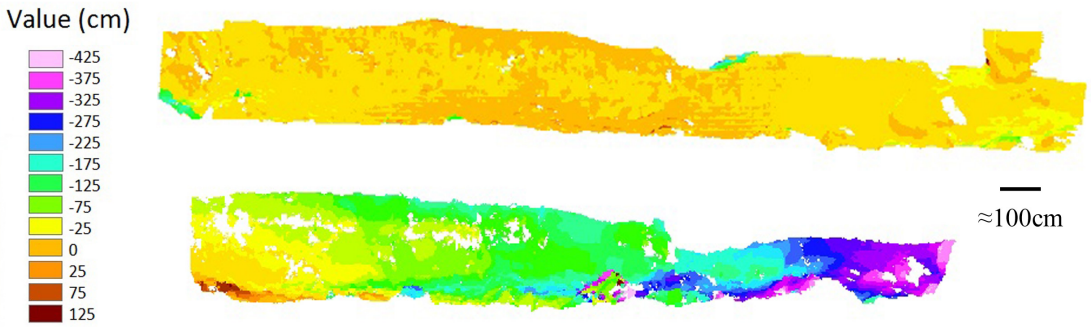

Fig. 59. DEM of difference of R4 obtained using a fixed 50mm and a 70mm lens in May 2011 (Top) and Sept 2011 (Bottom).

The DEM of difference created in May 2011 has a much broader area that exhibits little change between the two types of lenses whereas the DEM of difference created in September 2011 shows larger quantities and more dispersed error (Fig. 60.). This error is attributed to the reduced number of camera positions. Like aerial photogrammetry, photographs used for terrestrial photogrammetry should be acquired from many positions, but obstructions may prevent ideal photogrammetric conditions.

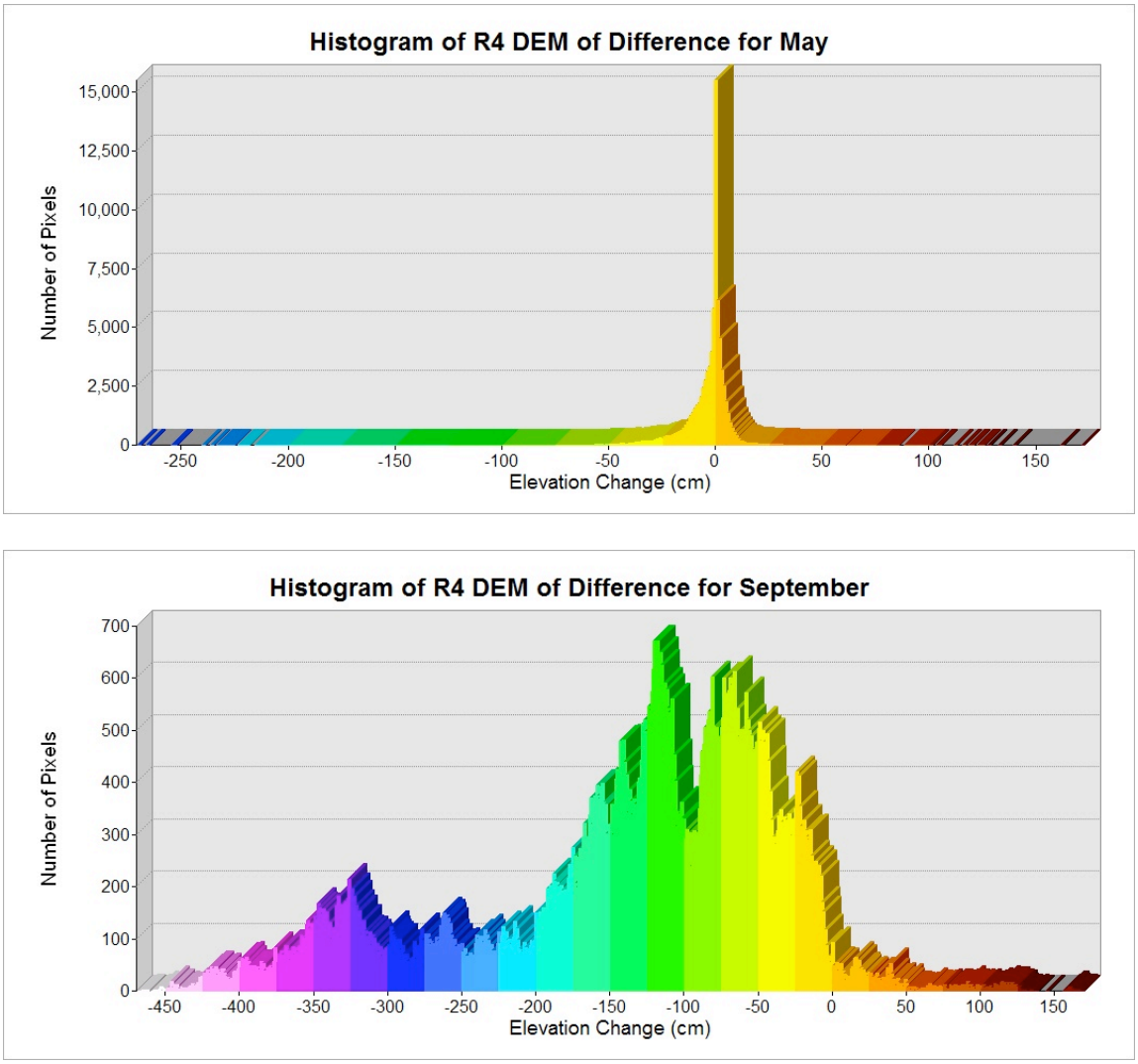

Fig. 60. Histograms of DEM of Difference from R4 showing that models created in May 2011 contain much less error than DEMs created in September 2011.

Discussion

Potential Improvements

Terrestrial photogrammetry has fundamental differences when compared to aerial photogrammetry, which present new challenges for obtaining photographs. Both concepts should be known well in theory *and* practice well before entering the field so that the best camera orientations can be used and accuracy of models can be maximized. Camera calibration and a test photogrammetric analysis should be the first step with a practice scene with ideal camera positions, GCPs, lighting, and good texture of the object being modeled. This step was not completed and caused less than ideal data to be collected. Familiarity with custom camera settings is necessary as picture quality is highly dependent on weather conditions, which change rapidly in alpine areas.

Fluency with the software package in which image analysis will be performed should also be accomplished before image acquisition. Typical software packages for remote sensing are fundamentally different in that all calculations are based on data acquired completely perpendicular to the land surface. These packages have still been used by applying coordinate transformations (Chandler, 1999), but extreme oblique imagery with insufficient accuracies of camera position make successful DTM creation difficult. As a user, the ability to fluently navigate detailed software packages is necessary and required to obtain the best results. Because some programs also require different input data than others, familiarity with the exact software to be used for analysis will help ensure that the proper data are collected in the field. If it is determined that more images need to be collected after leaving the field, acquiring more images

requires more time, money, and for some applications will not be valid because geomorphic change has already occurred.

The ability to create image masks for photogrammetric photographs is an advantage in oblique terrestrial photogrammetry because visual obstructions are frequently encountered. Even if a majority of the image is blocked by vegetation for example, if the AOI can be clearly seen, then the photograph can be used. This advantage can be utilized to obtain more images at different locations rather than creating image fans at a single location. More images would have been attempted in areas where trees were obstructions, but may not have prohibited good image acquisition for the AOI. Also, knowing that image masks can be applied, control points should be more densely focused around the AOI rather than dispersed throughout the entire view of the image.

Last, high-resolution sensors do not necessarily return better DTMs as one might expect. As was the case with DTMs created at R5, a lot of images at similar locations acquired with an 18MP sensor yielded poorer results than images acquired from a time-lapse capsule with a 3.1MP sensor at many different positions (Fig. 61.).

Fig. 61. 18MP Sensor from Canon Rebel T2i (Left) vs 3.1MP Sensor in Reconyx time-lapse capsules (Right). Even though image quality is poorer and resolution is lower, the images from the Reconyx capsules created a more accurate DTM.

Benchmarks used to synchronized data should be located as close as possible to the control points being surveyed. Finding a location for benchmarks can be difficult in areas where large quantities of change are probable because benchmarks need to remain stationary to remain valid.

Further analysis of photographs would be used to create a classification map to identify the exact water levels and geomorphic changes of the gravel bars related to clast size. In addition, studies in the past (Carbonneau, 2005; Carbonneau et al., 2004; Dugdale et al., 2010) have been used to create clast-size distributions of gravel bars from aerial images. Applying this concept to oblique images may yield yet another use of terrestrial photographs for making quantitative measurements.

Limitations

Whereas other technologies, such as lidar, exist that can obtain higher resolutions, this is often offset by very expensive operational costs. Although photogrammetry may be one the best mapping technologies available, it has its

limitations. New automated image matching algorithms save time, but sometimes produce significant systematic and gross errors, which require manually editing by the user. Eliminating these errors properly may require a moderate to high level of software fluency by the user. Therefore, time saved in the field is often replaced by extensive time using post-processing software, so that raw DEMs can be corrected to produce a more accurate final product.

For all photogrammetric studies, the geometry of camera positions relative to the object(s) being modeled must follow baselines rules. Traditional aerial photography becomes an easy process because aircraft can typically be moved in all three dimensions. Terrestrial photogrammetry of the land surface, however, is limited by elevation. Without the use of ladders, buildings, cliffs, etc. to achieve higher ground position, one must find objects that are oriented vertically to analyze.

Broader Impacts

The ability to easily calibrate cameras with unknown or limited EXIF metadata included in the images could allow new devices, like camera phones, to be calibrated and potentially create 3D models. Creating 3D models using camera phones is highly desirable because camera phones are very compact and many contain GPS devices that could provide useful data if attached to an UAV, kite, balloon, as has been done to provide very high-resolution imagery of events such as the BP Deepwater Horizon Oil Spill with compact consumer grade point-and-shoot cameras. This approach adds

versatility to studies where satellites or aerial photography may not be available or affordable (Dosemagen, 2010).

In addition, advances in computer processing have made DTM processing times shorterer. With the development of software becoming more and more automated, mass quantities of DEM data could be produced to create time-lapse videos of DEMs of change with a short-temporal resolution. 4D models can be used to study geomorphic processes that occur frequently, but do not require high-spatial resolution, so that processes could be observed without overcollecting massive quantities of data.

Conclusions

This paper has shown that terrestrial photogrammetry can be successfully used for change detection of a variety of areas within an alpine stream. DTMs were generated of a gravel bar from extreme oblique photographs (i.e. 64º from nadir) captured from nearby cliffs. Total RMSE values were 0.140 m and 0.324 m for DTMs from May 2011 and September 2011, respectively. RMSE values in the oblique direction were approximately three times larger than RMSE values in the across photograph direction.

Systematic errors existed in DEMs created in May 2011 and September 2011, whereas random errors were more prominent in the DEM from May 2011, which were attributed to difficulties estimating elevations through the water surface. A t-statistic filter was applied to the entire DEM of change using mean error values from ~100 control points for each DEM, which resulted in 51% of pixels remaining statistically significant. Applying the same t-statistic, using exact error values for sixty points from

cross-sections performed on the gravel bar to individual DEMs, showed that 81% of the points were statistically significant showing that error throughout the model varies.

A net deposition of 115 m^3 was calculated to be statistically significant for the DEM of difference from May 2011 to September 2011 on a gravel bar above a dynamic water level. Whereas deposition was larger, it was also more concentrated closest to the meander. Erosion on the other hand, was distributed over a much broader surface area on both sides of the bar.

CRP was performed at two sites downstream from restoration on two banks using different image sensors and camera position setups. DEMs of difference were created from images gathered at focal lengths of 50 mm and 70 mm for May 2011 and September 2011. Both models were created with a panoramic fan technique using four stations in May 2011 and two stations in September 2011. Using only two camera stations yielded higher RMSE errors in DTMs, and the distribution of errors showed minimal errors in the middle of the DTM and large errors propagating toward the edges. Errors from models created using four camera stations were much more limited, but larger errors also tended to occur on the edges of models; however, surfaces perpendicular to the direction of the lens were very small whereas slopes and complex surfaces exhibited higher error values.

A time-lapse capsule with an 8.5 mm lens and a 3.1MP sensor was used to create a DTM using 27 photographs, all of which were captured at different positions ~1 m apart. A consumer grade camera with a 50 mm lens was used to create a DTM of the same area using 25 photographs taken primarily from two camera stations. Although the

photographs taken with the larger image sensor have the potential for creating a more accurate DTM, the limited camera positions prevented successful DTM creation. Despite large distortions created from short focal lengths, limited details from low-resolution photographs, and large quantities of noisy pixels, an accurate DTM was successfully generated using a time-lapse capsule. Expanding DTM generation using images from unconventional sensors like camera phones or point-and-shoot cameras may provide more flexibility in creating low-resolution DTMs for other applications outside of geomorphology.

Time-lapse capsules were also used to capture photographs on a sub-daily interval from two stationary positions, from May 2011 to September 2011, downstream from the modified channel. Although drastic changes in discharge were observed, no visual indicators of bank erosion was seen. Time-lapse capsules still have the potential to capture geomorphic change from individual flows, but predicting changes at locations that have sufficient geometry for permanent camera setup, without encountering human disturbance, is difficult and needs to be overcome on a case-by-case basis.

The results of this study have provided a better understanding of the quantitative changes of elevations of a gravel bar in a modified alpine stream and the feasibility of terrestrial photogrammetry using consumer-grade cameras. The findings from this study show that camera geometries and image sensors that do not follow the original recommendations for aerial photogrammetry can still generate accurate DTMs sufficient for quantitative analysis, provided that images are acquired at more than two different camera stations with adequate separation.

CHAPTER IV

DISCUSSION

Broader Impacts

For river stabilization or restoration projects in alpine areas that are designed to imitate a meandering stream, it may be beneficial to design the channel slope and sinuosity near previously determined thresholds (Schumm and Khan, 1972). This important consideration will help limit deposition in the modified channel, which reduces the potential for erosion downstream.

The ability to easily calibrate cameras with unknown or limited EXIF metadata included in the images could allow new devices, like camera phones, to be calibrated and potentially create 3D models. Creating 3D models using camera phones is highly desirable because camera phones are very compact and many contain GPS devices that could provide useful data if attached to an UAV, kite, balloon, as has been done to provide very high-resolution imagery of events such as the BP Deepwater Horizon Oil Spill with compact consumer grade point-and-shoot cameras. This approach adds versatility to studies where satellites or aerial photography may not be available or affordable (Dosemagen, 2010).

In addition, advances in computer processing have made DTM processing times shorterer. With the development of software becoming more and more automated, mass quantities of DEM data could be produced to create time-lapse videos of DEMs of

change with a short-temporal resolution. 4D models can be used to study geomorphic processes that occur frequently, but do not require high-spatial resolution, so that processes could be observed without overcollecting massive quantities of data.

Limitations

Scientific studies can be performed at a wide variety of spatial scales, as well as temporal scales. In fluvial geomorphology, especially, conclusions of a single case study may reveal results that are contrary to results from streams that have similar locations, environments, characteristics, etc. Therefore, it is important that the results of this study are not widely assumed to apply for stream studies at a different spatial scale. The data in this study were primarily obtained at a cross-section to reach-scale and compared to other cross-sections or reaches in other areas of the stream. The conclusions of a fluvial geomorphology study on a reach-sized scale may agree and show trends with other rivers in a similar geographical context on a similar scales, but applying or even assuming these conclusions to be true for rivers in different environments or over larger scales could be misleading.

Alpine rivers, especially those near the headwaters are very heterogeneous. It should be noted that the equations that were used to calculate shear stress have underlying assumptions (Lorang and Hauer, 2003) such as uniform flow, that are not always valid for alpine streams.

Whereas other technologies such as lidar exist that can obtain higher resolutions, this is often offset by very expensive operational costs. Although photogrammetry may

be one the best mapping technologies available, it has its limitations. New automated image matching algorithms save time, but sometimes produce significant systematic and gross errors, which require manually editing by the user. Eliminating these errors properly may require a moderate to high level of software fluency by the user. Therefore, time saved in the field is often replaced by extensive time using post-processing software, so that raw DEMs can be corrected to produce a more accurate final product.

For all photogrammetric studies, the geometry of camera positions relative to the object(s) being modeled must follow baselines rules. Traditional aerial photography becomes an easy process because aircraft can typically be moved in all three dimensions. Terrestrial photogrammetry of the land surface, however, is limited by elevation. Without the use of ladders, buildings, cliffs, etc. to achieve higher ground position, one must find objects that are oriented vertically to analyze.

Future Recommendations

The largest difficulty of fieldwork for this study was identifying and actually surveying cross-sections. Most areas in the modified stream were shallow enough to allow crossing with waders; however, the natural channel presented some challenges even during low flows around 1.42 m^3/s. In May, daily discharges started around 1.42 m^3/s in the morning and peaked around 5.66 m^3/s only hours later, making surveys impossible to perform without high risk of injury. Data collection for cross-sections was, therefore, limited to daylight hours in the early morning, which was also the time of the

day that had the best lighting conditions for all terrestrial photographs (See Chapter III). In addition, dramatic shifts in weather patterns made fieldwork even more difficult to complete. For example, it snowed about 10 cm one day and the next day it was sunny and 21 ºC. The ability to perform more cross-sectional surveys directly upstream of the human-modified channel and at more locations within the modified channel could provide a better understanding between geomorphic changes, shear stress, and reach location.

Camera calibration and a test photogrammetric analysis should be done first with a practice scene with ideal camera positions, GCPs, lighting, and good texture of the object being modeled. This step was not completed and resulted in less than ideal data to be collected. Terrestrial photogrammetry has fundamental differences when compared to aerial photogrammetry, which present new challenges for obtaining photographs. Both concepts should be known well in theory *and* practice well before entering the field, so that the best camera orientations can be used and accuracy of models can be maximized. Familiarity with custom camera settings is necessary as picture quality is highly dependent on weather conditions, which change rapidly in alpine areas.

Fluency in the exact software package in which image analysis will be performed should also be obtained before image acquisition. Typical remote sensing software packages are fundamentally different in the fact that all calculations are based on data acquired completely perpendicular to the land surface. These packages have still been used by applying coordinate transformations (Chandler, 1999), but extreme oblique imagery with insufficient accuracies of camera position make successful DTM creation

difficult. As a user, the ability to fluently navigate detailed software packages is necessary and required to obtain the best results. Because some programs also require different input data than others, familiarity with the exact software to be used for analysis will help ensure that the proper data are collected in the field. If it is determined that more images need to be collected after leaving the field, acquiring more images requires more time, money, and for some applications will not be valid because geomorphic change has already occurred.

The ability to create image masks for photogrammetric photographs is a huge advantage in oblique terrestrial photogrammetry because visual obstructions are frequently encountered. If a majority of an image is blocked by vegetation for example, if the AOI can be clearly seen, then the photograph can be used. This advantage can be utilized to obtain more images at different locations rather than creating image fans at a single location. More images would have been attempted in areas where trees were obstructions, but may not have prohibited good image acquisition for the AOI. Also, knowing that image masks can be applied, control points should be more densely focused around the AOI rather than dispersed throughout the entire view of the image.

Last, higher resolution sensors do not necessarily return better DTMs as one might expect. As was the case with DTMs created at R5, a lot of images at similar locations acquired with an 18MP sensor still yielded poor results than images acquired from a time-lapse capsule with a 3.1MP sensor at many different positions. Benchmarks used to synchronized data should be located as close as possible to the control points being surveyed. Finding a location for benchmarks can be difficult in areas where large

quantities of change are probable because benchmarks need to remain stationary to remain valid.

Further analysis of photographs would be used to create a classification map to identify the exact water levels and geomorphic changes of the gravel bars related to grain size. In addition, studies in the past (Carbonneau, 2005; Carbonneau et al., 2004; Dugdale et al., 2010) have been used to create clast-size distributions of gravel bars from aerial images. Applying this concept to oblique images may yield yet another use of terrestrial photographs for making quantitative measurements.

CHAPTER V

CONCLUSIONS

Summary

River Restoration

The river restoration project in Ouray, CO, decreased the overall slope of the river and increased the sinuosity of the river for the portion that was modified. Meandering streams typically deposit large quantities of material fine-grained material that has traveled long distances from its source. Creating an artificial meandering stream in an alpine environment forces deposition of large gravel and cobbles as bars. However, deposition of material in the modified channel reduces the quantity of bedload material and suspended sediment, which could potentially increase erosion downstream because water that was once carrying sediment now has more power to erode and transport sediment.

Pebble counts show a large increase in the abundance of fine-grained sediment (<4mm) at R1 from May 2011 to September 2011, while all sites in September 2011 show a decrease in the abundance of fine-grained sediment as one moves downstream. The decrease in abundance of fine-grained sediments at R5 from May 2011 to September 2011 also supports the possibility of suspended sediment decreasing from deposition in the modified channel, which would increase the potential suspended sediment capacity downstream. Although this process may be occurring in the

Uncompahgre River, tracking individual grains and taking water samples to measure suspended sediment should confirm this. If the modified channel is not dredged annually, deposition in the modified channel may decrease, which may decrease erosion downstream.

Terrestrial Photogrammetry

This paper has shown that terrestrial photogrammetry can be successfully used as a method of measuring volumetric change for a variety of areas within an alpine stream. DTMs with total RMSEs of 0.140 m and 0.324 m for May 2011 and September 2011, respectively were generated of a gravel bar from extreme oblique photographs (i.e. 64º from nadir) captured from nearby cliffs. RMSE values in the oblique viewing direction were approximately three-times larger than RMSE values in the across photograph direction.

Systematic errors existed in DEMs created in May 2011 and September 2011, whereas random errors were more prominent in the DEM from May 2011, which were attributed to difficulties estimating elevations in and around a water surface.

A t-statistic filter was applied to the entire DEM of change using mean error values from about 100 control points for each DEM, which resulted in only 51% of pixels remaining statistically significant. Applying the same t-statistic using exact error values for sixty points from cross-sections performed on the gravel bar to individual DEMs showed that 81% of points were statistically significant, showing that error throughout the model varies considerably.

A net deposition of 115 m^3 was calculated to be statistically significant for the DEM of difference from May 2011 to September 2011 on a gravel bar above a dynamic water level. Deposition was larger, it was also more concentrated closest to the meander whereas erosion was distributed over a much broader surface area on both sides of the bar. Whereas net deposition on the gravel bar was visually observed in the field, broader areas of erosion were not observed and would have otherwise been unnoticed.

CRP was performed at two sites downstream from restoration at two banks using different image sensors and camera position setups. DEMs of difference were created from images obtained at focal lengths of 50 mm and 70 mm for May 2011 and September 2011 separately. Both models were created using a panoramic-image fan technique with four stations for May 2011 and two stations for September 2011. Using only two camera stations yielded higher RMSE errors in DTMs, and the distribution of errors showed small but present errors in the center of the DTM and large errors propagating toward the edges. Errors from models created using four camera stations were much more limited, but errors that did exist also tended to occur on the edges of models. Surfaces perpendicular to the viewing direction of the lens were very small whereas slopes and complex surfaces exhibited higher error values.

A time-lapse capsule with an 8.5 mm lens and a 3.1MP sensor was used to create a DTM using 27 photographs, all of which were captured at different positions ~1m apart. A consumer-grade camera with a 50 mm lens was used to create a DTM of the same area using 25 photographs taken primarily from two camera stations using the fan technique. Although the photographs taken with the larger image sensor have the

potential for creating a more accurate DTM, the limited camera positions prevented successful DTM creation. Despite large distortions created from short focal lengths, limited details from low-resolution photographs, and large quantities of noisy pixels, an accurate DTM was successfully generated using a time-lapse capsule. Expanding DTM generation using images from unconventional sensors like camera phones or point-and-shoot cameras may provide more flexibility in creating low-resolution DTMs for other applications outside geomorphology.

Time-lapse capsules were also used to capture photographs on a sub-daily interval from two stationary positions from May 2011 to September 2011 downstream from the modified channel. Although drastic changes in discharge were observed, no visual indicators of bank erosion were observed. Time-lapse capsules still have the potential to capture geomorphic change from individual flows, but predicting changes at individual locations that have sufficient geometry for permanent camera setup without encountering human disturbance are difficulties that need to be overcome on a case-by-case basis.

The results of this study have provided a better understanding of the quantitative changes of elevations of a gravel bar in a modified alpine stream and the feasibility of terrestrial photogrammetry using consumer-grade cameras. The findings from this study show that camera geometries and image sensors that do not follow the original recommendations for aerial photogrammetry can still generate accurate DTMs sufficient for quantitative analysis provided images are acquired at more than two different camera stations with adequate separation.

REFERENCES

Adams, J.C., Chandler, J.H., 2002. Evaluation of lidar and medium scale photogrammetry for detecting soft-cliff coastal change. The Photogrammetric Record. 17, 405-418.

Adenlof, K.A., Wohl, E.E., 1994. Controls on bedload movement in a subalpine stream of the Colorado Rocky Mountains, U.S.A. Arct. Alp. Res. 26(1), 77-85.

Anonymous, Station Information - USGS Water Data for the Nation. U.S. Geological Survey, pp. Metadata for USGS Gauging Station #09146020.

Anonymous, 2011. The Public Laboratory for Open Technology and Science. In: Jeffrey Warren (Ed.).

Ashmore, P., Sauks, E., 2006. Prediction of discharge from water surface width in a braided river with implications for at-a-station hydraulic geometry. Water Resour. Res. 42(3), 1-11.

Baily, B., Collier, P., Farres, P., Inkpen, R., Pearson, A., 2003. Comparative assessment of analytical and digital photogrammetric methods in the construction of DEMs of geomorphological forms. Earth Surf. Process. Landf. 28(3), 307-320.

Birch, J.S., 2009a. Using 3DM Analyst Mine Mapping Suite for Slope Stability — Case Studies Geotechnical Engineering in Open Pit Mines Seminar Australian Centre for Geomechanics, Brisbane, Australia, pp. 1-15.

Birch, J.S., 2009b. Using 3DM Analyst Mine Mapping Suite for Slope Stability — Case Studies Geotechnical Engineering for Open Pit Mines. ADAM Technology 3D Measurement Software and Solutions, Brisbane, Australia, pp. 1-15.

Brasington, J., Langham, J., Rumsby, B., 2003. Methodological sensitivity of morphometric estimates of coarse fluvial sediment transport. Geomorphology. 53(3-4), 299-316.

Brasington, J., Smart, R.M.A., 2003. Close range digital photogrammetric analysis of experimental drainage basin evolution. Earth Surf. Process. Landf. 28(3), 231-247.

Brecher, H.H., Thompson, L.G., 1993. Measurement of the retreat of Qori Kalis Glacier in the Tropical Andes of Peru by Terrestrial Photogrammetry. Photogramm. Eng. Remote Sens. 59(6), 1017-1022.

Butler, J.B., Lane, S.N., Chandler, J.H., Porfiri, E., 2002. Through-water close range digital photogrammetry in flume and field environments. Photogramm. Rec. 17(99), 419-439.

Carbonneau, P.E., 2005. The threshold effect of image resolution on image-based automated grain size mapping in fluvial environments. Earth Surf. Process. Landf. 30(13), 1687-1693.

Carbonneau, P.E., Lane, S.N., Bergeron, N.E., 2004. Catchment-scale mapping of surface grain size in gravel bed rivers using airborne digital imagery. Water Resour. Res. 40(7), 1-11.

Ceballos, J.L., Euscategui, C., Ramirez, J., Canon, M., Huggel, C., Haeberli, W., Machguth, H., 2006. Fast shrinkage of tropical glaciers in Colombia. Annals of Glaciology, Vol 43, 2006. 43, 194-201.

Chandler, J., 1999. Effective application of automated digital photogrammetry for geomorphological research. Earth Surf. Process. Landf. 24(1), 51-63.

Chandler, J., Ashmore, P., Paola, C., Gooch, M., Varkaris, F., 2002. Monitoring river-channel change using terrestrial oblique digital imagery and automated digital photogrammetry. Annals of the Association of American Geographers. 92(4), 631-644.

Chow, V.T., 1959. Open-Channel Hydraulics. McGraw-Hill, New York.

Clow, D.W., 2010. Changes in the timing of snowmelt and streamflow in Colorado: A response to recent warming. J. Clim. 23(9), 2293-2306.

Coudrain, A., Francou, B., Kundzewicz, Z.W., 2005. Glacier shrinkage in the Andes and consequences for water resources. Hydrological Sciences Journal. 50(6), 925-932.

Dietrich, W., E,, Whiting, P., 1989. Boundary shear stress and sediment transport in river meanders of sand and gravel. In: S. Ikeda, G. Parker (Eds.), River Meandering. American Geophysical Union Water Resources Monograph 12, pp. 1-50.

Dosemagen, S., 2010. Grassroots aerial photography: Mapping the BP oil disaster, 2010 Geological Society of America Annual Meeting. GSA, Denver, CO, pp. 504.

Dugdale, S.J., Carbonneau, P.E., Campbell, D., 2010. Aerial photosieving of exposed gravel bars for the rapid calibration of airborne grain size maps. Earth Surf. Process. Landf. 35(6), 627-639.

Elliott, J.G., Capesius, J.P., 2009. Geomorphic changes resulting from floods in reconfigured gravel-bed river channels in Colorado, USA. In: L. A. James, S. L. Rathburn, G. R. Whittecar (Eds.), Management and Restoration of Fluvial Systems with Broad Historical Changes and Human Impacts. Geological Society of America Special Papers. Geological Soc Amer Inc, Boulder, pp. 173-198.

Elliott, J.G., Hammack, L.A., 2000. Entrainment of riparian gravel and cobbles in an alluvial reach of a regulated canyon river. Regulated Rivers: Research & Management. 16(1), 37-50.

Flynn, K.M., Kirby, W.H., Hummel, P.R., 2006. User's manual for program PeakFQ annual flood-frequency analysis using Bulletin 17B guidlines, Geological Survey Techniques and Methods Book 4. U.S. Geologrical Survey, pp. 1-42.

Fraser, C.S., 1998. Automated processes in digital photogrammetric calibration, orientation, and triangulation. Digit. Signal Prog. 8(4), 277-283.

Gong, J.Y., Li, Z.L., Zhu, Q., Sui, H.G., Zhou, Y., 2000. Effects of various factors on the accuracy of DEMs: An intensive experimental investigation. Photogramm. Eng. Remote Sens. 66(9), 1113-1117.

Griffiths, G.A., 1980. Stochastic estimation of bed load yield in pool-and-riffle mountain streams. Water Resour. Res. 16(5), 931-937.

Hasegawa, H., Matsuo, K., Koarai, M., Watanabe, N., Masaharu, H., Fukushima, Y., 2000. DEM Accuracy and the base to height (B/H) ratio of stereo images. In: D. Fritsch and M. Molenaar (Ed.), XIXth Congress. International Society of Photogrammetry and Remote Sensing, Amsterdam, pp. 356-359.

Jensen, J.R., 2007. Remote Sensing of the Environment: An Earth Resource Perspective. Prentice-Hall Series in Geographic Information Science. Pearson - Prentice Hall, Upper Saddle River, NJ.

Komar, P.D., 1987. Selective gravel entrainment and the empirical evaluation of flow competence. Sedimentology. 34(6), 1165-1176.

Lane, S.N., Chandler, J.H., 2003. Editorial: The generation of high quality topographic data for hydrology and geomorphology: New data sources, new applications and new problems. Earth Surf. Process. Landf. 28(3), 229-230.

Lane, S.N., Westaway, R.M., Hicks, D.M., 2003. Estimation of erosion and deposition volumes in a large, gravel-bed, braided river using synoptic remote sensing. Earth Surf. Process. Landf. 28(3), 249-271.

Langbein, W.B., Leopold, L.B., 1964. Quasi-Equilibrium states in channel morphology. Am. J. Sci. 262(6), 782-794.

Lawler, D.M., 2005. The importance of high-resolution monitoring in erosion and deposition dynamics studies: Examples from estuarine and fluvial systems. Geomorphology. 64(1-2), 1-23.

Lorang, M.S., Hauer, F.R., 2003. Flow competence and streambed stability: an evaluation of technique and application. J. N. Am. Benthol. Soc. 22(4), 475-491.

Luedke, G.R., Burbank, S. Wilbur, 1962. Geology of the Ouray Quadrangle, Colorado. In: The Colorado State Metal Mining Fund Board (Ed.). Department of the Interior - USGS, Ouray, CO.

Marcus, W.A., Fonstad, M.A., 2008. Optical remote mapping of rivers at sub-meter resolutions and watershed extents. Earth Surf. Process. Landf. 33(1), 4-24.

Mathewson, C.C., Keaton, J. R., 1992. Methodology for the evaluation and mitigation of multiple natural hazards, CCNAA-AIT Joint Seminar on Prediction & Damage Mitigration of Meteorologically Indicued Natural Disasters. National Taiwan University, pp. 135-144.

Matthews, N.A., 2008. Aerial and close-range photogrammetric technology: Providing resource documentation, interpretation, and preservation. Technical Note 428, Bureau of Land Management, Denver, Colorado.

Middleton, G.V., Southard, J.B., 1984. Mechanics of sediment movement. S.E.P.M. Short Course Number 3. Sponsored by the Eastern Section S.E.P.M., Providence.

Pasumansky, A., 2011. Agisoft Lens. Agisoft LLC, St. Petersburg, Russia.

Petrie, G., Walker, A.S., 2007. Airborne digital imaging technology: A new overview. Photogramm. Rec. 22(119), 203-225.

Pyle, C.J., Richards, K.S., Chandler, J.H., 1997. Digital photogrammetric monitoring of river bank erosion. The Photogrammetric Record. 15(89), 753-764.

Rignot, E., Rivera, A., Casassa, G., 2003. Contribution of the Patagonia Icefields of South America to sea level rise. Science. 302(5644), 434-437.

Rondinelli, P., 2011. River Cleaning. In: Tyler Depke (Ed.), Ouray, CO.

Schumm, S.A., 1977. The Fluvial System. John Wiley & Sons, New York.

Schumm, S.A., 1979. Geomorphic thresholds: The concept and its applications. Transactions of the Institute of British Geographers. 4(4), 485-515.

Schumm, S.A., Khan, H.R., 1972. Experimental study of channel patterns. Geol. Soc. Am. Bull. 83(6), 1755-1770.

Smith, S.M., Prestegaard, K.L., 2005. Hydraulic performance of a morphology-based stream channel design. Water Resour. Res. 41(11), 1-17.

Thomas, H., Cantré, S., 2009. Applications of low-budget photogrammetry in the geotechnical laboratory. The Photogrammetric Record. 24(128), 332-350.

VanderZee, D., 2010. Reconyx Lens Specs. In: Tyler Depke (Ed.). Reconyx.

Westaway, R.M., Lane, S.N., Hicks, D.M., 2003. Remote survey of large-scale braided, gravel-bed rivers using digital photogrammetry and image analysis. Int. J. Remote Sens. 24(4), 795-815.

Wohl, E., 2006. Human impacts to mountain streams. Geomorphology. 79(3-4), 217-248.

Wolman, M.G., 1954. A method of sampling coarse river-bed material. American Geophysical Union Transactions. 35(6), 951-956.

Wolman, M.G., Miller, J.P., 1960. Magnitude and frequency of forces in geomorphic processes. J. Geol. 68(1), 54-74.

Yilmaz, H.M., 2010. Close range photogrammetry in volume computing. Experimental Techniques. 34(1), 48-54.

APPENDIX

FIGURES

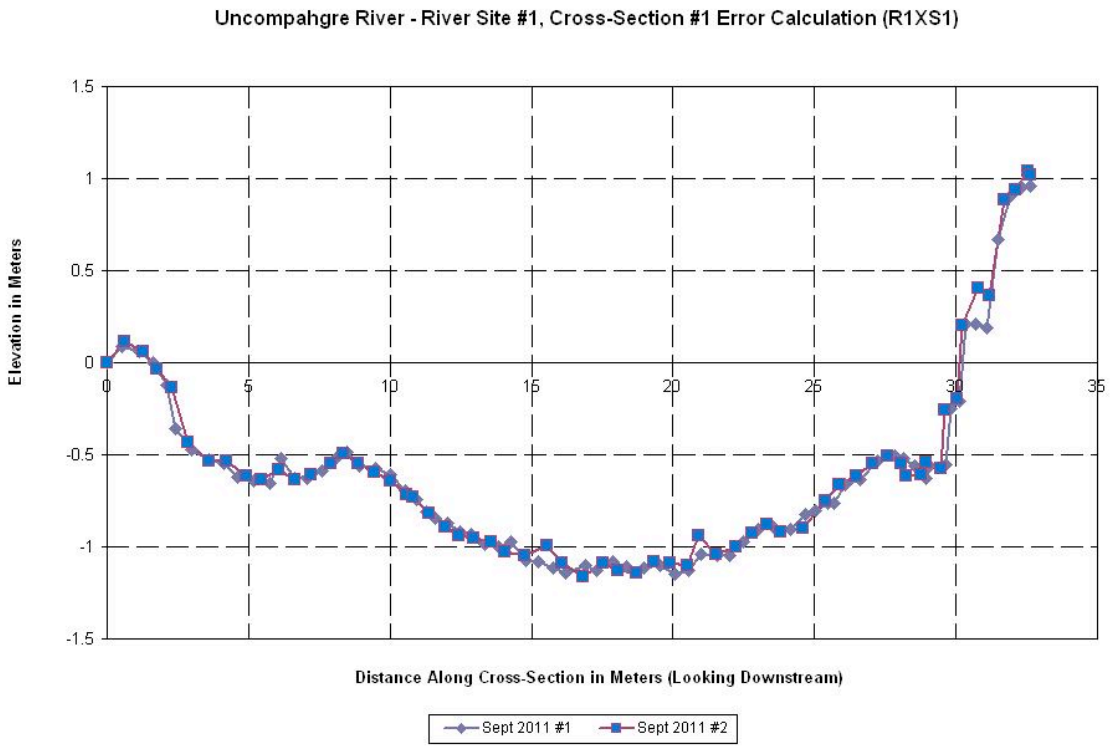

Fig. A-1. Cross-sectional error calculation using R1XS1.

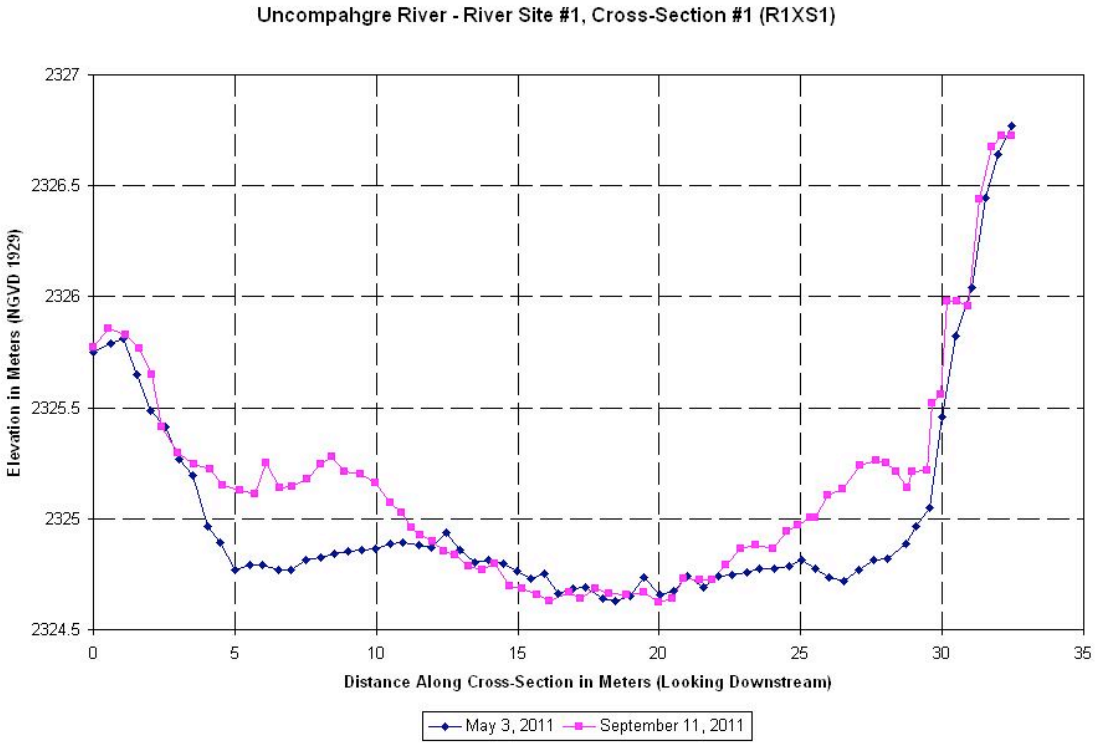

Fig. A-2. Total station cross-sectional survey at R1XS1.

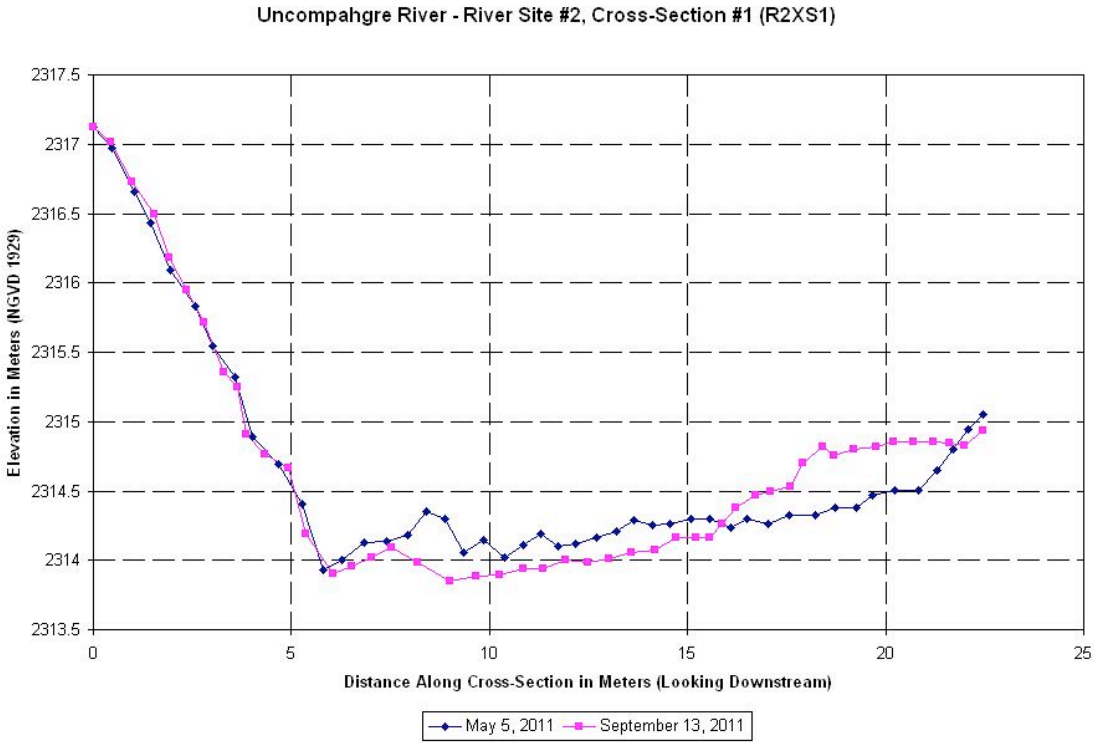

Fig. A-3. Total station cross-sectional survey at R2XS1.

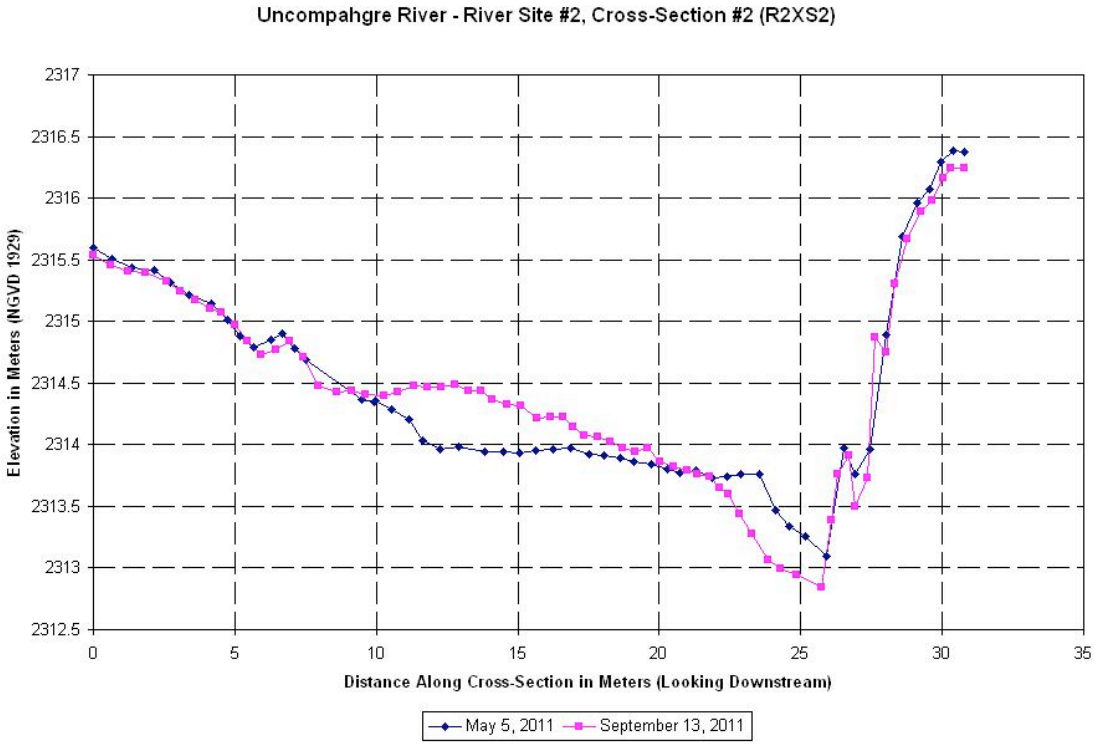

Fig. A-4. Total station cross-sectional survey at R2XS2.

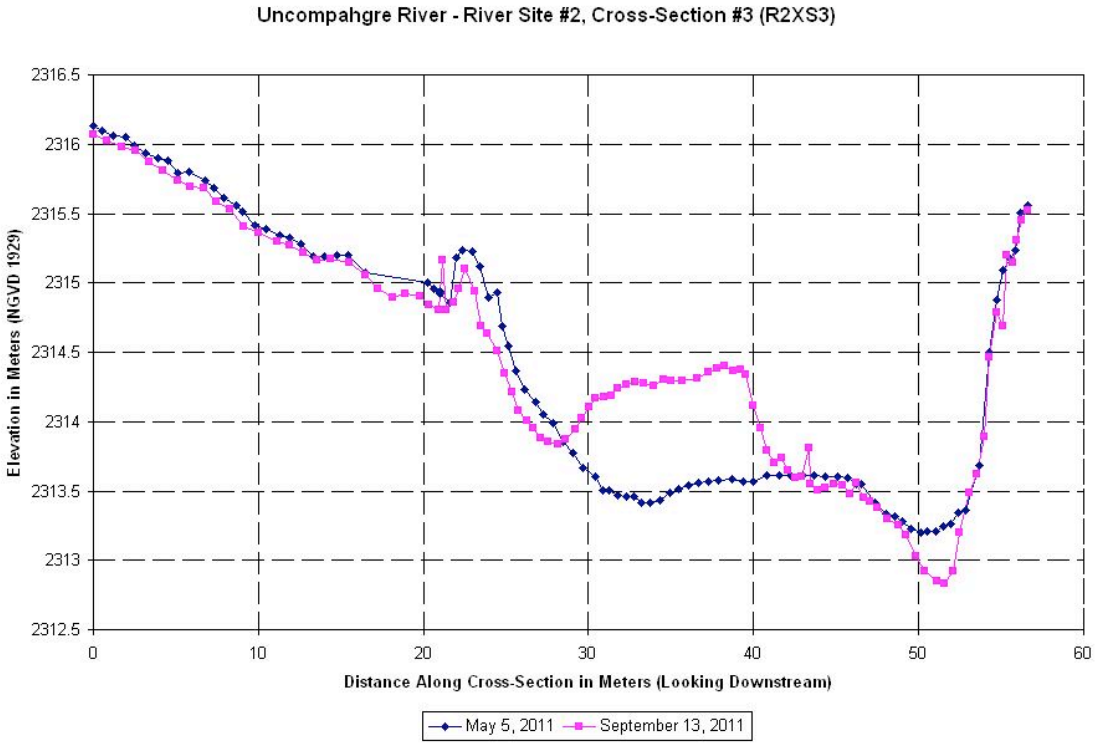

Fig. A-5. Total station cross-sectional survey at R2XS3.

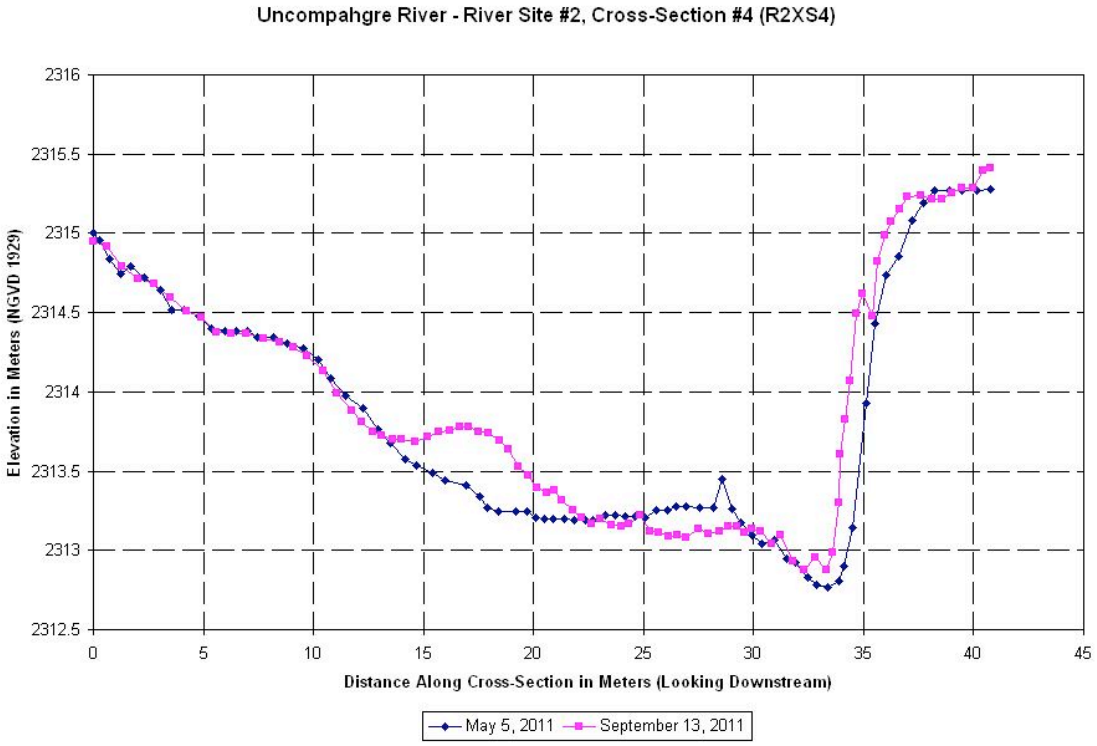

Fig. A-6. Total station cross-sectional survey at R2XS4.

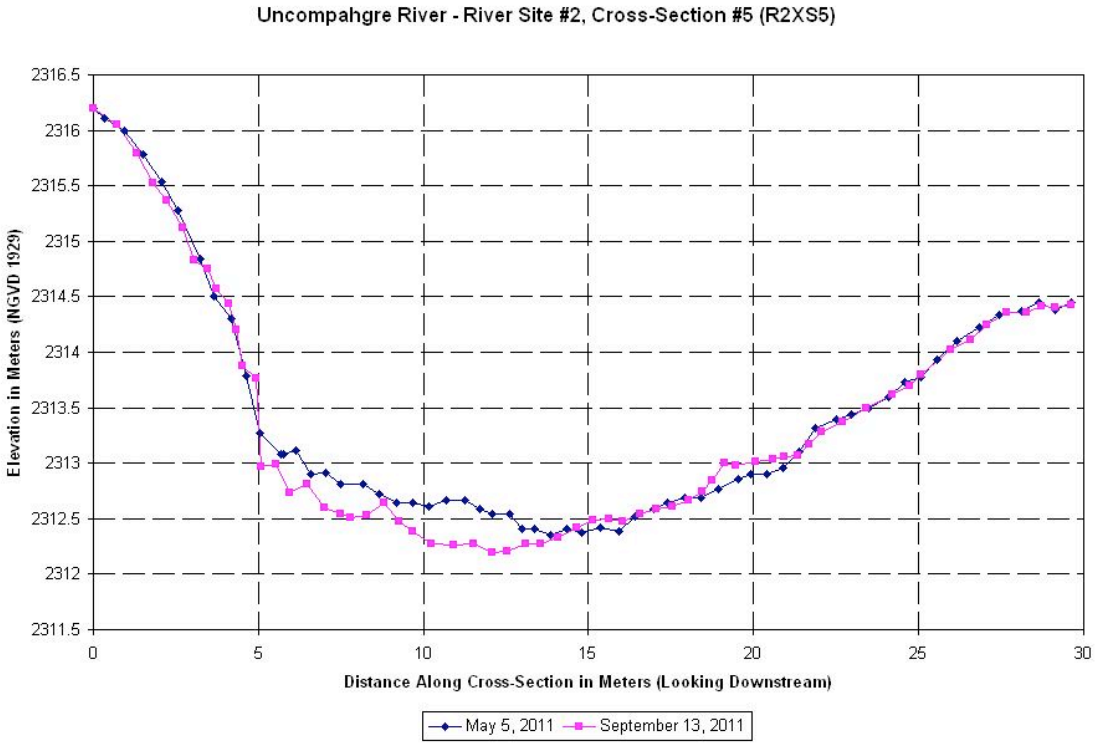

Fig. A-7. Total station cross-sectional survey at R2XS5.

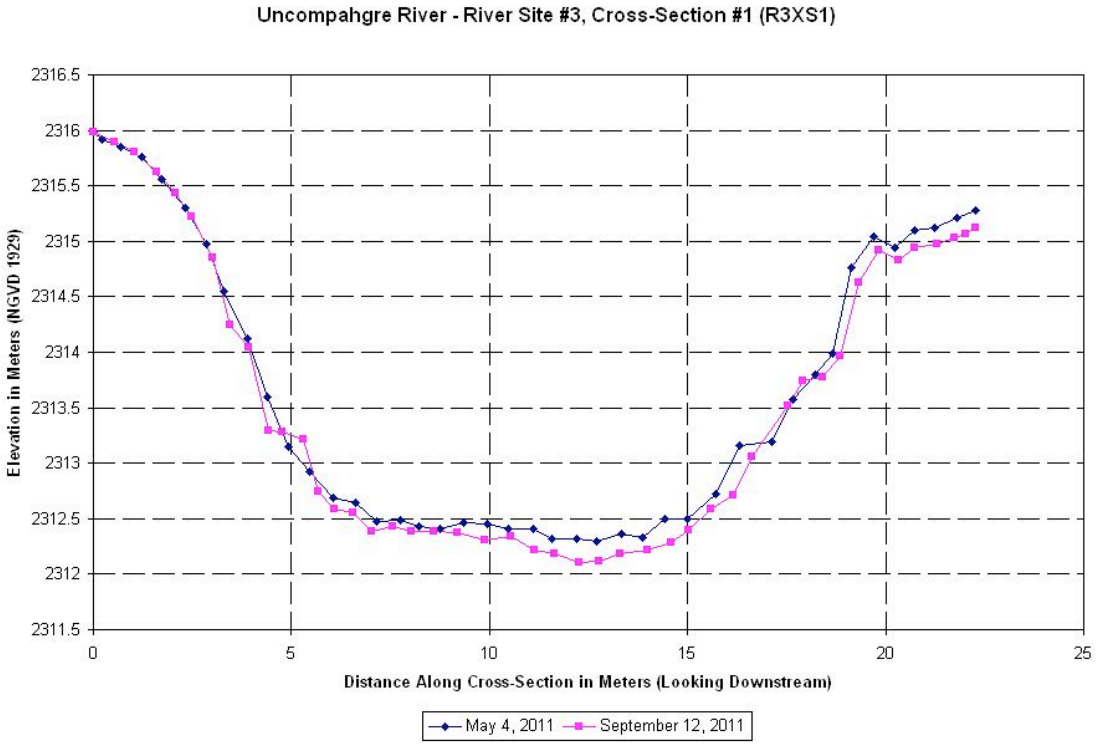

Fig. A-8. Total station cross-sectional survey at R3XS1.

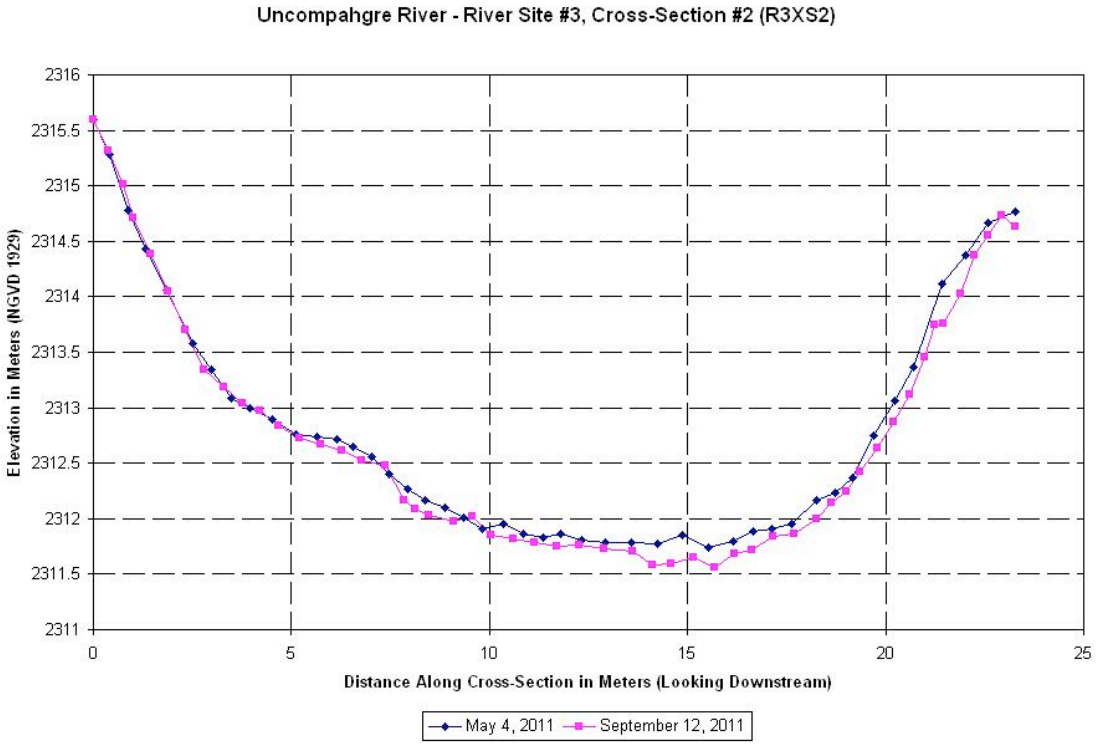

Fig. A-9. Total station cross-sectional survey at R3XS2.

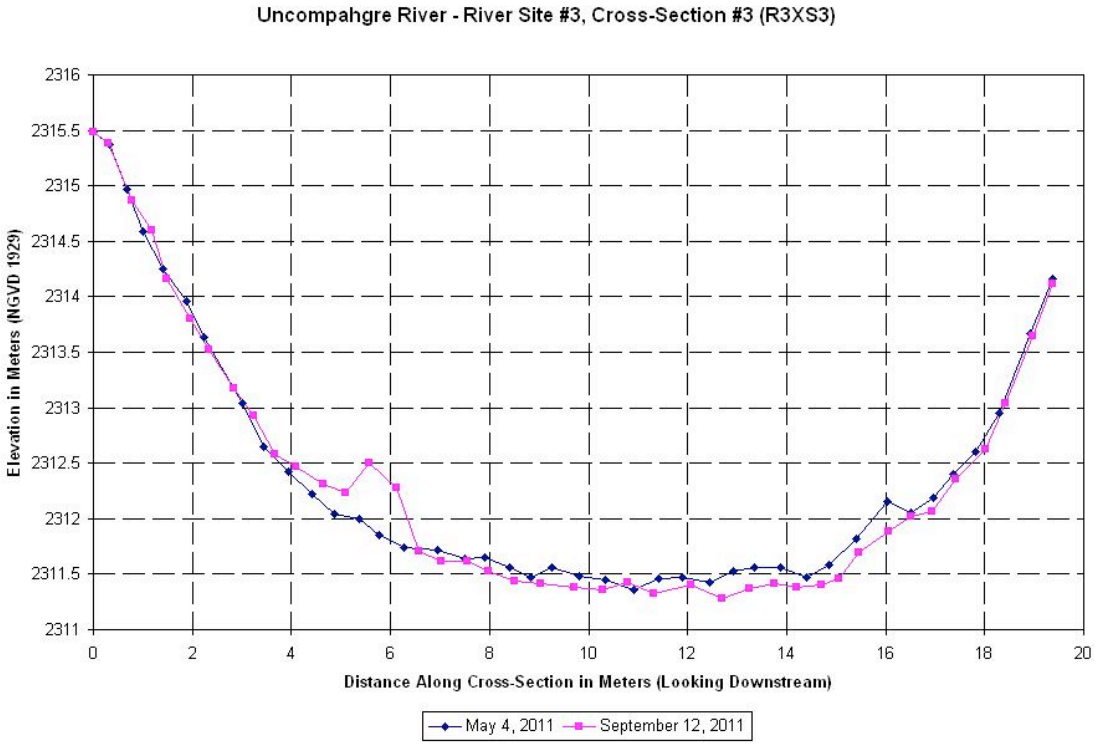

Fig. A-10. Total station cross-sectional survey at R3XS3.

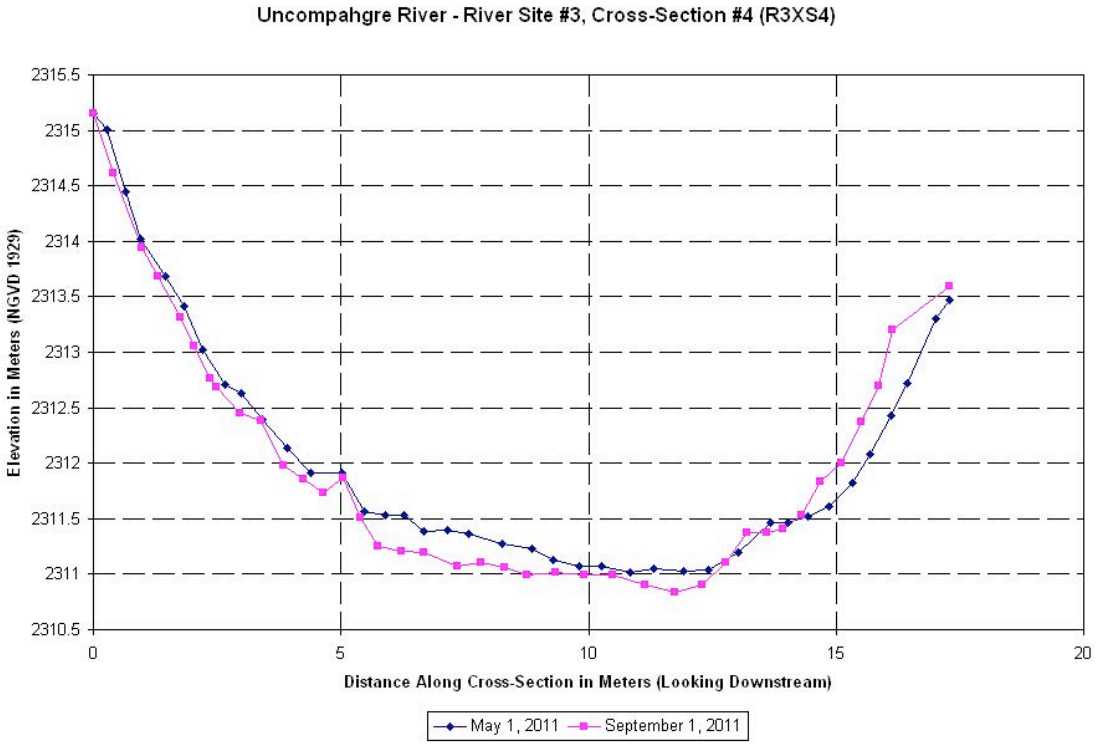

Fig. A-11. Total station cross-sectional survey at R3XS4.

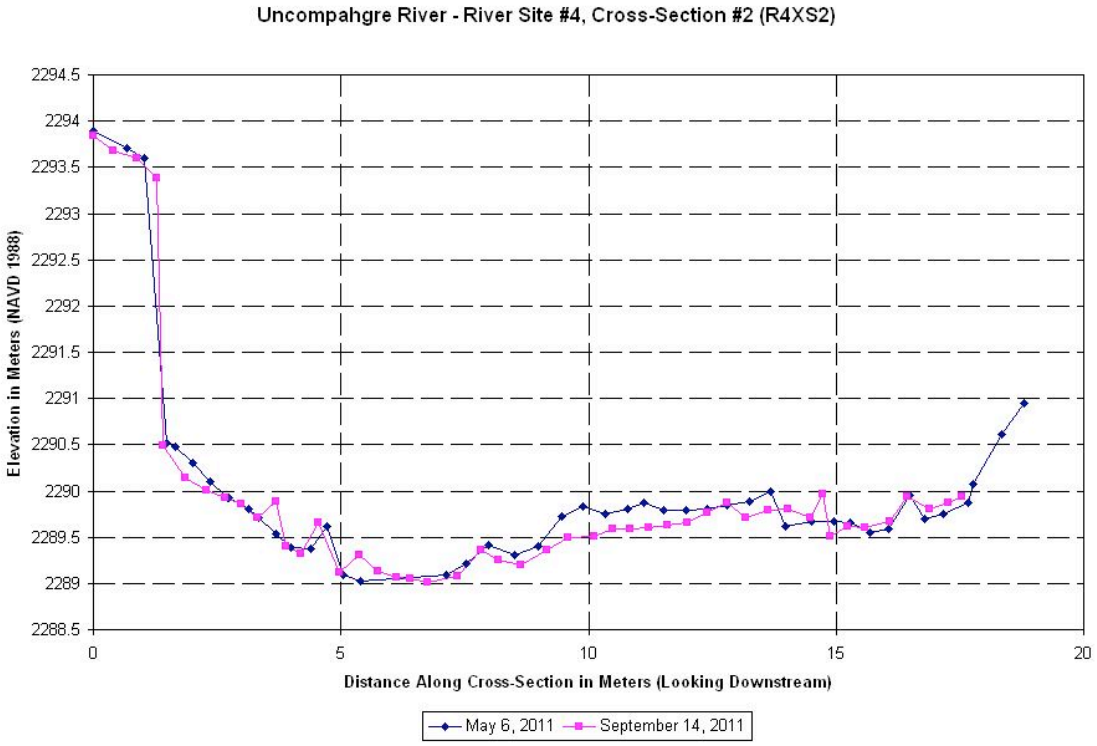

Fig. A-12. Total station cross-sectional survey at R4XS2.

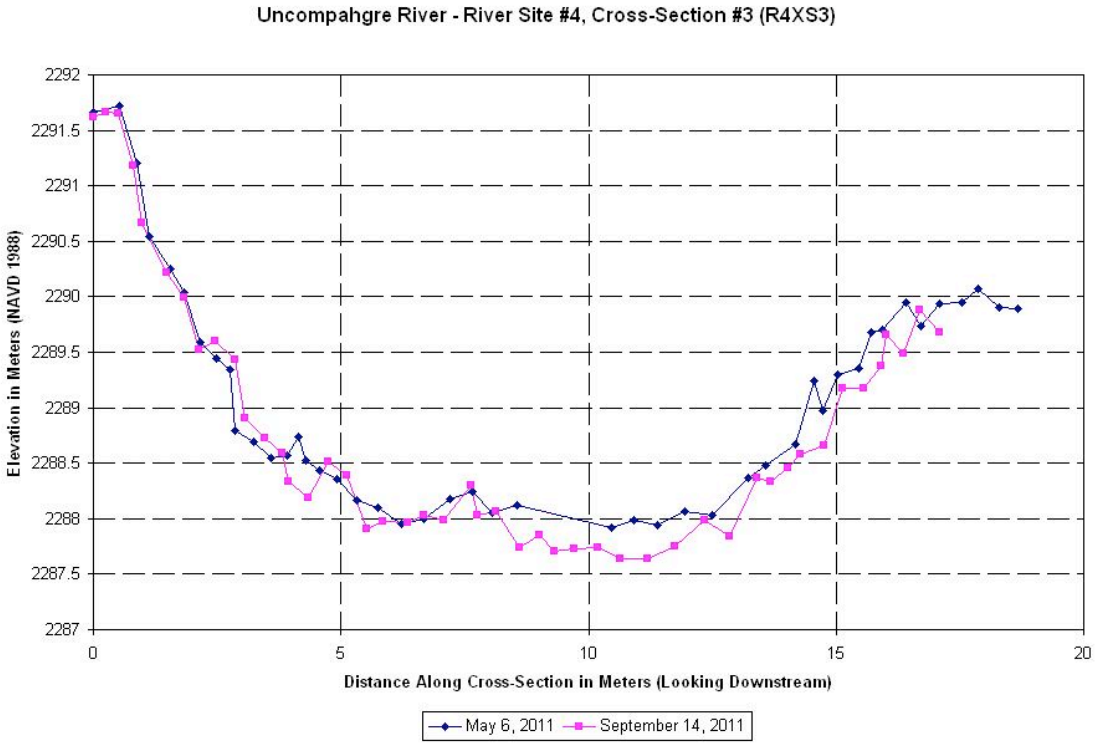

Fig. A-13. Total station cross-sectional survey at R4XS3.

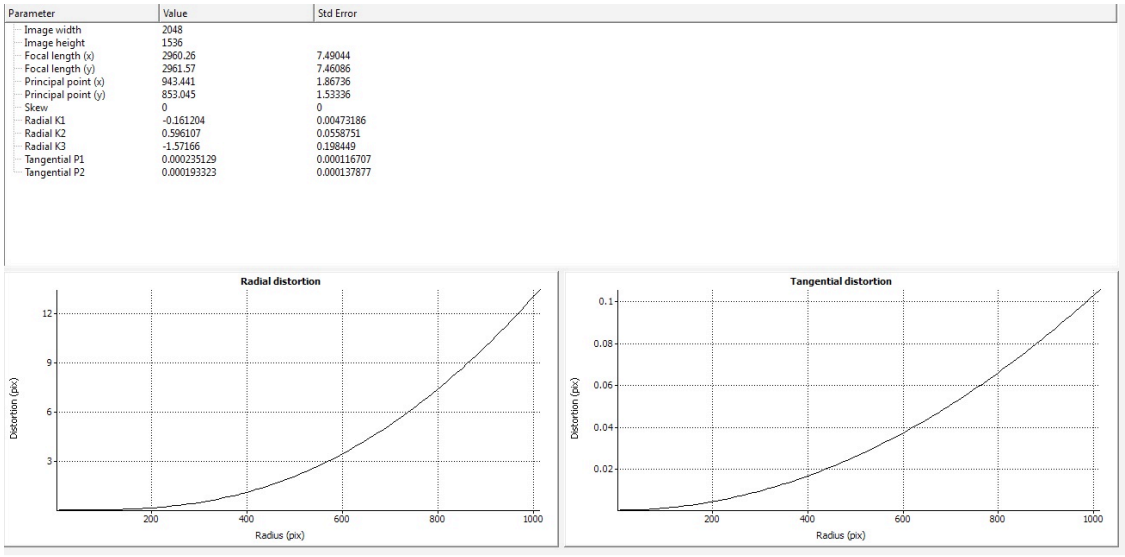

Parameter	Value	Std Error
Image width	2048	
Image height	1536	
Focal length (x)	2960.26	7.49044
Focal length (y)	2961.57	7.46086
Principal point (x)	943.441	1.86736
Principal point (y)	853.045	1.53336
Skew	0	0
Radial K1	-0.161204	0.00473186
Radial K2	0.596107	0.0558751
Radial K3	-1.57166	0.198449
Tangential P1	0.000235129	0.000116707
Tangential P2	0.000193323	0.000137877

Fig. A-14. Lens Parameters for Reconyx Time-Lapse Capsule (~8.5mm).

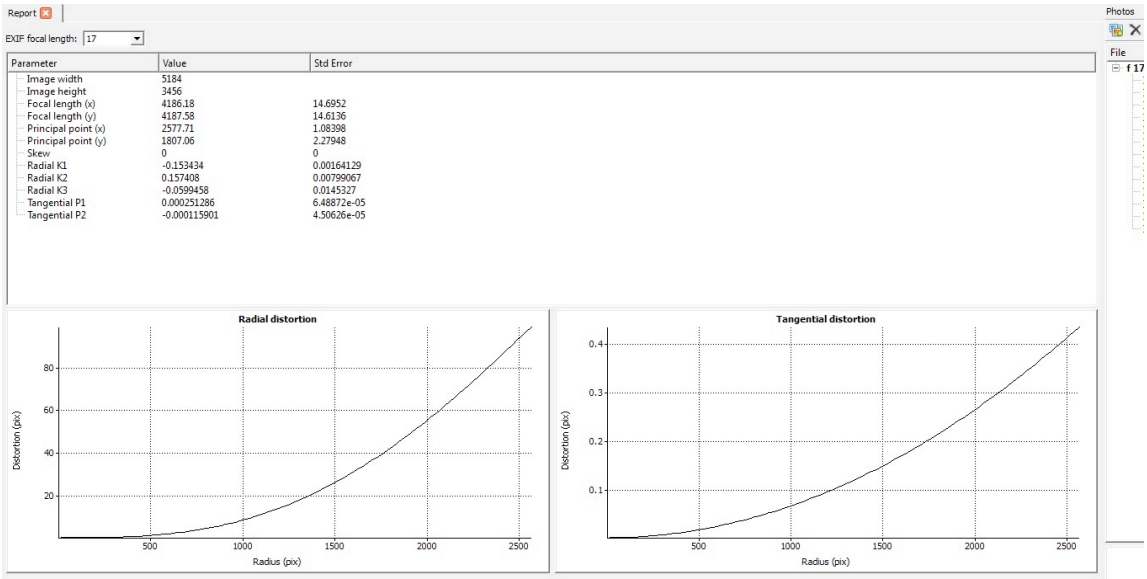

Fig. A-15. Lens Parameters for Sigma 17-70 mm f/2.8-4 DC Macro OS HSM Lens @ 17 mm.

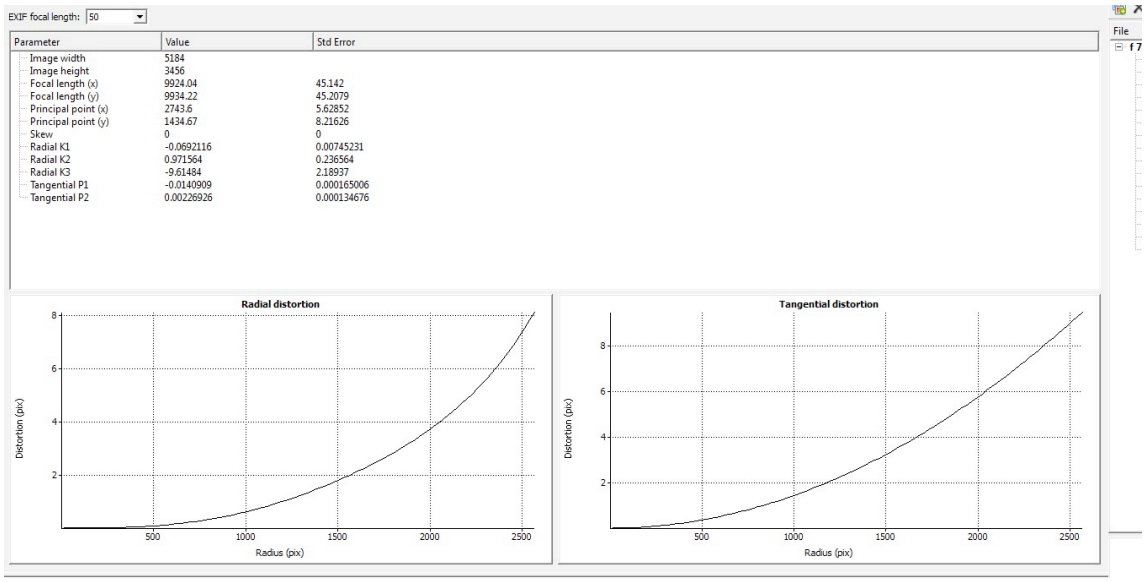

Fig. A-16. Lens Parameters for Canon EF 50 mm f/1.8 II.

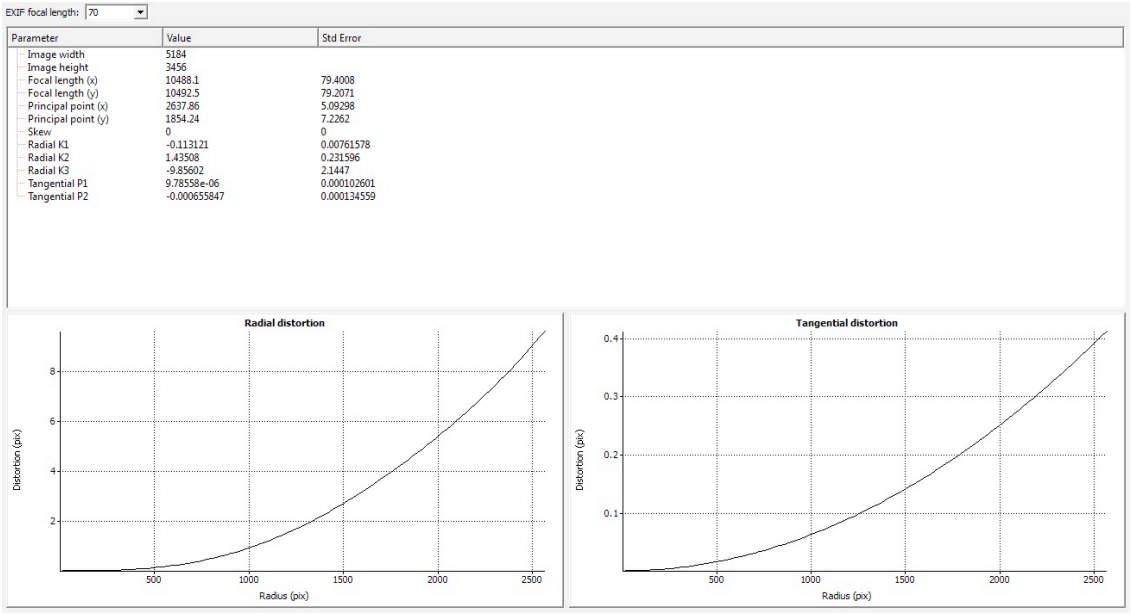

Fig. A-17. Lens Parameters for Sigma 70-300mm f/4-5.6 DG APO Macro Telephoto Zoom Lens @ 70mm.

Fig. A-18. Standing on gravel bar at R2 in September 2011.

TABLES

Table A-1. Camera Station Base-to-Height Ratios.

Camera Stations	B-H Ratio
EM1-EM2	1.05
EM2-EM3	0.72
WM1-WM2	0.58

Table A-2. All RMSE (m) values for all DTMs organized by river site, lens used, and accuracy setting used in Agisoft Photoscan Pro. In models where bold values are present, these are the only values used for calculating the average.

		RMSE (m)			
Model Name	Point #	Total	X	Y	Z
R2 70mm May High					
	point 11	**0.171**	**0.081**	**0.026**	**0.148**
	point 12	**0.204**	**-0.125**	**-0.031**	**-0.157**
	point 13	1.180	-0.827	-0.668	-0.513
	point 14	**0.093**	**0.044**	**-0.011**	**-0.081**
	point 15	**0.092**	**0.000**	**0.017**	**0.090**
	point 16	1.930	1.421	0.966	0.879
	point 17	5.601	4.221	2.670	2.536
	Average	0.140	0.063	0.021	0.119
Outside AOI Mask					
	point 24	7.776	6.018	3.49	3.473
	point 26	13.93	10.091	8.682	4.102
	point 27	5.435	3.976	3.318	1.651
	point 28	8.743	6.565	5.101	2.705
	point 29	6.929	5.415	3.651	2.317
	point 3	13.103	-8.976	-8.118	-5.022
	point 5	20.961	-15.545	-10.888	-8.898
	point 6	18.138	-13.817	-8.968	-7.592
	point 8	4.076	-3.436	-1.701	-1.384
	Average	12.061	3.495	2.647	2.391
R2 70mm Sept High					
	point 1	6.156	-6.062	0.624	-0.871
	point 2	**0.148**	**0.088**	**0.116**	**-0.024**
	point 3	1.866	-1.848	0.151	-0.213

		RMSE (m)			
Model Name	Point #	Total	X	Y	Z
	point 4	5.295	5.135	-1.150	0.595
	point 5	**0.203**	**-0.081**	**-0.182**	**0.039**
	point 6	4.746	4.522	-1.384	0.406
	point 7	**0.480**	**-0.470**	**0.097**	**-0.001**
	point 8	**0.464**	**0.462**	**-0.031**	**-0.014**
	Average	0.324	0.275	0.107	0.020
R4 50mm May Low					
	point 1	**0.067**	**-0.015**	**-0.011**	**0.065**
	point 10	0.099	0.071	0.063	0.029
	point 11	**0.033**	**-0.004**	**-0.027**	**0.018**
	point 12	**0.032**	**-0.010**	**-0.025**	**0.017**
	point 13	**0.052**	**0.010**	**-0.020**	**-0.047**
	point 14	**0.031**	**0.013**	**-0.007**	**-0.028**
	point 15	**0.026**	**0.024**	**-0.003**	**-0.009**
	point 2	0.074	-0.042	-0.060	0.009
	point 3	**0.015**	**-0.015**	**-0.002**	**0.002**
	point 4	0.093	-0.083	0.042	0.007
	point 5	**0.054**	**-0.025**	**0.046**	**-0.016**
	point 6	**0.031**	**0.012**	**-0.009**	**-0.027**
	point 7	**0.013**	**0.008**	**0.008**	**-0.006**
	point 8	**0.058**	**0.001**	**0.050**	**0.029**
	point 9	0.135	-0.094	0.092	0.030
	Average	0.037	0.012	0.019	0.024
R4 70mm May Low					
	point 1	**0.02**	**0.007**	**0.016**	**0.010**
	point 10	**0.046**	**0.042**	**0.013**	**-0.014**
	point 11	**0.042**	**-0.021**	**-0.029**	**-0.021**
	point 12	**0.035**	**-0.011**	**-0.020**	**0.026**
	point 13	12.643	-12.532	1.565	-0.584
	point 14	9.039	-8.789	2.044	-0.525
	point 15	**0.028**	**0.027**	**-0.009**	**0.000**
	point 2	**0.044**	**-0.021**	**-0.036**	**-0.014**
	point 3	**0.017**	**0.004**	**0.016**	**-0.001**
	point 4	0.092	-0.064	0.063	0.020
	point 5	**0.058**	**-0.019**	**0.054**	**0.006**
	point 6	**0.024**	**0.002**	**-0.023**	**-0.007**
	point 7	**0.005**	**0.004**	**-0.003**	**0.000**

		RMSE (m)			
Model Name	Point #	Total	X	Y	Z
	point 8	**0.03**	**-0.014**	**0.021**	**0.016**
	point 9	0.131	-0.111	0.071	-0.002
	Average	0.032	0.016	0.022	0.010
R4 50mm Sept Low					
	point 1	**0.307**	**0.093**	**0.226**	**0.185**
	point 10	**0.390**	**-0.073**	**0.307**	**0.229**
	point 11	**0.237**	**-0.055**	**0.206**	**-0.103**
	point 12	13.537	0.600	13.518	0.398
	point 13	7.152	0.362	7.141	0.167
	point 14	3.152	0.184	3.146	0.043
	point 15	1.880	0.035	-1.877	-0.089
	point 16	5.805	-0.151	-5.800	-0.210
	point 17	8.079	-0.275	-8.069	-0.279
	point 2	**0.349**	**0.052**	**0.276**	**-0.208**
	point 3	1.945	0.101	-1.925	-0.259
	point 4	**0.674**	**-0.439**	**-0.502**	**0.094**
	point 5	1.588	-1.463	-0.302	0.538
	point 6	1.631	-0.066	-1.627	-0.094
	point 7	1.604	1.419	-0.324	-0.674
	point 8	**0.693**	**0.421**	**-0.513**	**-0.198**
	point 9	1.947	-0.251	-1.927	0.108
	Average	0.442	0.189	0.338	0.170
R4 70mm Sept Low					
	point 1	**0.239**	**-0.159**	**-0.153**	**0.092**
	point 10	3.103	-1.401	2.757	-0.264
	point 11	10.109	-7.985	3.768	-4.922
	point 12	16.1	-2.488	15.854	-1.293
	point 13	9.416	-2.760	8.912	-1.273
	point 14	5.553	-2.918	4.562	-1.230
	point 15	3.398	-2.874	-1.029	-1.492
	point 16	6.114	-2.847	-5.262	-1.258
	point 17	8.194	-2.716	-7.668	-0.981
	point 2	**0.301**	**0.104**	**0.277**	**-0.054**
	point 3	2.025	-0.281	-1.923	-0.569
	point 4	1.513	-1.368	-0.084	-0.641
	point 5	2.656	-2.604	0.438	-0.292
	point 6	**0.277**	**0.127**	**-0.228**	**-0.092**

		RMSE (m)			
Model Name	Point #	Total	X	Y	Z
	point 7	1.661	0.648	1.355	-0.710
	point 8	1.766	-0.777	1.252	-0.974
	point 9	**0.137**	**-0.072**	**0.104**	**0.054**
	Average	0.116	0.191	0.073	0.073
R5 Reconyx Low					
	point 1	**0.217**	**0.006**	**0.166**	**-0.139**
	point 10	2.445	0.713	-1.967	1.265
	point 11	**0.166**	**-0.094**	**-0.048**	**0.129**
	point 12	**0.228**	**0.121**	**0.004**	**-0.193**
	point 2	**0.194**	**0.019**	**-0.163**	**0.103**
	point 3	1.260	0.015	-1.033	0.721
	point 4	1.205	-0.004	-0.988	0.690
	point 5	0.499	0.020	0.426	-0.259
	point 6	**0.201**	**-0.007**	**-0.143**	**0.141**
	point 7	2.102	-0.070	-1.713	1.216
	point 8	**0.194**	**-0.044**	**0.184**	**-0.041**
	point 9	1.279	-1.096	-0.132	0.647
	Average	0.200	0.049	0.118	0.124
R5 50mm Sept Low					
	point 1	**0.371**	**0.346**	**0.130**	**-0.039**
	point 10	0.938	0.061	-0.604	0.715
	point 11	**0.242**	**0.171**	**0.110**	**-0.131**
	point 2	1.708	1.075	-1.222	0.518
	point 4	2.109	0.881	-1.641	0.988
	point 5	**0.507**	**-0.466**	**-0.199**	**0.025**
	point 6	1.618	0.676	-1.464	-0.131
	point 7	1.261	-0.734	-0.986	0.280
	point 8	**0.159**	**-0.051**	**-0.041**	**0.145**
	point 9	2.963	-2.260	1.912	-0.132
	Average	0.259	0.120	0.085	0.085

VITA

Name: Tyler J. Depke

Address: Texas A&M University
Department of Geology and Geophysics
MS 3115
College Station, TX 77843

E-mail Address: tyler.depke@gmail.com

Education: M.S. Geology, Texas A&M, 2012
B.S. Geology, Hope College, 2009

Professional Experience:

1. Computing Geoscientist for ExxonMobil's Information Technology Company

2. Graduate Teaching Assistant in the Dept. of Geology and Geophysics, Texas A&M

3. Independent Researcher in the School for International Training, Bolivia

4. Undergraduate Researcher for the Dept. of Geological and Environmental Sciences, Hope College, Holland, MI

5. Civil Engineering Intern for the Engineering Division, Village of Gurnee, IL

6. Technology Lab Tutor for the Techlab, Hope College, Holland, MI

Awards:

Michigan Space Grant Consortium Undergraduate Research Fellowship, NASA:
Digitally Mapping Mineral and Structural Patterns in Southwestern Sweden
National Geographic Channel's Preserve Our Planet Short Film Contest
Eagle Scout Rank Troop 96 Grayslake, IL
Sigma Xi Senior Research Award
Texas A&M Graduate Studies Multimedia Scholarship
Honors Convocation Award, Hope College
Hope Grant, Hope College
National Honors Society
U.S. Army Reserve National Scholar Athlete Award
MIAA Honor Roll of Athletes
Dean's List